# Electronic Supplementary Material

# Vanadyl complexes supported by *O*,*O*- and *N*,*O*-chelate ligation: Structures and polymerization catalysis

Kaname Shibata,[a] Kenji Michiue,[a] Ignas Motuzis,[b] Mark R.J. Elsegood,[b] and Carl Redshaw[c,d]*

[a] *R&D Centre, Mitsui Chemical Inc., 580-32 Naguara, Sodegaura, Chiba 299-0265, Japan.*

[b] *Chemistry Department, Loughborough University, Loughborough, Leicestershire, LE11 3TU, UK*
[c] *Department of Chemistry, Graduate School of Science, Tokyo Metropolitan University, 1-1 Minami Osawa, Hachioji, Tokyo, 192-0397, Japan.*
[d] *School of Chemistry, Pharmacy and Pharmacology, University of East Anglia, Norwich Research Park, Norwich, NR4 7TJ, U.K.*
*E.mail: credshaw@tmu.ac.jp*

**Contents** **Page Numbers**

*X-ray Crystallography*

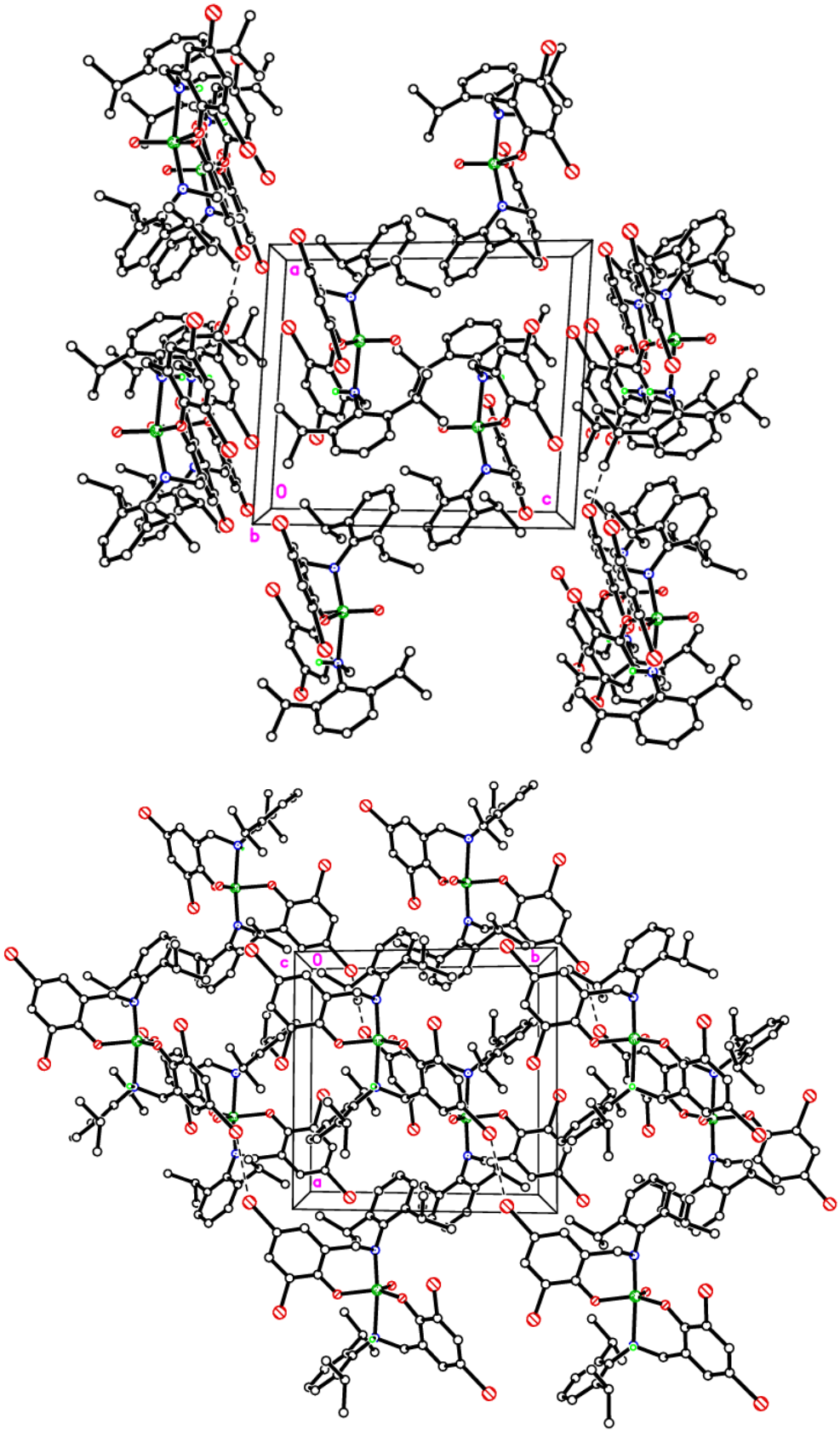

**Figure S1.** Alternative views of the packing of **1** viewed parallel to *b* (top) and *c* (bottom) showing halogen-bonding interactions Br(2)···(Br(4') = 3.535 Å.

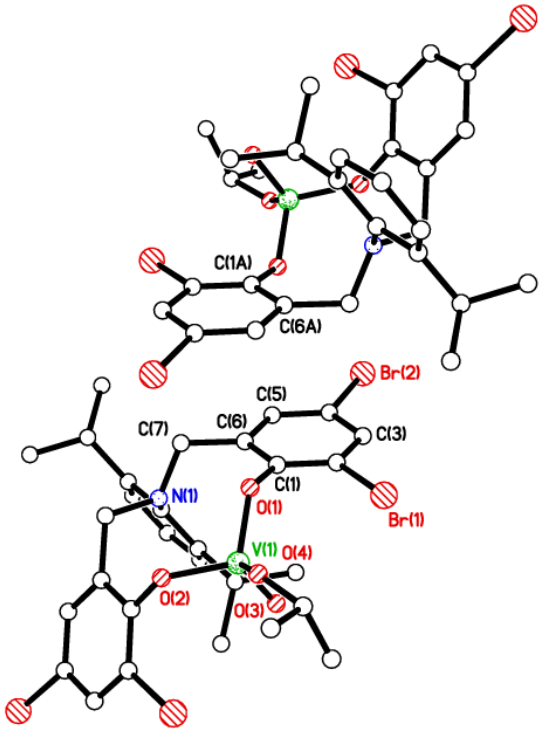


**Figure S2.** Alternative view of the packing of **2** showing the slipped π···π interactions between symmetry-related brominated rings with closest C···C separation of *ca*. 3.45 Å.

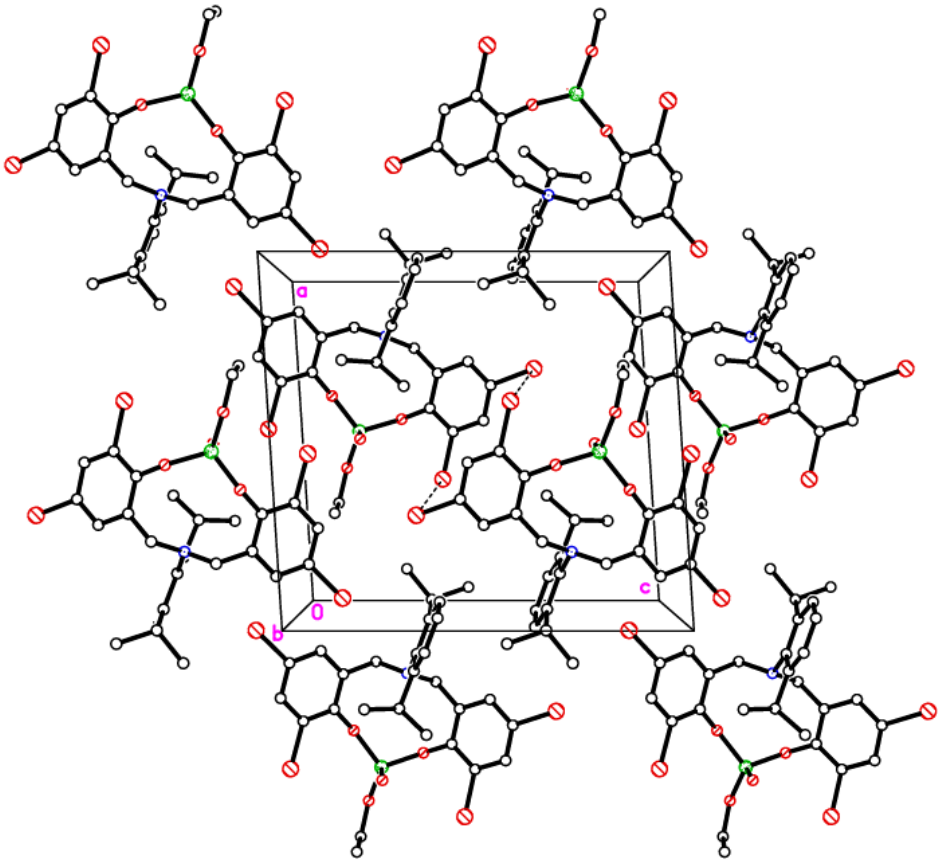

**Figure S3.** Alternative view of the packing of **3** viewed parallel to *b* showing centro-symmetric had-to-tail halogen-bond interactions Br(2)···Br(3') = 3.787 Å.

Discussion of [2,6-*i*Pr$_2$C$_6$H$_3$N=CH-2-(OH)-C$_6$H$_2$Br$_2$-3,5)] (**LH**), [2,6-*i*Pr$_2$C$_6$H$_3$CH$_2$NH-2-(OH)-C$_6$H$_2$Br$_2$-3,5)] (**LH$_2$**) and **[L'H][Et$_3$NH]** (where L'H = {[(2-(O)C$_6$H$_2$Br$_2$-3,5)CH$_2$][(2-(OH)C$_6$H$_2$Br$_2$-3,5)CH$_2$]$_2$(μ-NC$_6$H$_3$-*i*Pr$_2$-2,6)}.

To gain some insight into the formation of the ligand set observed in **2** (and **3**), we reacted equimolar amounts of dibromosalicylic aldehyde with 2,6-diisopropylaniline following the method of Hu *et al*. [S1] After work-up and crystallization, X-ray diffraction (Fig. S4) revealed the product to be the expected Schiff-base compound [2,6-*i*Pr$_2$C$_6$H$_3$N=CH-2-(OH)-C$_6$H$_2$Br$_2$-3,5)] (**LH**). There are two molecules in the asymmetric unit, one substantially 2-fold disordered the other ordered. Each molecule has an intramolecular O–H···N H-bond forming an S(6) ring (Table S1). The twist angle between the two rings in the ordered molecule is 64.41(9)°. Those in the disordered molecule are similar but less reliable due to the disorder. One molecule is modelled as mostly 2-fold disordered with only atoms C(29) > C(31), and C(36) > C(38) common to both

components. The major component occupancy is 52.34(17)%. The ring attached to O(2) has two possible orientations approx. 180° rotated. Alternative views of **LH** are given in Fig. S5.

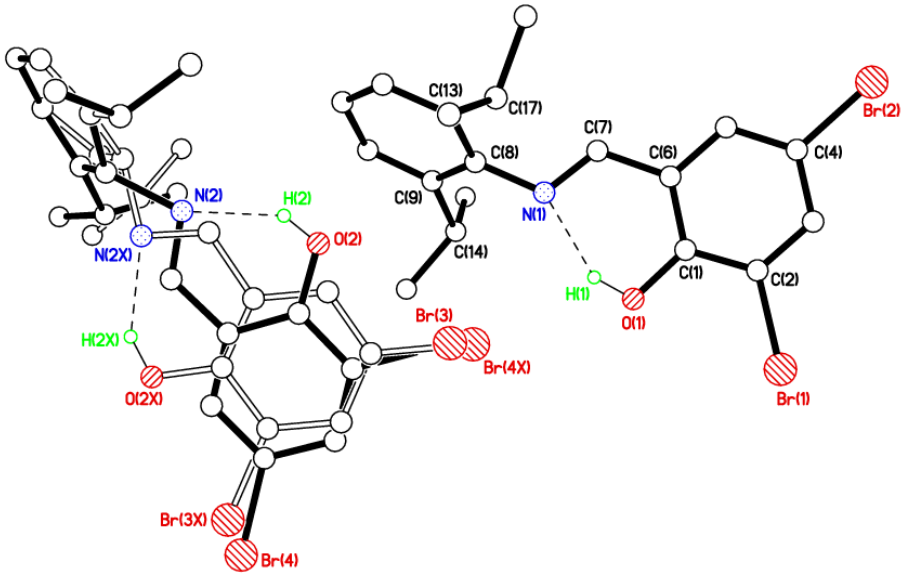


**Figure S4**. Molecular structure of [2,6-*i*Pr$_2$C$_6$H$_3$N=CH-2-(OH)-C$_6$H$_2$Br$_2$-3,5)] (**LH**) with most H atoms omitted for clarity. Selected bond lengths (Å) and angles (°): N(1)–C(7) 1.277(3), N(1)–C(8) 1.427(3), C(6)–C(7) 1.455(3); C(7)–N(1)–C(8) 117.9(2), N(1)–C(7) – C(6) 121.8(2).

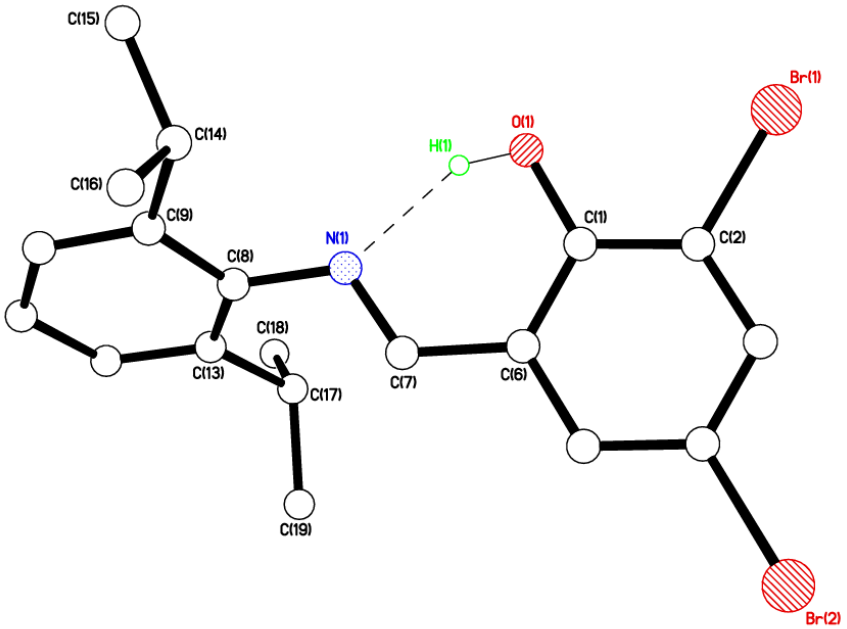
C(15)
C(14)
C(16)
C(9)
C(8)
N(1)
H(1)
O(1)
C(1)
C(2)
Br(1)
C(18)
C(13)
C(17)
C(7)
C(6)
C(19)
Br(2)

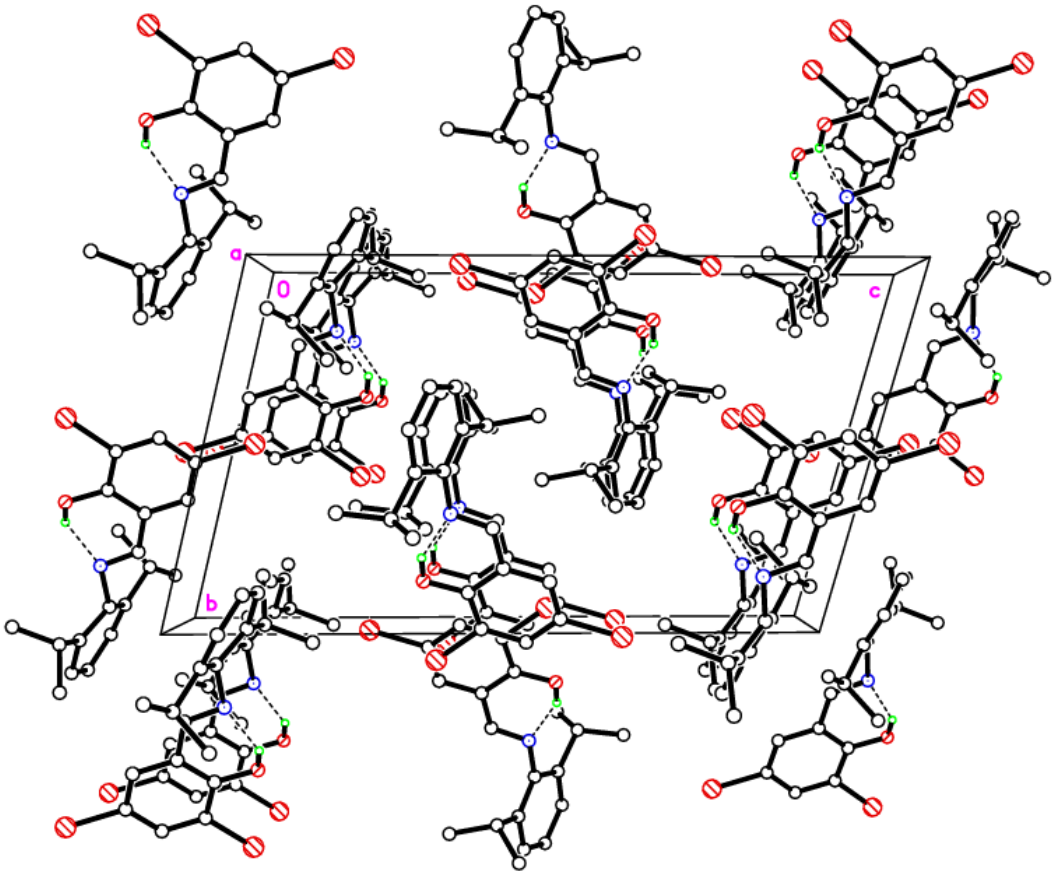
a
0
c
b

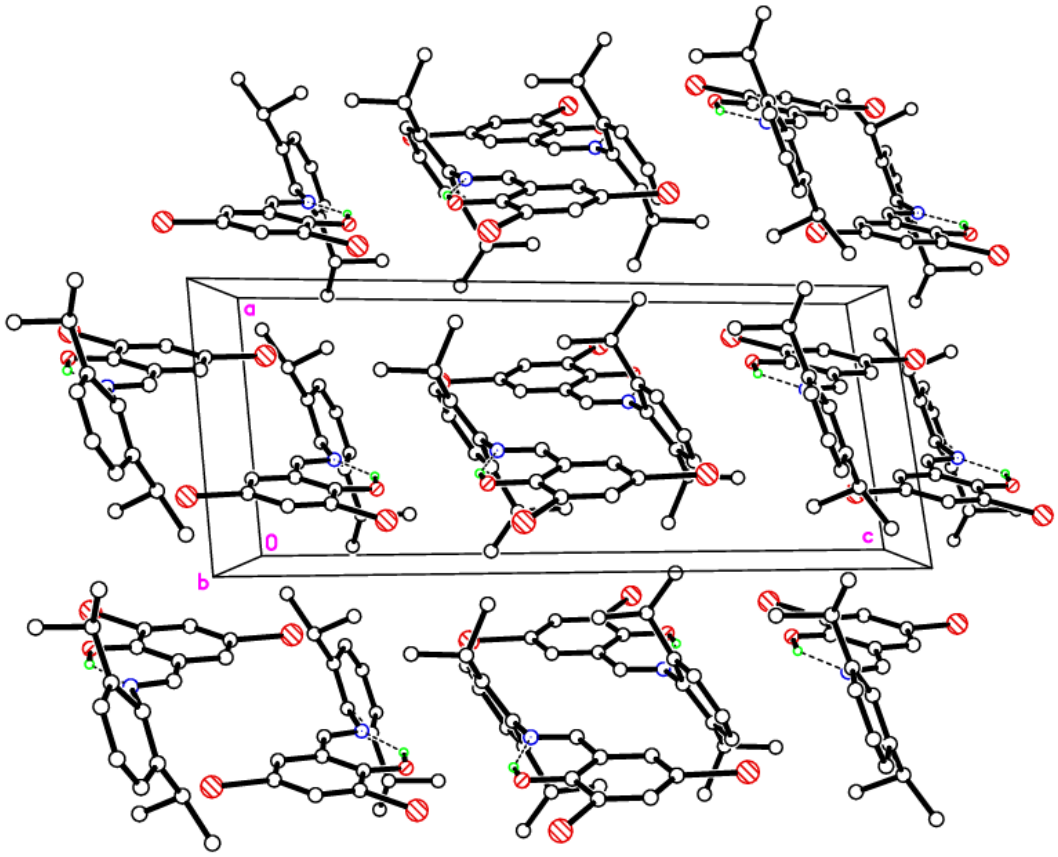


**Figure S5.** Alternative views of **LH** with a single molecule highlighting the intramolecular S(6) H-bonding motif (top) and packing plots viewed parallel to *a* and *b* (middle & bottom).

**Table S1**. Hydrogen bond geometry (Å, º) for **LH**.

| *D*—H···*A* | *D*—H | H···*A* | *D*···*A* | *D*—H···*A* |
|---|---|---|---|---|
| O1—H1···N1 | 0.84 (2) | 1.86 (2) | 2.621 (3) | 150 (3) |
| O1—H1···Br4*X* | 0.84 (2) | 2.97 (3) | 3.399 (2) | 115 (3) |
| O2—H2···N2 | 0.84 | 1.91 | 2.642 (7) | 144 |
| O2*X*—H2*X*···N2*X* | 0.84 | 1.88 | 2.615 (6) | 146 |

The product formed upon reduction of **LH** with $NaBH_4$, **$LH_2$**, was then structurally characterized (Fig. S6). There is one molecule in the asymmetric unit, and one intramolecular O–H···N bond present. The H-bond gives rise to an S(6) ring. Molecules form H-bonded dimers via additional pairs of N–H···O H-bonds and are related by a 2-fold axis. Within this dimer, the brominated rings π···π stack with quite short closest contacts of: C(3)···C(3') = 3.420 Å and C(5)···C(6') = 3.364 Å. Alternative views of **$LH_2$** are given in Fig. S7.

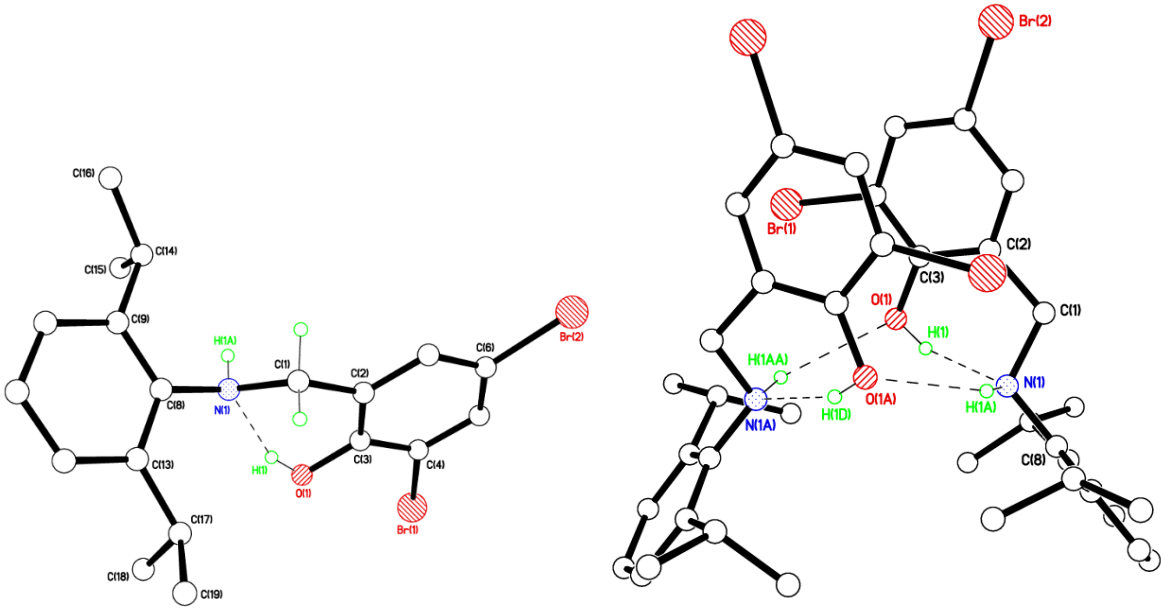


**Figure S6**. Left: Molecular structure of [2,6-*i*Pr$_2$C$_6$H$_3$CH$_2$NH-2-(OH)-C$_6$H$_2$Br$_2$-3,5)] (**LH$_2$**); Right: H-bonded dimers of **LH$_2$**. Most H atoms omitted for clarity. Selected bond lengths (Å) and angles (°): C(1)–N(1) 1.4799(11), N(1)–C(8) 1.4447(11), C(1)–C(2) 1.5121(12); N(1)–C(1)–C(2) 112.38(7), C(1)–N(1)–C(8) 112.99(7).

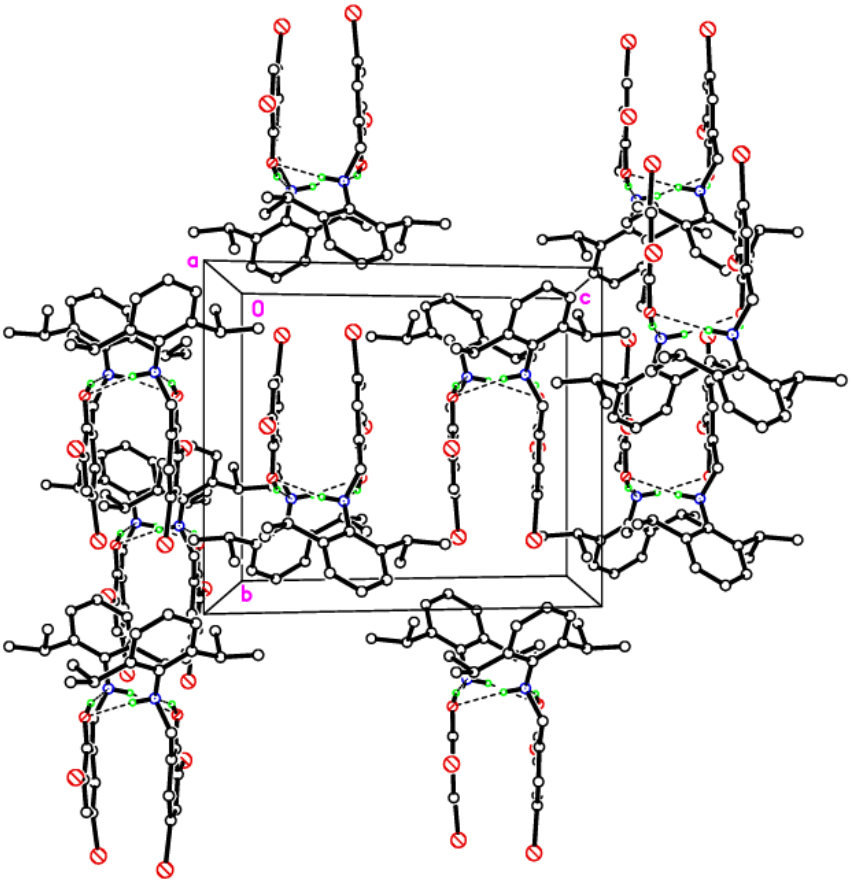
a
0
c
b

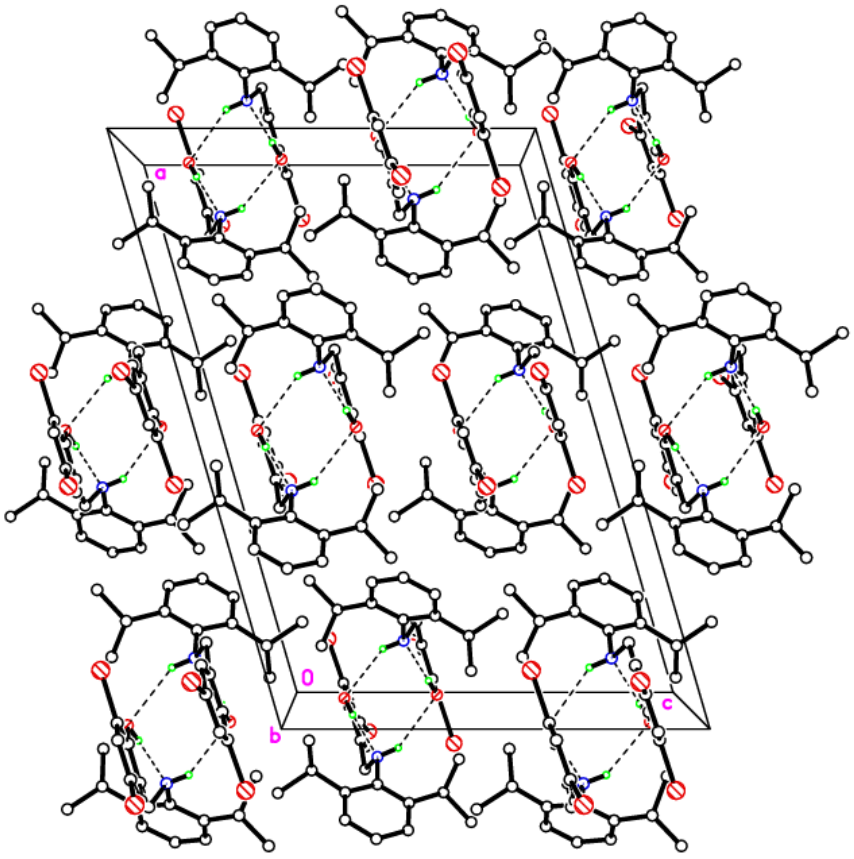
a
0
c
b

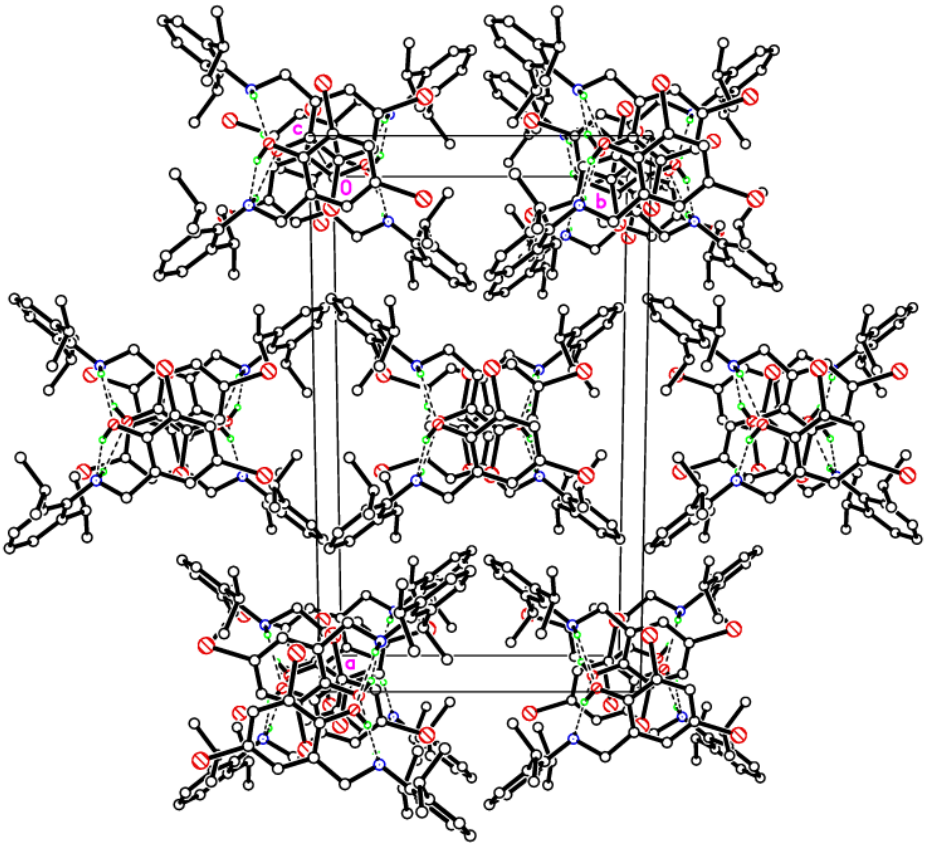

**Figure S7.** Alternative views of the packing of **$LH_2$** viewed parallel to *a*, *b*, and *c* (top, middle & bottom) highlighting pairs of H-bonded molecules and their packing.

**Table S2**. Hydrogen bond geometry (Å, º) for $LH_2$.

| *D*—H···*A* | *D*—H | H···*A* | *D*···*A* | *D*—H···*A* |
|---|---|---|---|---|
| N1—H1*A*···O1$^{i}$ | 0.868 (16) | 2.560 (16) | 3.3399 (11) | 149.9 (13) |
| O1—H1···N1 | 0.817 (17) | 1.878 (18) | 2.6500 (11) | 157.0 (16) |

Symmetry code: (i) -*x*+1, *y*, -*z*+1/2.

Carrying out the above reaction either in the presence of $Et_3N$ or $Et_3N$/2-chloromethylpyridine hydrochloride also yielded [2,6-*i*$Pr_2C_6H_3$CH=N-2-(OH)-$C_6H_2Br_2$-3,5)], and in the latter case some $Et_3NHCl$.

We then reacted the precursor ligands together in equimolar amounts and subsequently subjected the system to sodium borohydride and triethylamine as described previously. Following work-up, pale brown crystals were isolated in low isolated yield (<5%) and were subjected to a structure determination. The molecular structure is shown in Figure S8, with selected bond lengths and

angles given in the caption. In the asymmetric unit, there is one triethylammonium cation & one anion. The anion holds a negative 1– charge (on O(2) due to missing hydrogen) and is paired with triethylammonium ($HNEt_3^+$) to form a salt. Intramolecular, strong, charge-assisted H-bonding is present between O(1)–H(1)···O(2) and N(2)–H(2)···O(2) (see Table S3).

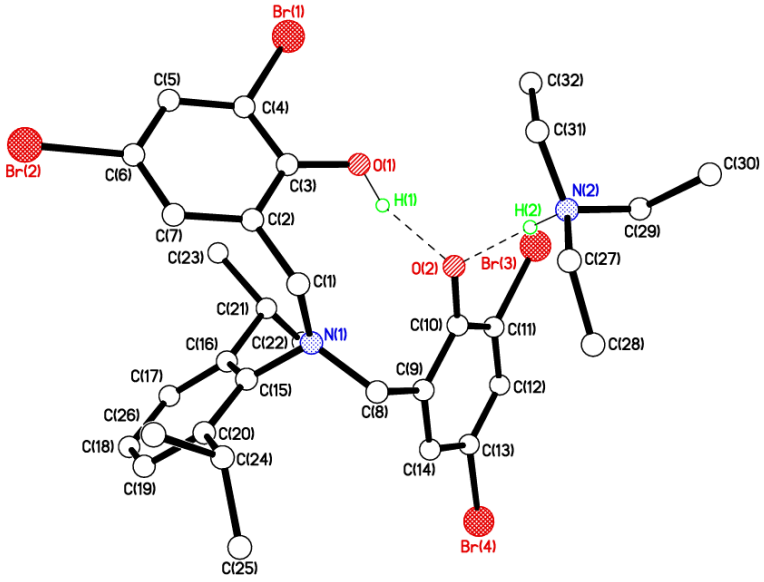


**Figure S8**. Molecular structure of **[L'H][Et$_3$NH]** (where L'H = {[(2-(O)$C_6H_2Br_2$-3,5)$CH_2$][(2-(OH)$C_6H_2Br_2$-3,5)$CH_2$]$_2$(μ-$NC_6H_3$-*i*$Pr_2$-2,6)}. Most H atoms omitted for clarity. Selected bond lengths (Å) and angles (°): N(1)–C(1) 1.455(4), N(1)–C(8) 1.472(4), N(1)–C(15) 1.442(4); C(1)–N(1)–C(8) 116.9(3), C(8)–N(1)–C(15) 115.1(2), N(1)–C(1)–C(2) 112.5(2), N(1)–C(8)–C(9) 111.8(3).

In the packing, there are weak hydrogen bonding interactions between C(31)–H(31A)···Br(3) and C(1)–H(1B)···Br(4) (see Table S3). There are also halogen bonding interactions Br(2)···Br(3) (3.527 Å). A view of the packing is given in Fig. S9.

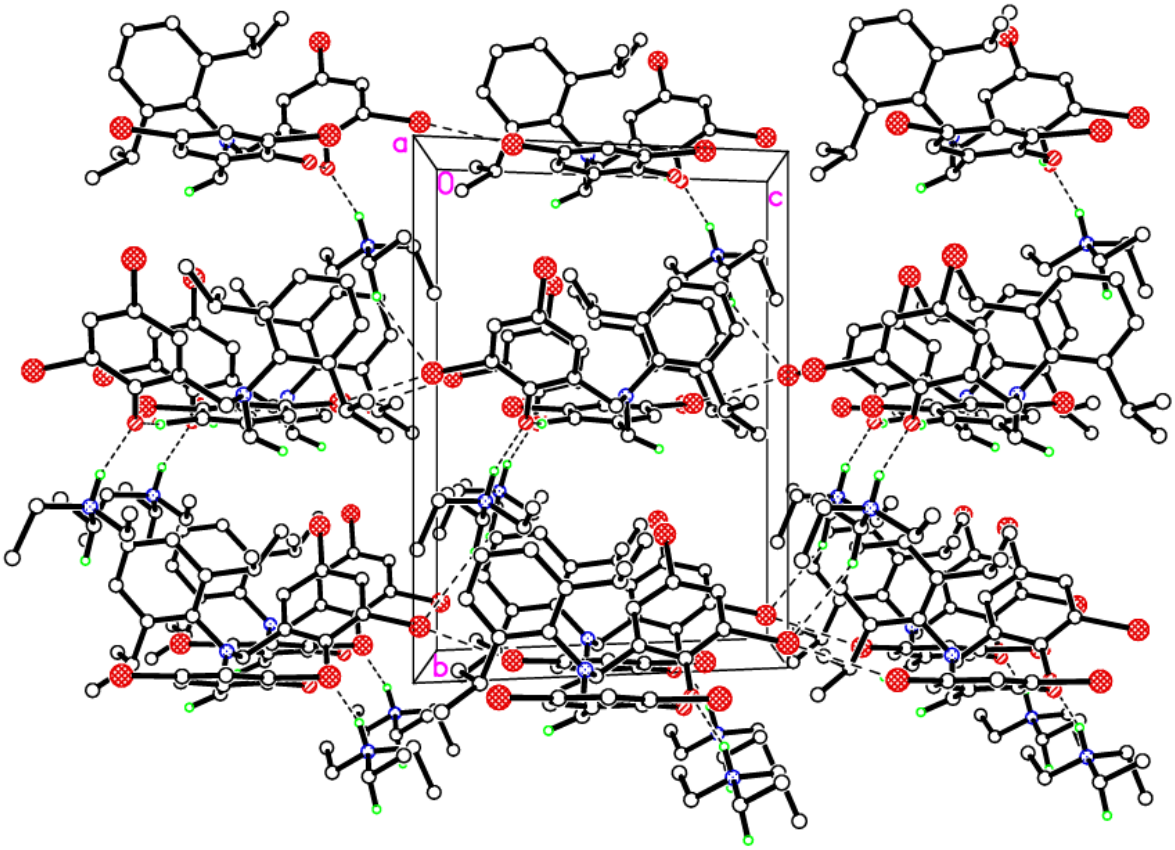
a
0
c
b

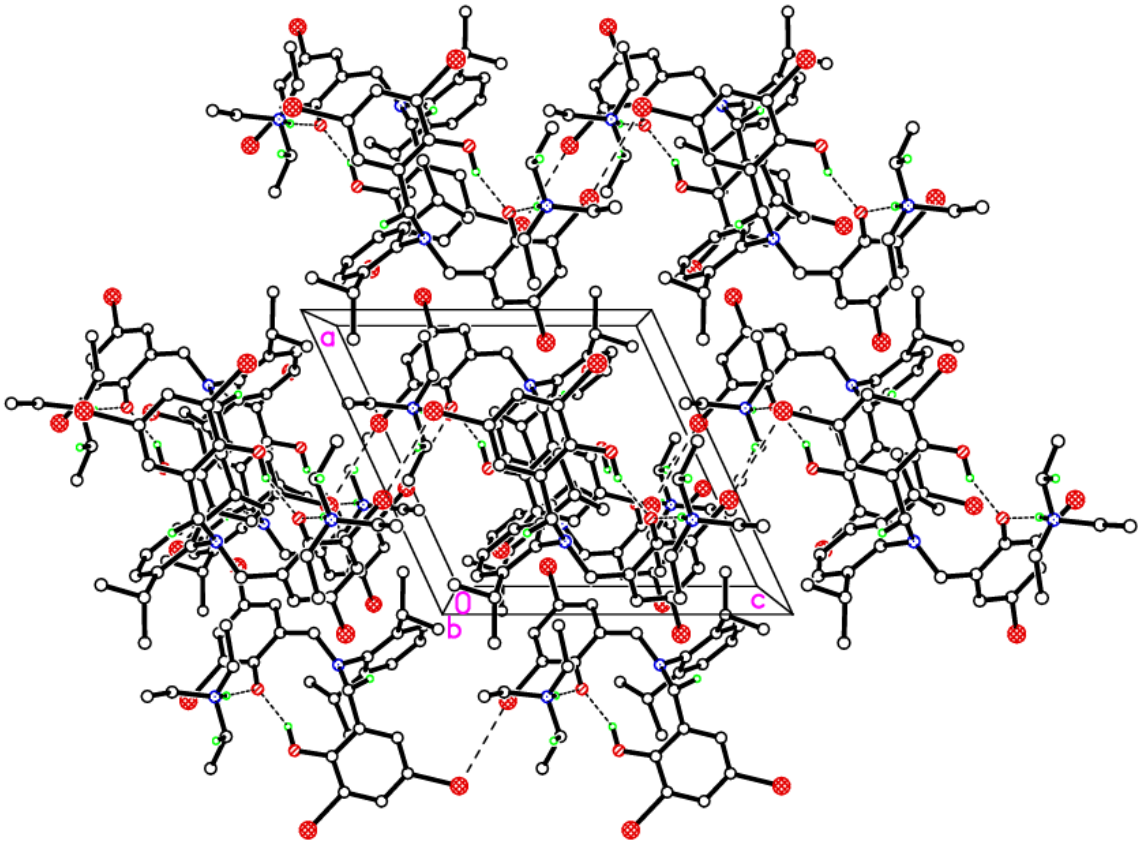
a
0
c
b

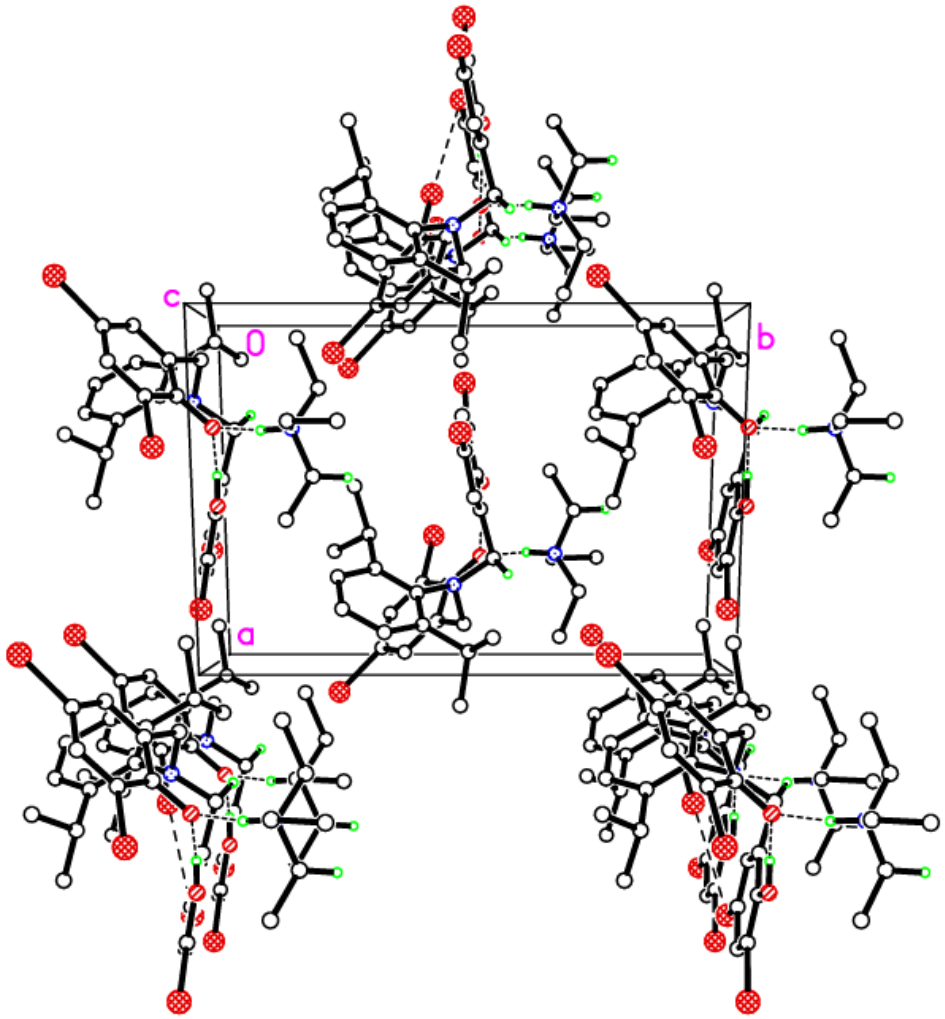


**Figure S9.** Alternative views of the packing of [$Et_3NH$][**L'H**] viewed parallel to *a*, *b*, and *c* (top, middle, & bottom) showing strong cation···anion H-bond interactions, weak H-bonding C(31)–H(31A)···Br(3) = 3.02 and C(1)–H(1B)···Br(4) = 3.08 Å, and halogen-bonding Br(2)···Br(3') =3.527 Å.

**Table S3**. *Hydrogen-bond geometry (Å, º) for* **[L'H][$Et_3NH$]**

| *D*—H···*A* | *D*—H | H···*A* | *D*···*A* | *D*—H···*A* |
|---|---|---|---|---|
| C1—H1*B*···Br4$^{i}$ | 0.99 | 3.08 | 3.592 (3) | 114 |
| O1—H1···O2 | 0.88 (5) | 1.73 (5) | 2.553 (3) | 156 (4) |
| N2—H2···O2 | 0.92 (5) | 1.69 (5) | 2.581 (4) | 164 (5) |
| C29—H29*A*···Br3 | 0.99 | 3.12 | 3.698 (4) | 118 |
| C31—H31*A*···Br3$^{ii}$ | 0.99 | 3.02 | 3.874 (4) | 145 |

Symmetry codes: (i) -*x*+2, *y*+1/2, -*z*+1; (ii) -*x*+1, *y*+1/2, -*z*.

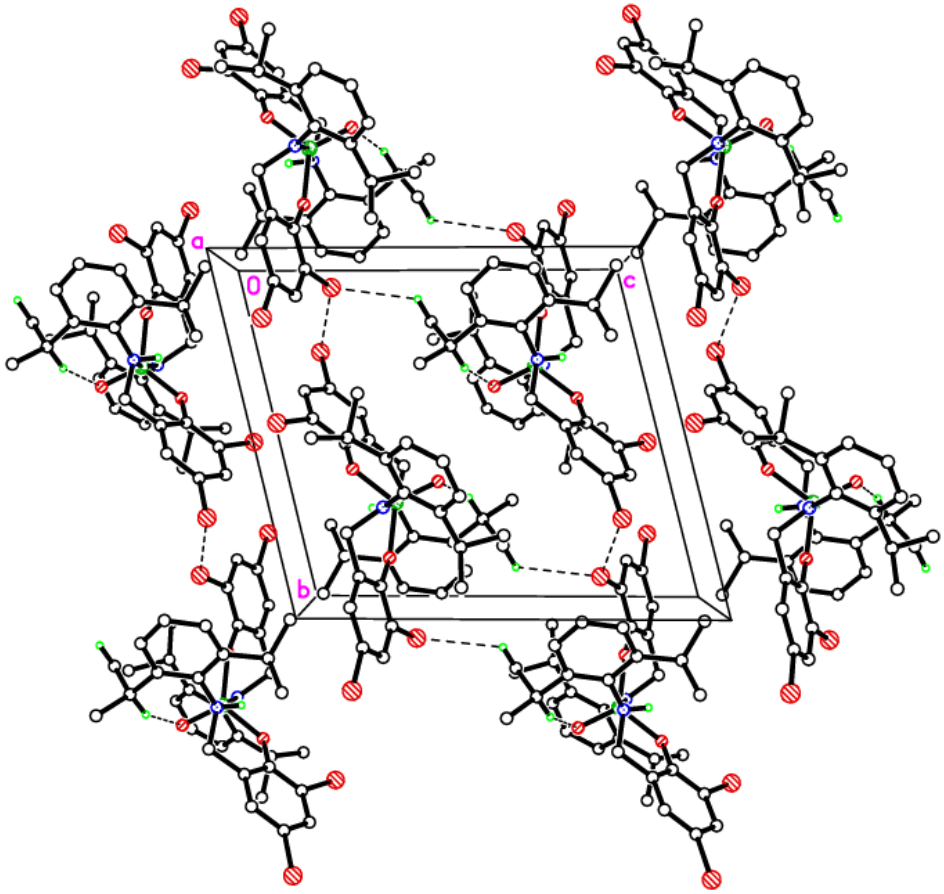
a
0
c
b

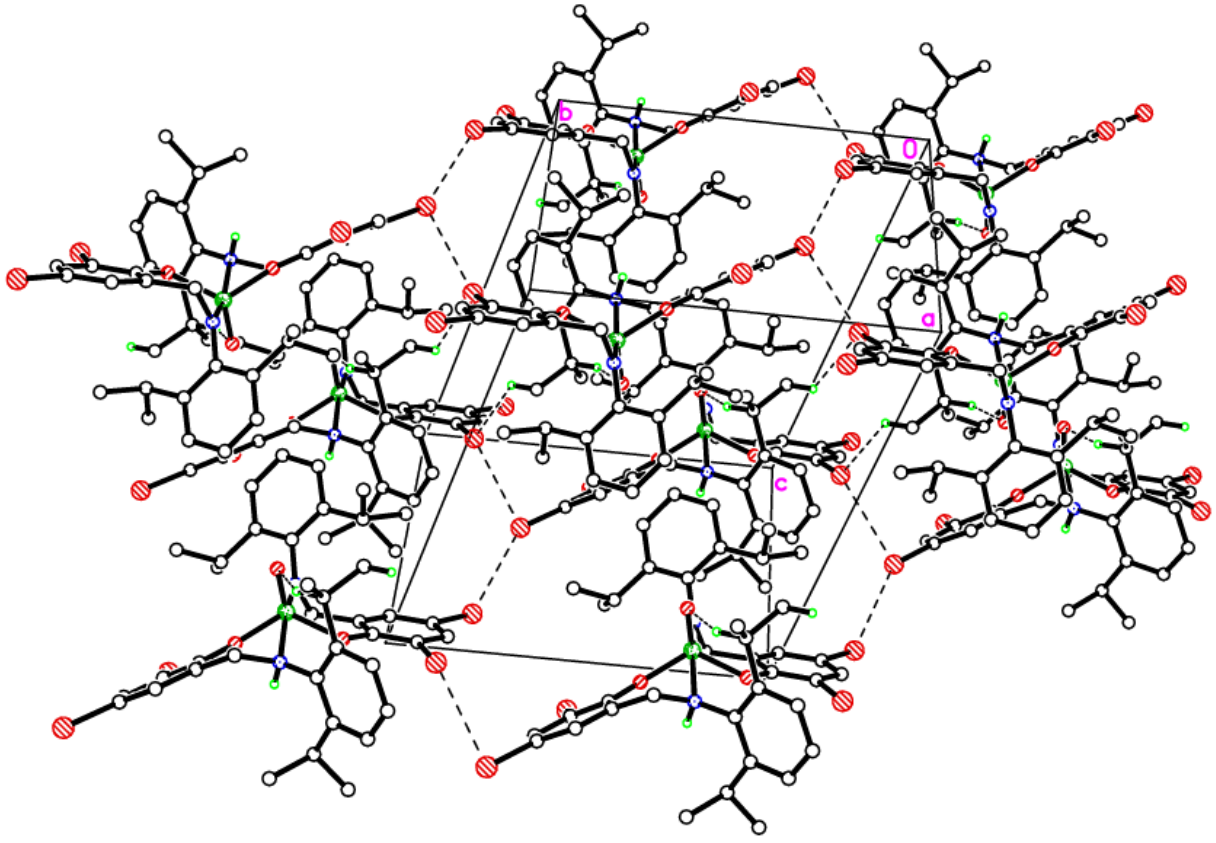
b
0
a
c

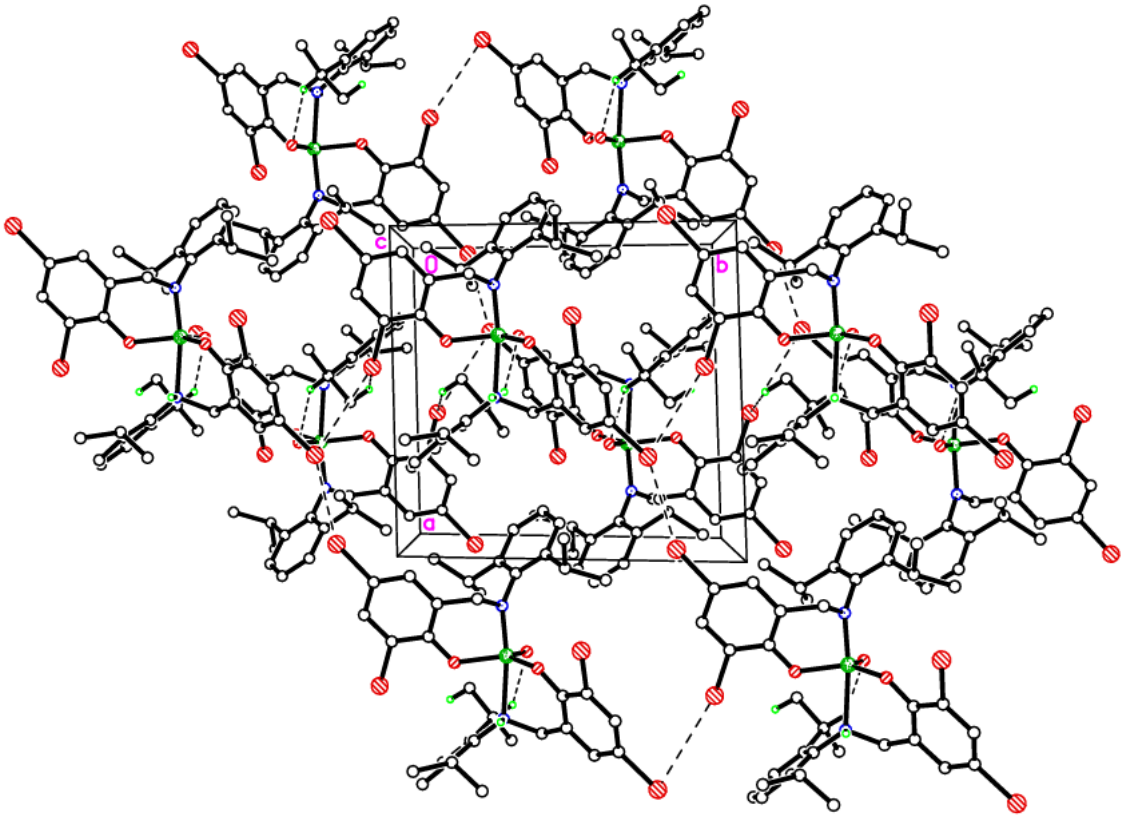


**Figure S10.** Alternative views of the packing of **4** viewed parallel to *a* (top), off-axis (middle), and *c* (bottom) showing weak H-bonds C(15)–H(15A)···Br(3') = 3.032 Å and two unique halogen bonds Br(3)···Br(2') = 3.830 and Br(2)···Br(4) = 3.630 Å forming sheets in the *a*/*b* plane.

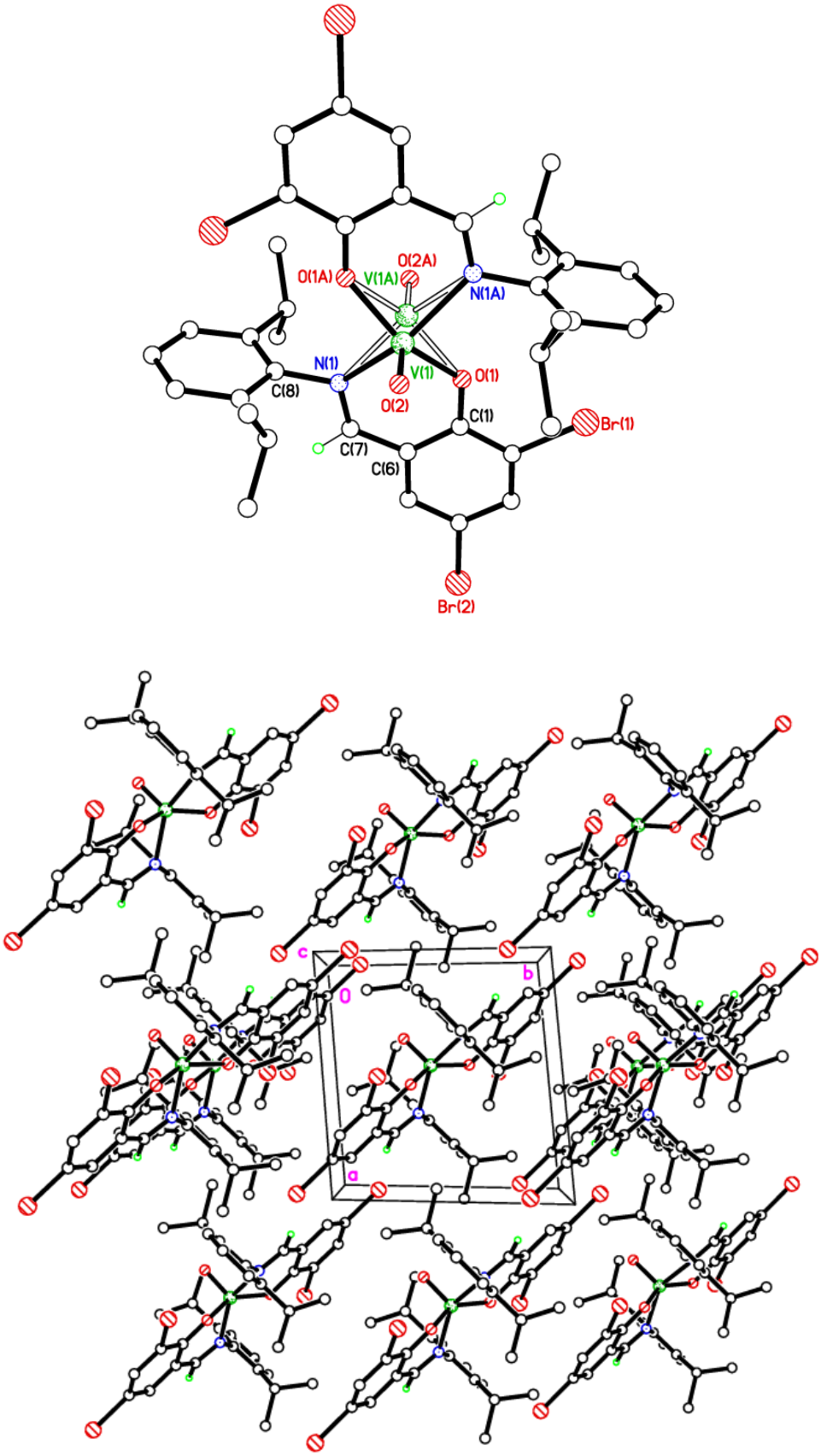


**Figure S11.** Alternative views of **5** showing 50/50 V=O disorder (top) and packing viewed parallel to c (bottom).

Discussion of **5** *vs* **6**

In **6**, V(1) lies 0.464(3) Å out of the O(1)/C(1)/C(6)/C(7)/N(1) plane. In **5** the V(1) atom was 0.533(4) Å out of the plane, so slightly more than in **6**. The ring C(8) > C(13) is almost perpendicular to the C(1) > C(6) plane at 87.84(6)°. Thus, the individual molecules are very similar in **5** and **6**. As in **5**, the V=O moiety is disordered exactly 50/50 above and below the $O_2N_2$ plane. In the structure of **6** the dominant feature is centrosymmetric, head-to-tail Br(2)···O(2') interactions at 3.342 Å (Fig. S12), which are not seen in the packing of **5**. However, these cannot happen all of the time since the O(2') atom would only be there half the time. Thus, these interactions must occur randomly, half the time, along the *b* axis, forming weakly bound chains. Unlike in **5**, H(7) does not form a weak interaction with any other atom. Alternative views of **6** are given in Fig. S13.

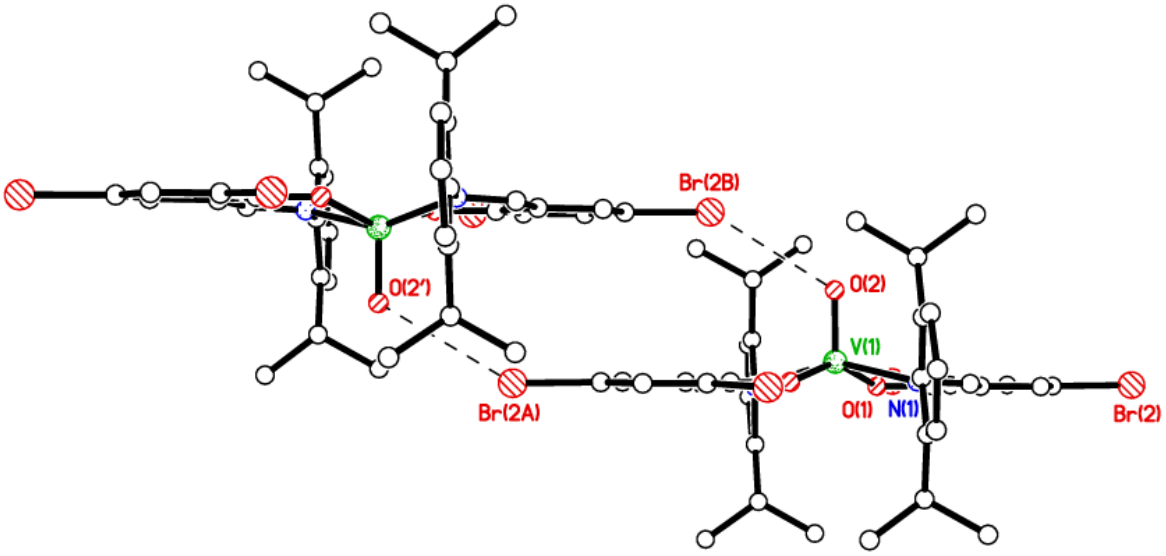


**Figure S12**. Head-to-tail Br(2)···O(2') interactions in **6** which occur 50% of the time. H atoms omitted for clarity.

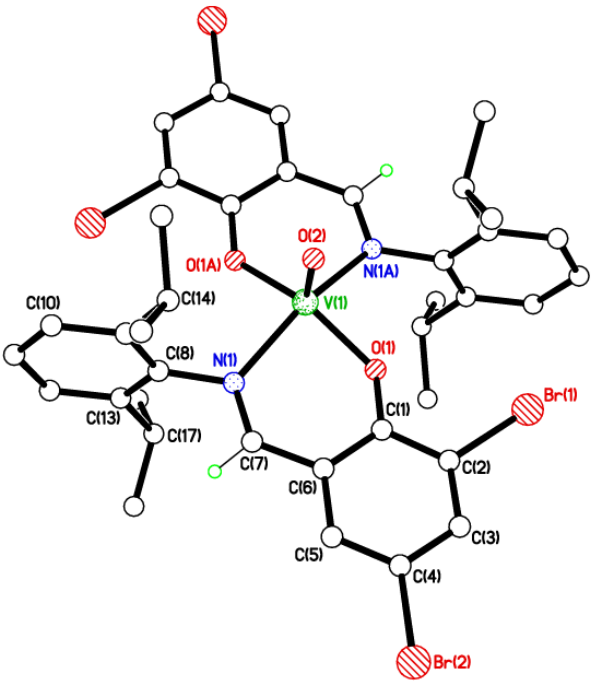
O(2)
O(1A)
N(1A)
C(10)
C(14)
V(1)
C(8)
N(1)
O(1)
Br(1)
C(13)
C(17)
C(1)
C(7)
C(2)
C(6)
C(3)
C(5)
C(4)
Br(2)

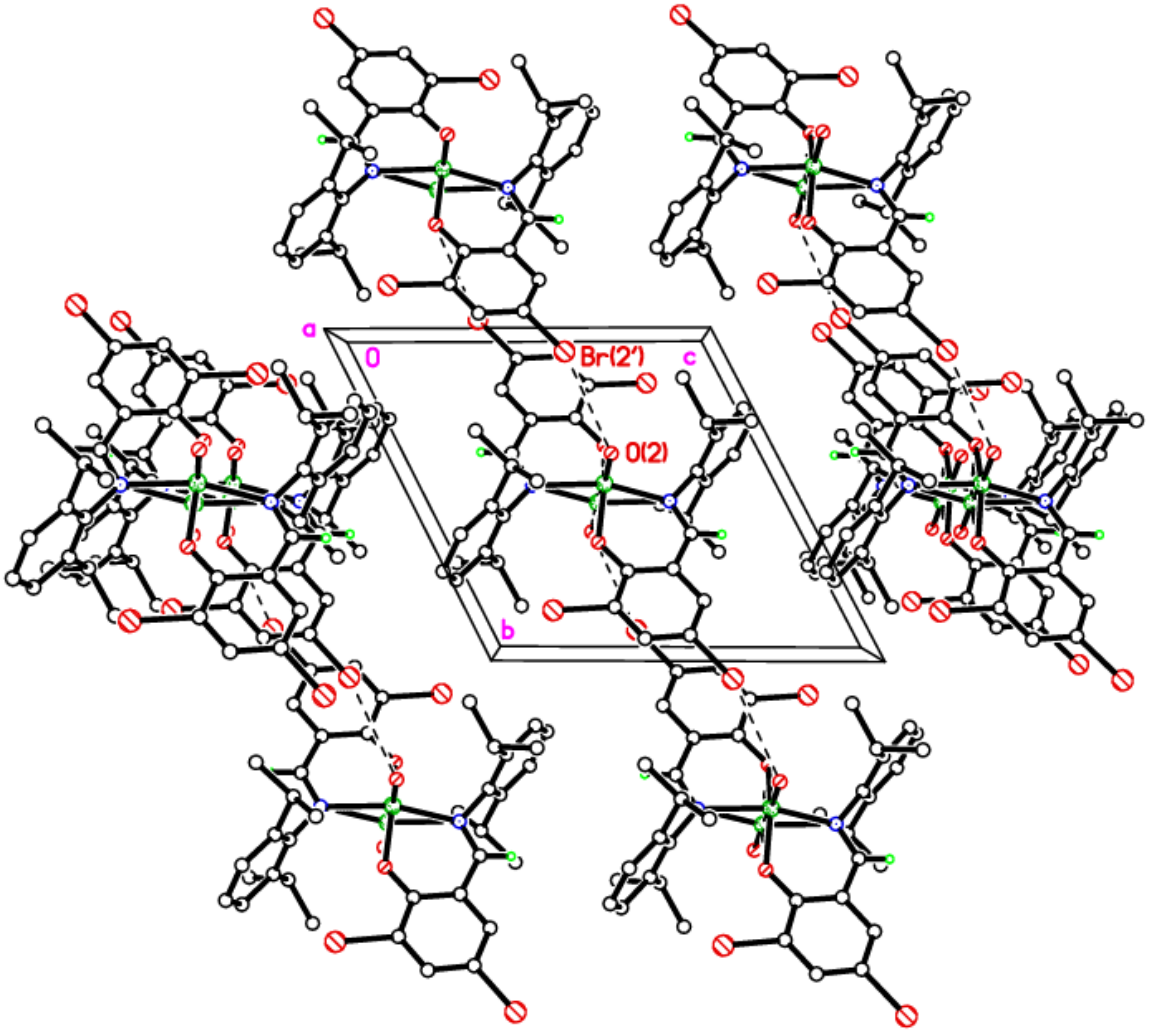
a
0
Br(2')
c
O(2)
b

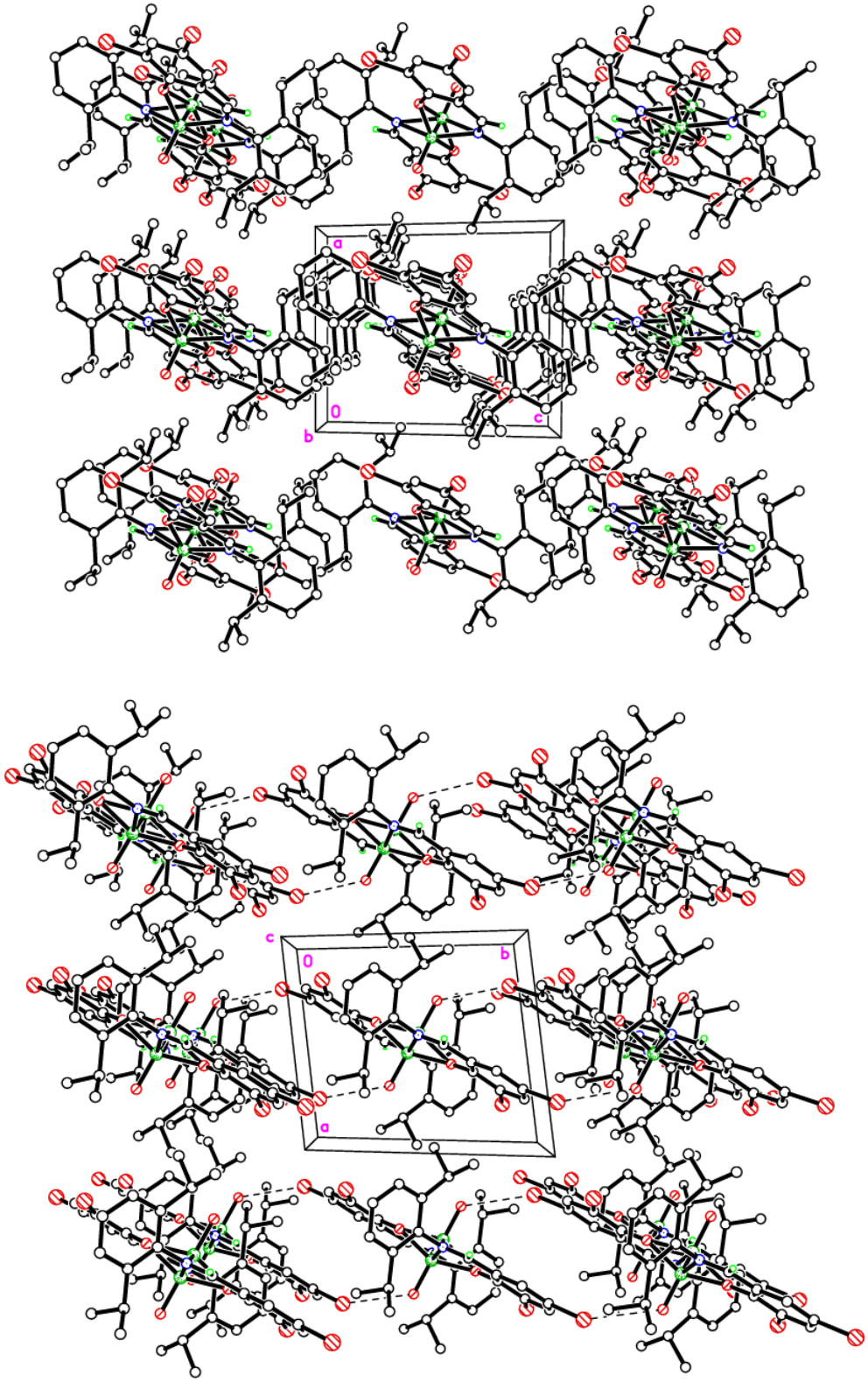


**Figure S13.** Alternative views of **6** showing a single molecule with the 50/50 V=O disorder omitted for clarity (top), and packing plots viewed parallel to *a*, *b*, and *c* showing centro-symmetric, head-to-tail halogen to oxygen interactions Br(2)···O(2') = 3.342 Å.

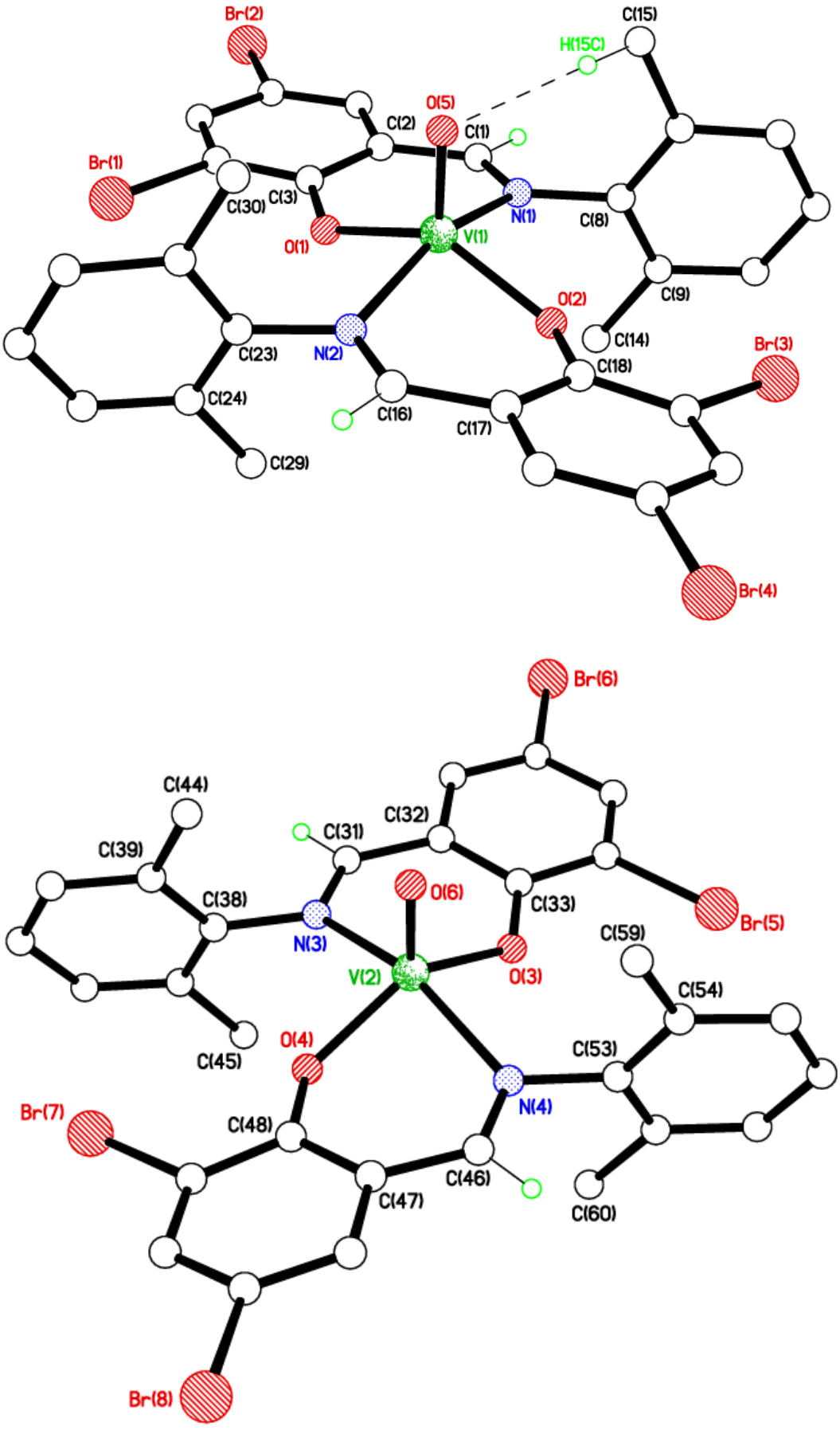
Br(2)
C(15)
H(15C)
O(5)
C(2)
C(1)
Br(1)
C(30)
C(3)
N(1)
C(8)
O(1)
V(1)
O(2)
C(9)
C(14)
C(23)
N(2)
Br(3)
C(18)
C(24)
C(16)
C(17)
C(29)
Br(4)
Br(6)
C(44)
C(32)
C(31)
C(39)
C(38)
O(6)
C(33)
Br(5)
N(3)
C(59)
V(2)
O(3)
C(54)
O(4)
C(45)
C(53)
N(4)
Br(7)
C(48)
C(46)
C(47)
C(60)
Br(8)

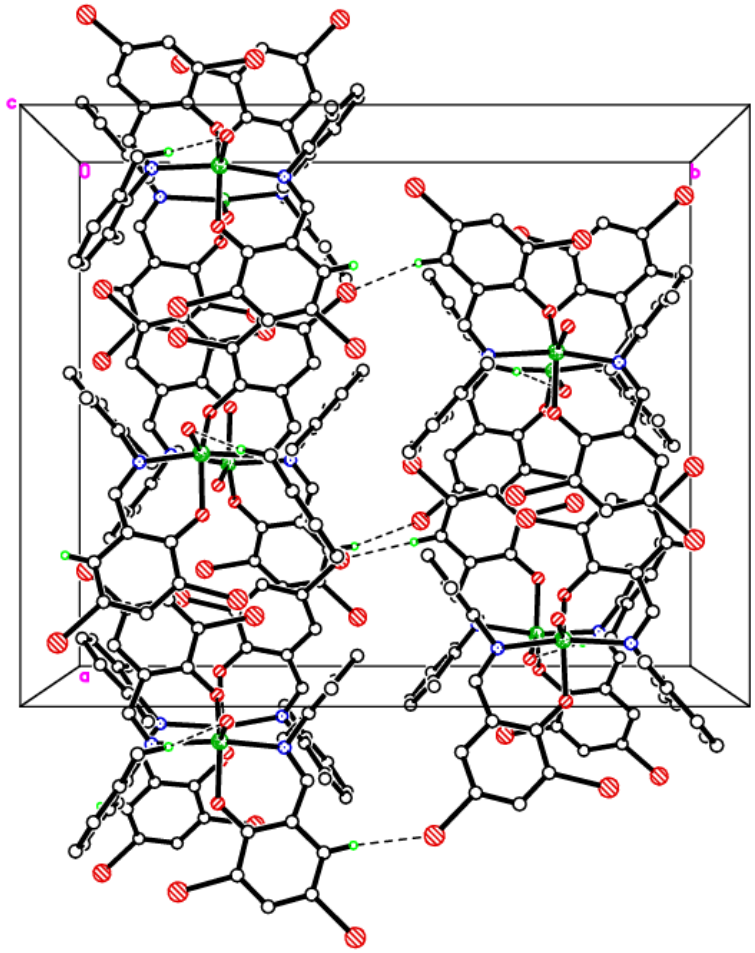

**Figure S14.** Alternative views of **7** showing both unique molecules with minor V=O disorder components omitted for clarity (top & middle), and the packing viewed parallel to *c* showing weak H-bond interactions between stack of molecules, C(22)–H(22)···Br(8') = 3.00 Å and C(37)–H(37)···Br(2') = 3.01 Å.

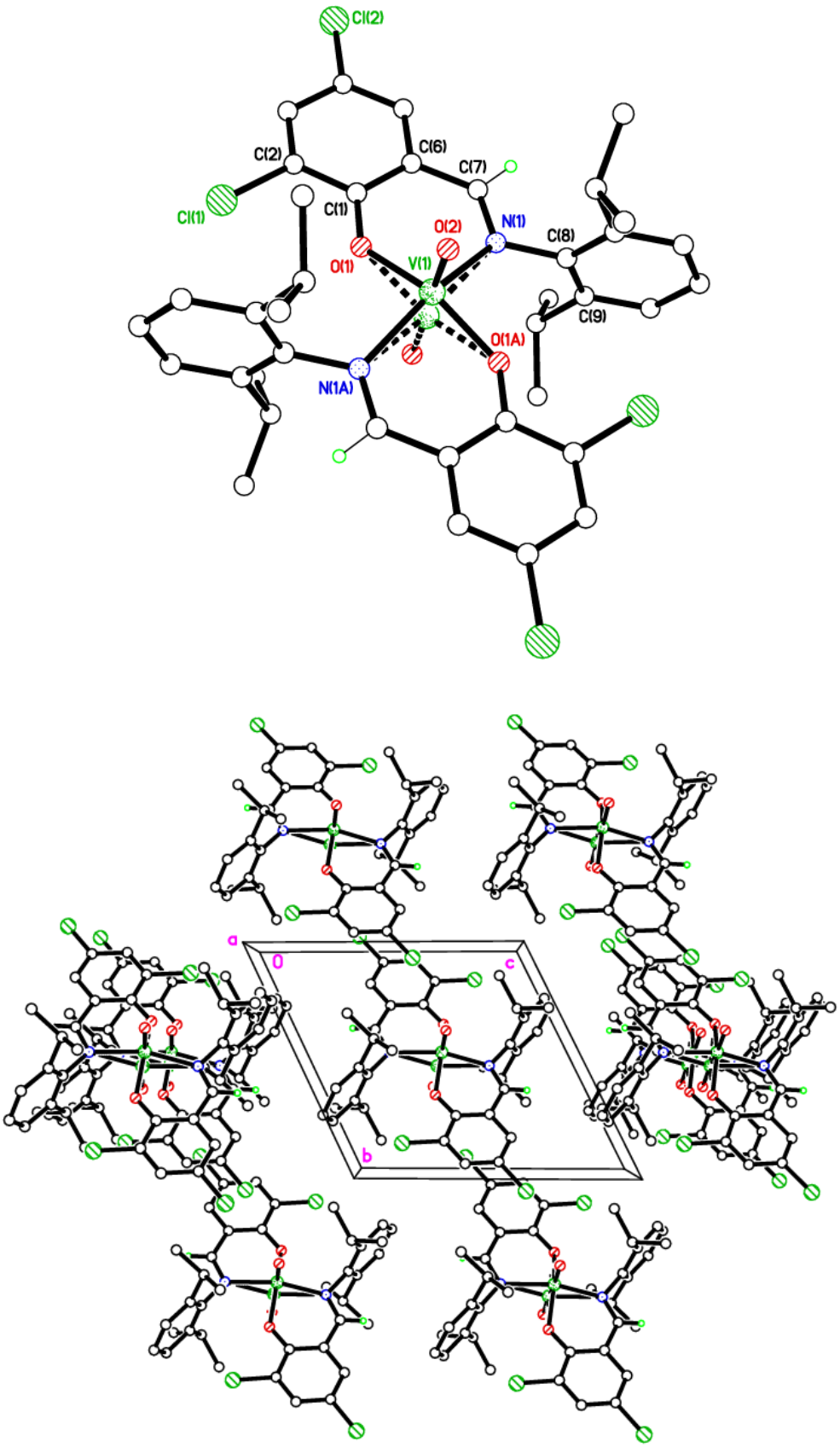


**Figure S15.** Alternative views of **8** (triclinic polymorph) showing V=O 50/50 disorder (top) and packing viewed parallel to *a*.

Discussion of **9**.

The molecular structure of **9** is shown in Fig. S16, with selected bond lengths and angles given in the caption. There is one complex molecule is the asymmetric unit. The V(IV) centre has $\tau = 0.16$, so the geometry is closest to square-based pyramidal.

In the packing, there are some quite off-set π···π interactions between symmetry-related aromatic rings including C(10) > C(12), with closest contact of *ca*. 3.54 Å. The closest halogen-halogen {Cl(3)···Cl(4')} interactions are at 3.641 Å. For an alternative view of the packing in **9**, see Fig. S17.

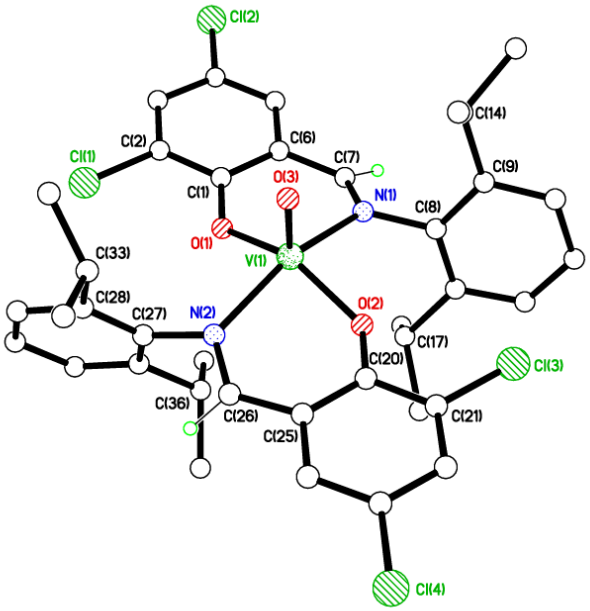


**Figure S16**. View of the molecular structure of **9** with most H atoms omitted for clarity. Selected bond lengths (Å) and angles (°): V(1)–O(1) 1.9120(14), V(1)–O(2) 1.8974(15), V(1)–O(3) 1.5880(17), V(1)–N(1) 2.1472(15), V(1)–N(2) 2.1212(15); O(1)–V(1)–O(2) 145.38(9), N(1)–V(1)–N(2) 154.83(6).

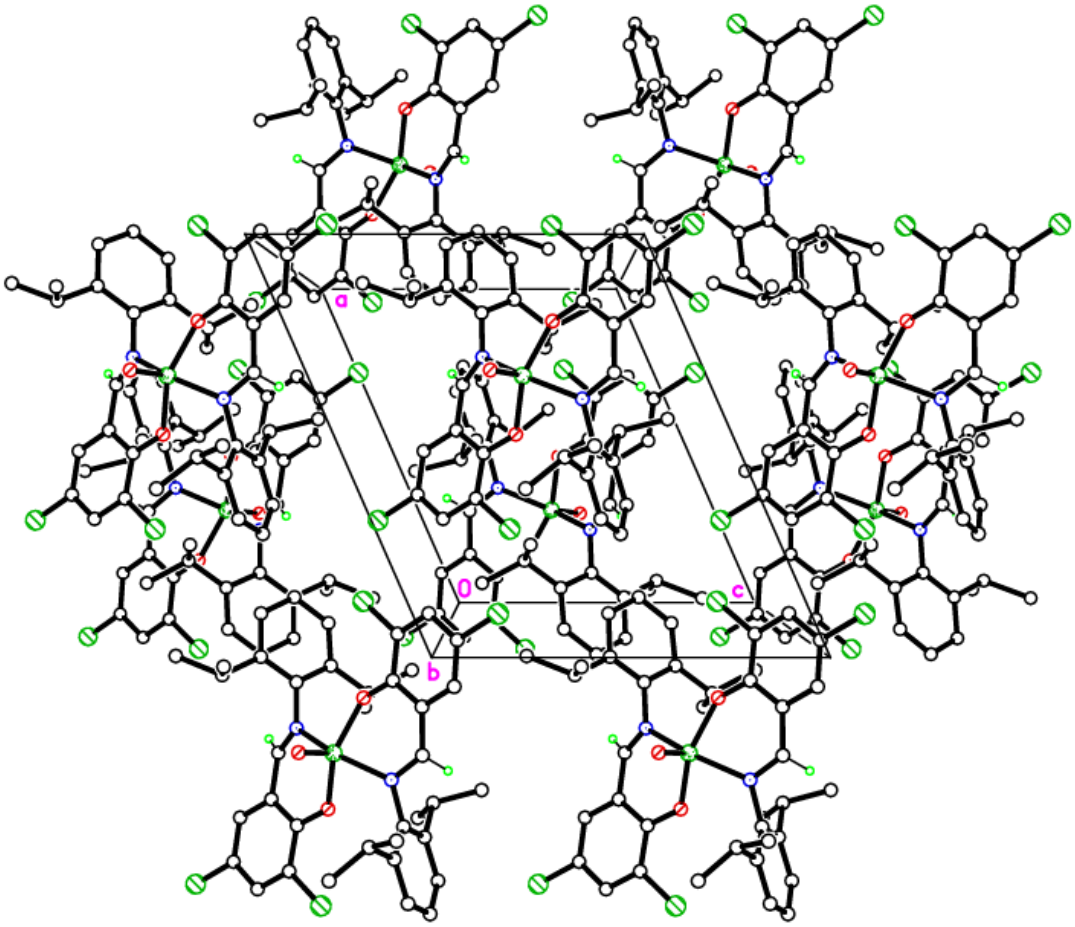


**Figure S17.** Alternative view of the packing of **9** (monoclinic polymorph) viewed parallel to *b*.

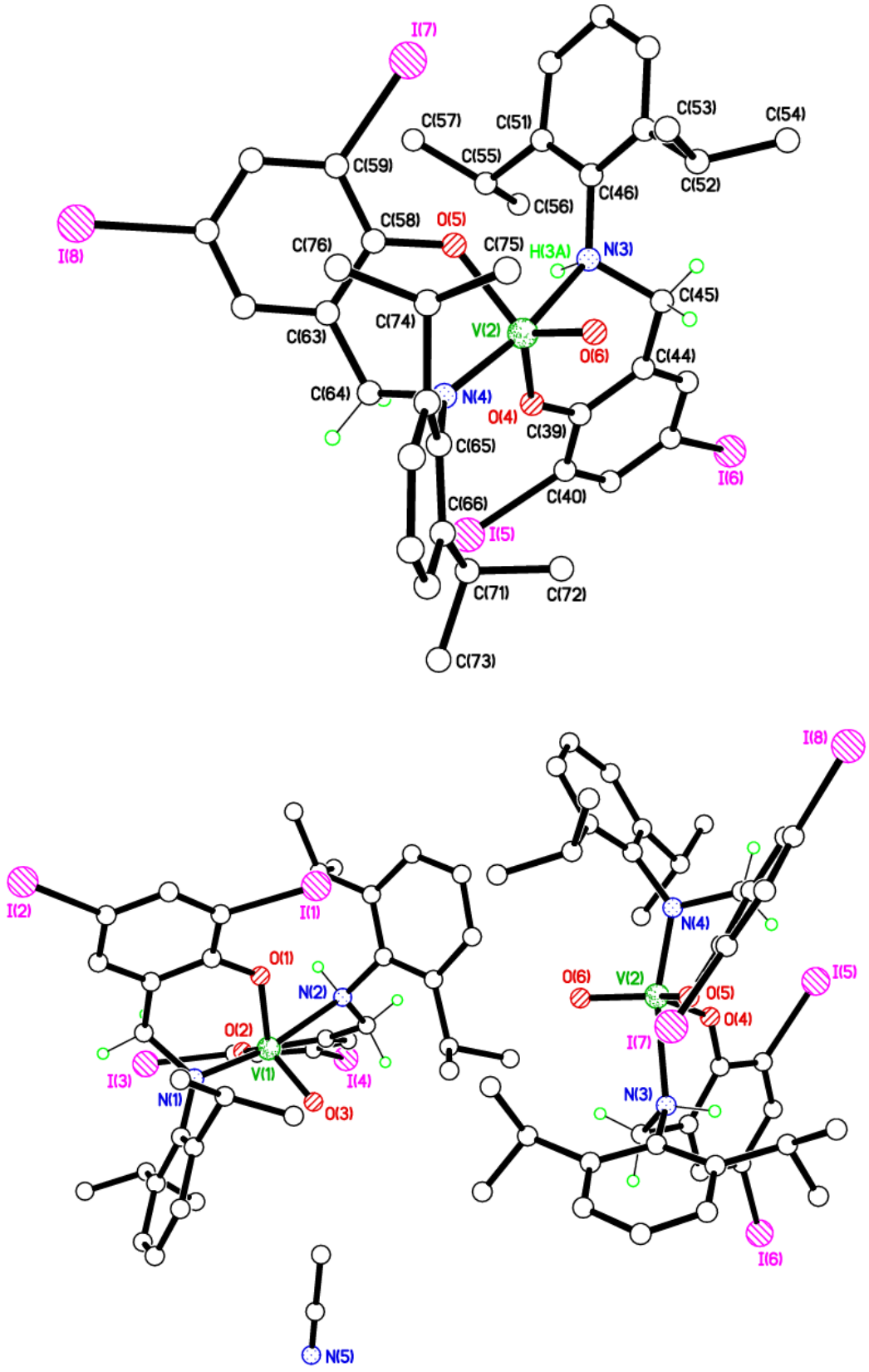


**Figure S18.** Alternative views of the packing of **10** showing the second unique molecule (top) and the full asymmetric unit (bottom).

## Ring opening polymerization

### *ε-Caprolactone*

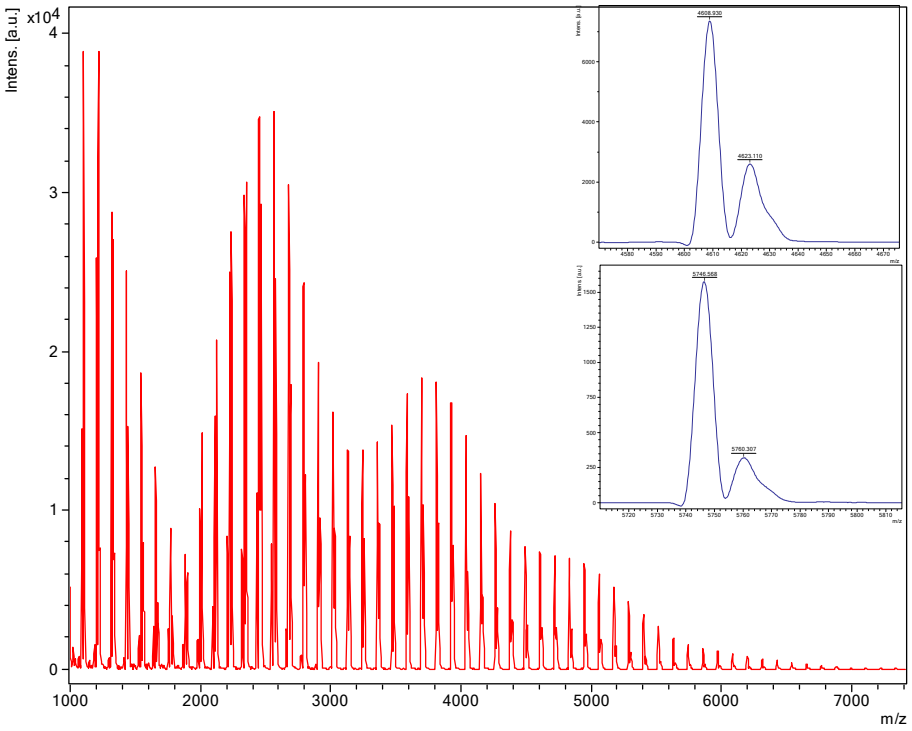


**Figure S19.** MALDI-ToF of PCL using **8** in toluene at 130 °C under air (entry 12, table 3). Present are chain polymers of the type H-PCL-OH, $Na^+$ [M = 17 (OH) + 1(H) + n × 114.14 (CL) + 22.99 ($Na^+$)] (e.g. n = 40 calculated peak 4606.6; observed peak 4608.9; for n = 50: calculated peak 5748.0; observed peak 5746.3).

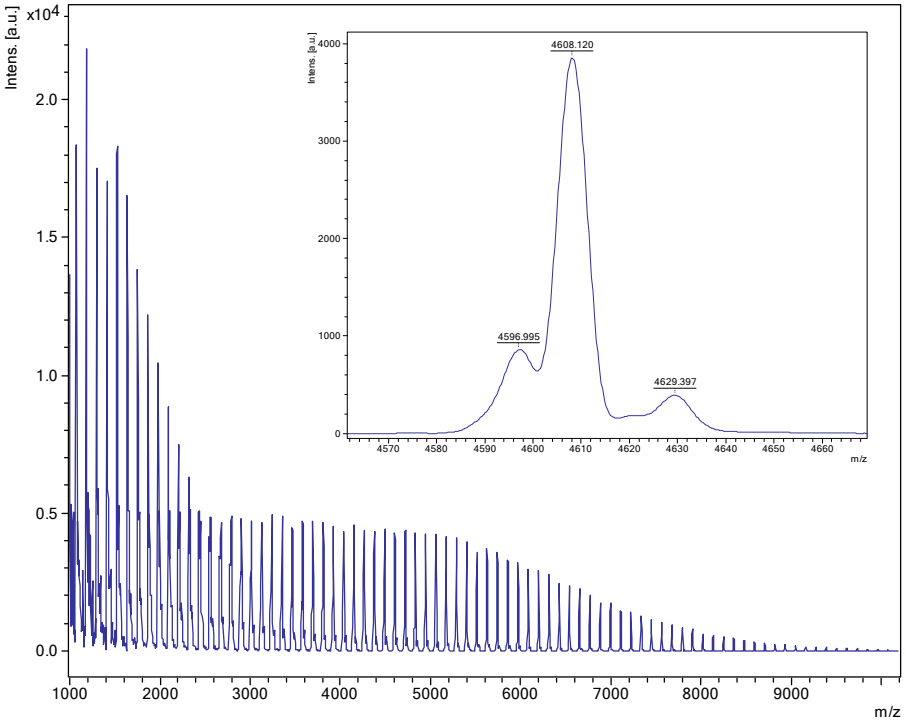

**Figure S20.** MALDI-ToF spectra of PCL using **10** in toluene at 130 °C under air in the presence of BnOH (entry 21, table 3). Present are chain polymers of the type H-PCL-OH, $Na^+$ [M = 17 (OH) + 1(H) + n × 114.14 (CL) + 22.99 ($Na^+$)] (e.g. for n = 20: calculated peak 2323.8; observed peak 2321.3; n = 40 calculated peak 4606.6; observed peak 4608.2).

**Kinetic runs for ε-CL**

No 2 VO(OiPr)

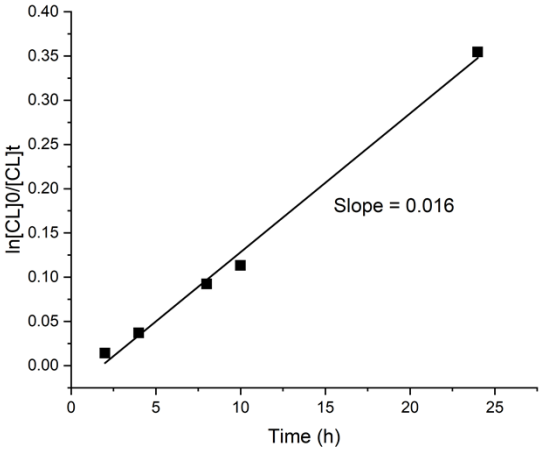


**Figure S21**. Kinetic run for compound **2** with ε-CL.

**OEt No. 3**

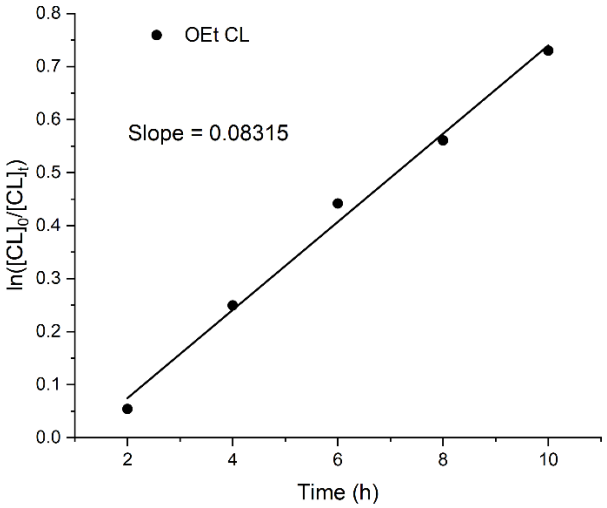

**Figure S22**. Kinetic run for compound **3** with ε-CL.

Njc5

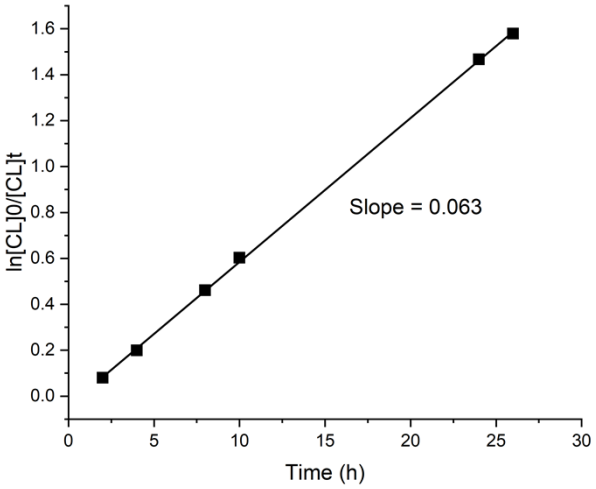


**Figure S23**. Kinetic run for compound **5** with ε-CL.

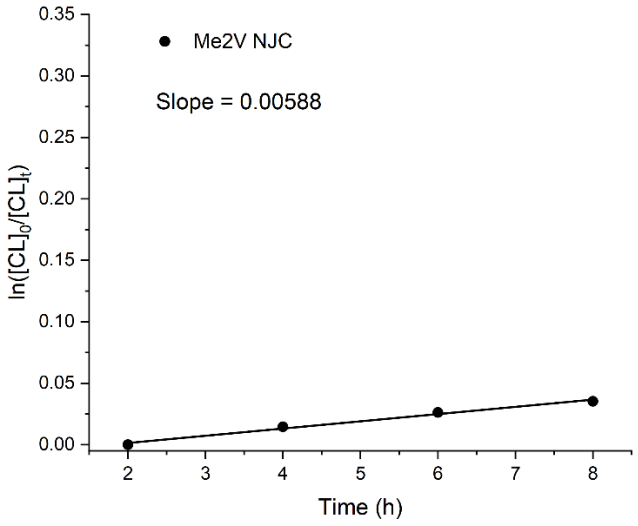


**Figure S24**. Kinetic run for compound **7** with ε-CL.

3,5-dichloro complex:

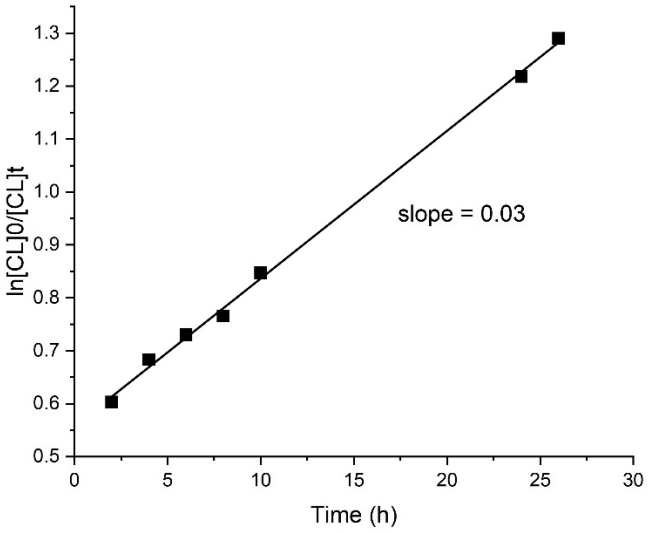


**Figure S25**. Kinetic run for compound **8** with ε-CL.

3,5-diiodo complex:

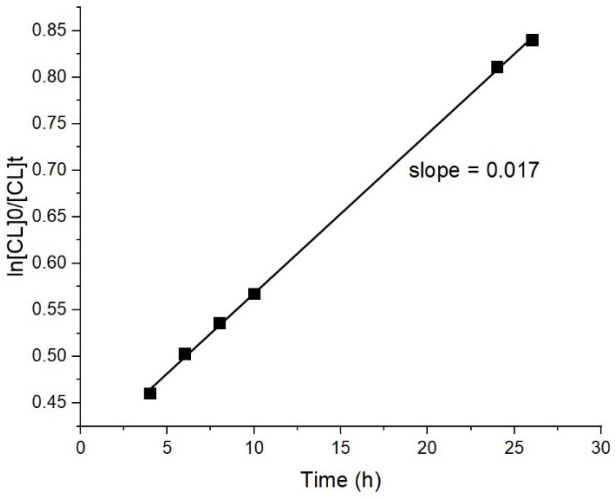


**Figure S26**. Kinetic run for compound **10** with ε-CL.

## GPC traces for PCL

Cl2V tol air CL

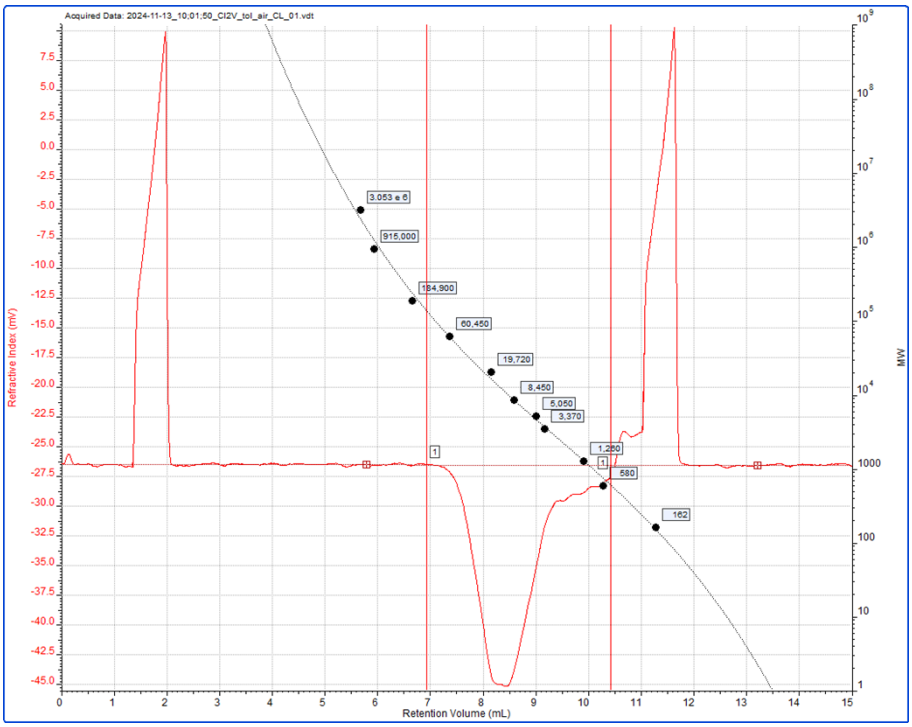
Acquired Data: 2024-11-13_10;01;50_CI2V_tol_air_CL_01.vdt
Refractive Index (mV)
MW
Retention Volume (mL)
3.053 e 6
915,000
184,900
60,450
19,720
8,450
5,050
3,370
1,260
580
162

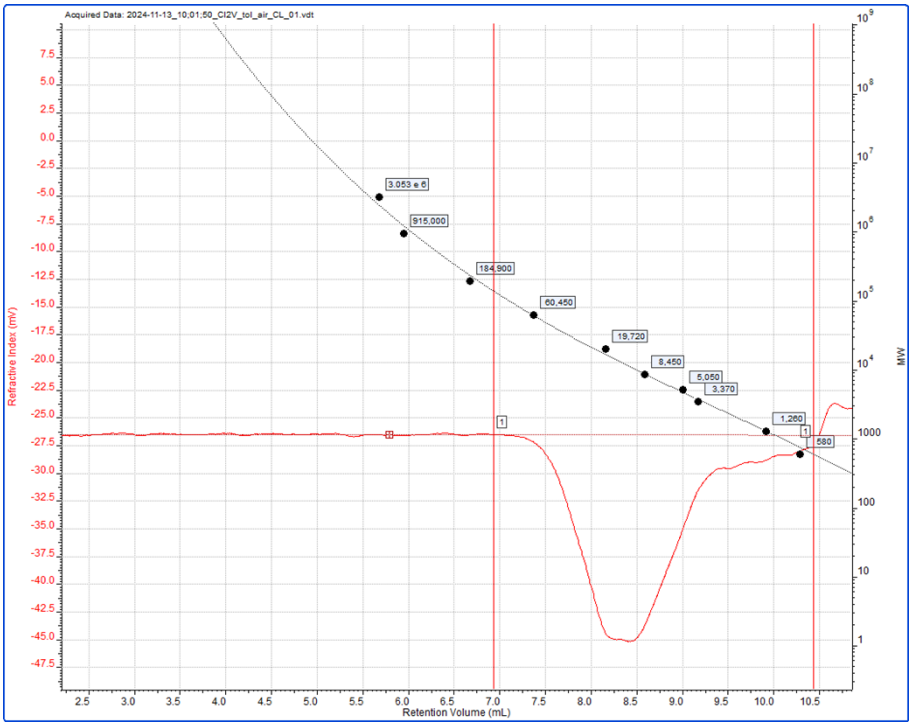
Acquired Data: 2024-11-13_10;01;50_CI2V_tol_air_CL_01.vdt
Refractive Index (mV)
MW
Retention Volume (mL)
3.053 e 6
915,000
184,900
60,450
19,720
8,450
5,050
3,370
1,260
580

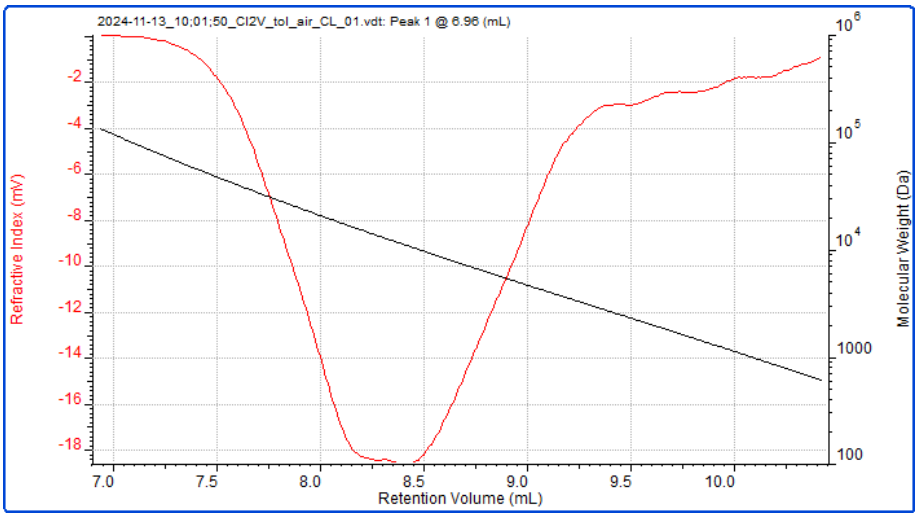


**Figure S27.** GPC trace for PCL from entry 12, Table 1.

Peak 1

Ret Vol (mL) 6.964

*M*n (Da) 5,904

*M*w (Da) 12,579

*M*z (Da) 19,882

*M*p (Da) 124,988

*M*w/*M*n 2.131

CL BnOH tol N2 Cl2V

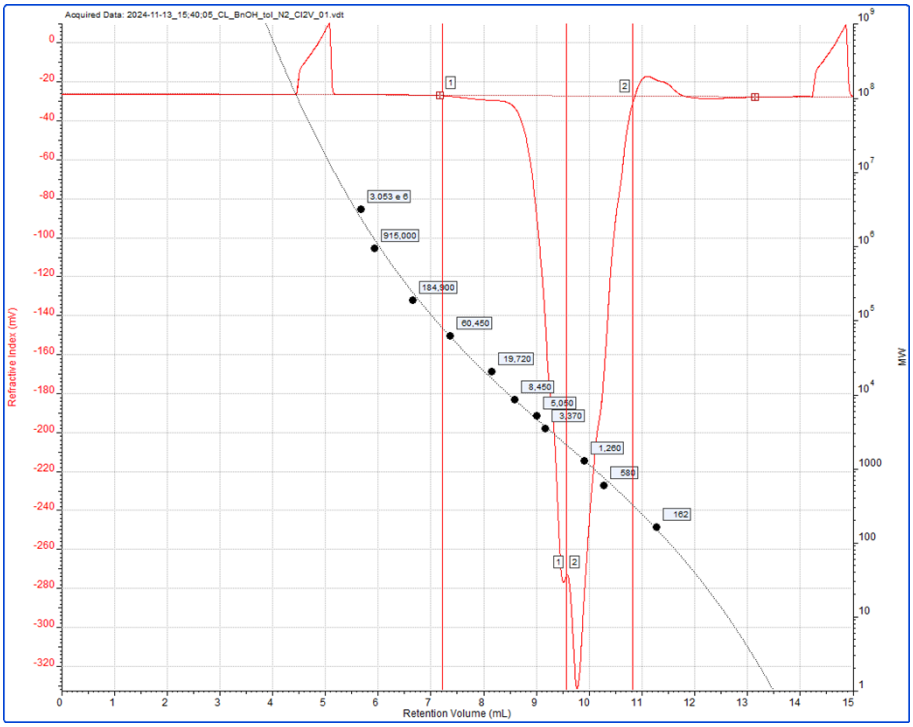
Acquired Data: 2024-11-13_15:40:05_CL_BnOH_tol_N2_Cl2V_01.vdt
Refractive Index (mV)
MW
Retention Volume (mL)
3.053 e 6
915,000
184,900
60,450
19,720
8,450
5,050
3,370
1,260
580
162

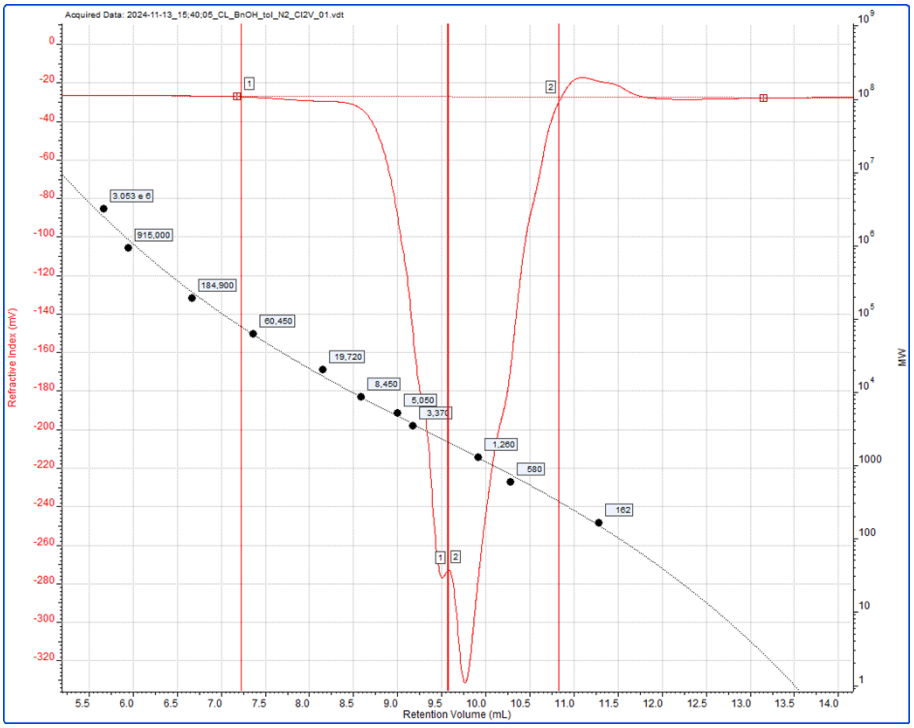
Acquired Data: 2024-11-13_15:40:05_CL_BnOH_tol_N2_Cl2V_01.vdt
Refractive Index (mV)
MW
Retention Volume (mL)
3.053 e 6
915,000
184,900
60,450
19,720
8,450
5,050
3,370
1,260
580
162

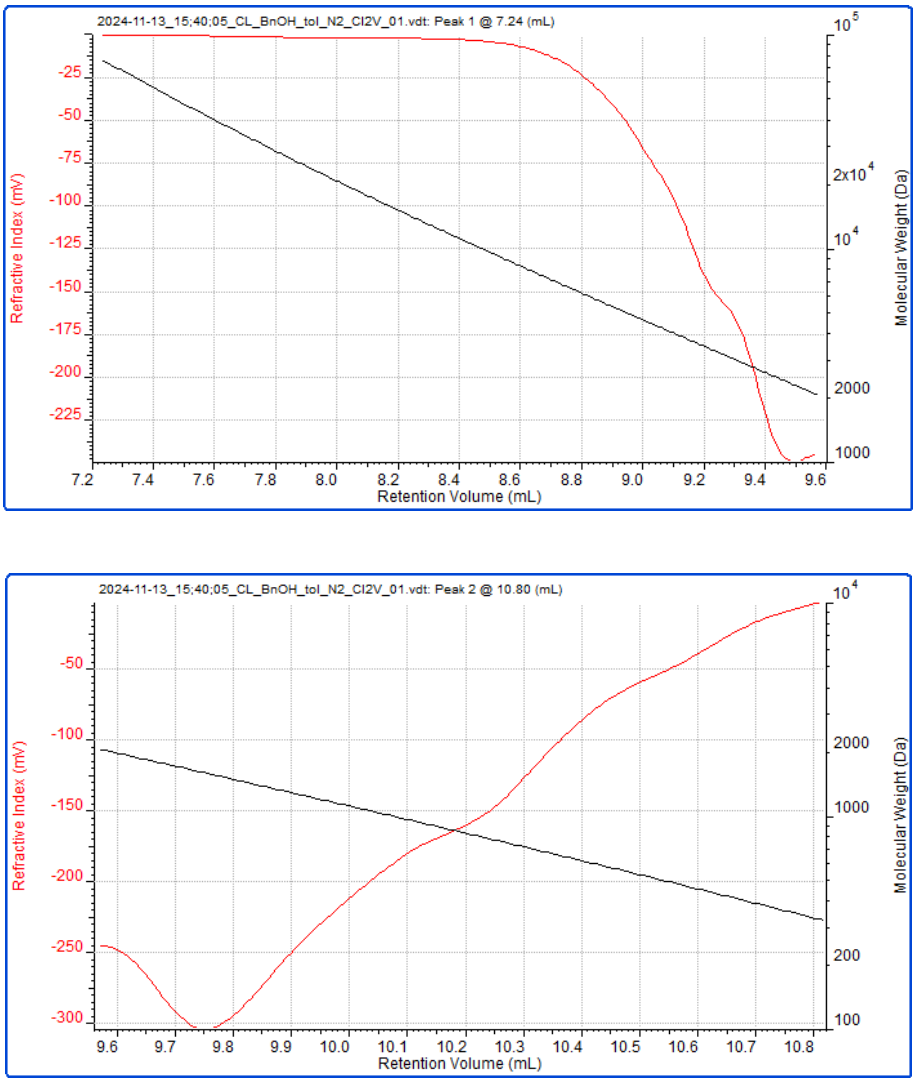


**Figure S28.** GPC trace for PCL from entry 13, Table 1.

| Peak | 1 | 2 |
|---|---|---|
| Ret Vol (mL) | 7.237 | 10.802 |
| *M*n (Da) | 2,975 | 1,090 |
| *M*w (Da) | 3,537 | 1,283 |
| *M*z (Da) | 6,150 | 1,444 |
| *M*p (Da) | 75,685 | 326 |
| *M*w/*M*n | 1.189 | 1.177 |

melt air CL 3,5-Cl2

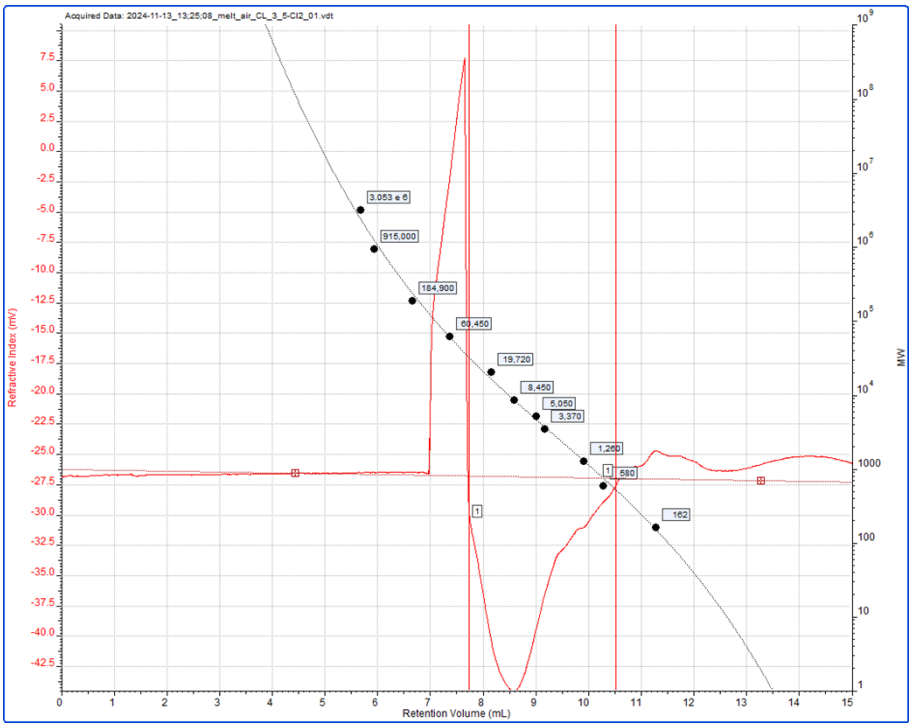


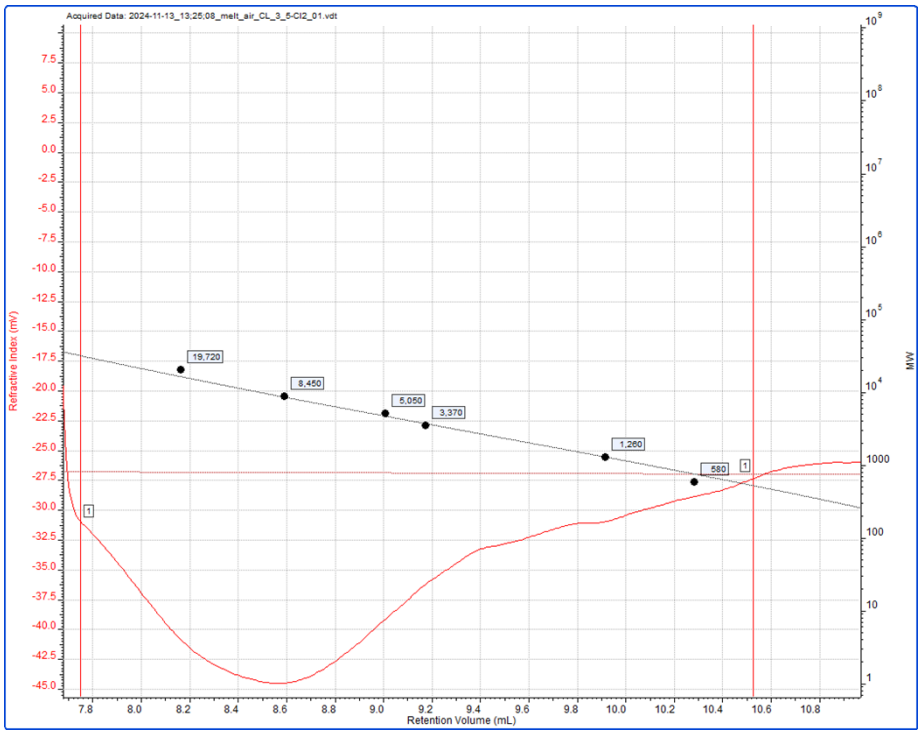

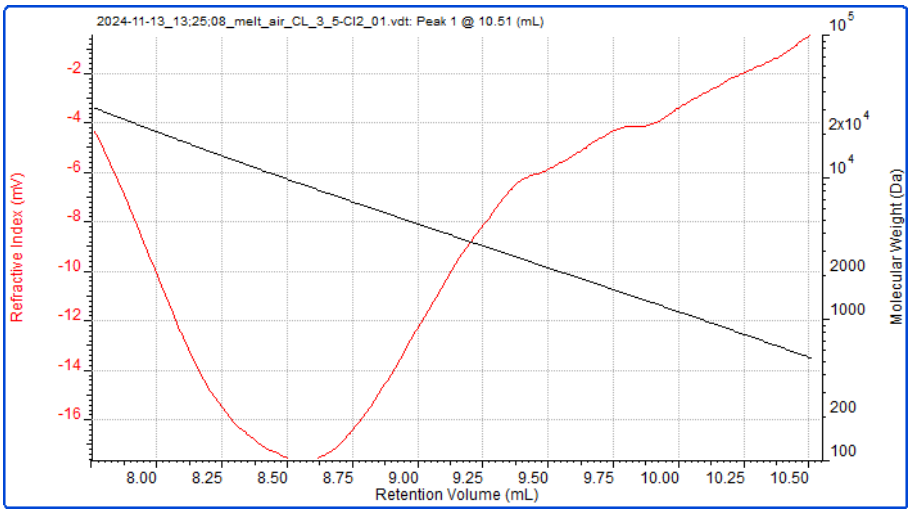


**Figure S29.** GPC trace for PCL from entry 16, Table 1.

Peak 1

Ret Vol (mL) 10.506

*M*n (Da) 7,625

*M*w (Da) 15,591

*M*z (Da) 20,322

*M*p (Da) 524

*M*w/*M*n 2.045

I2 tol air BnOH CL

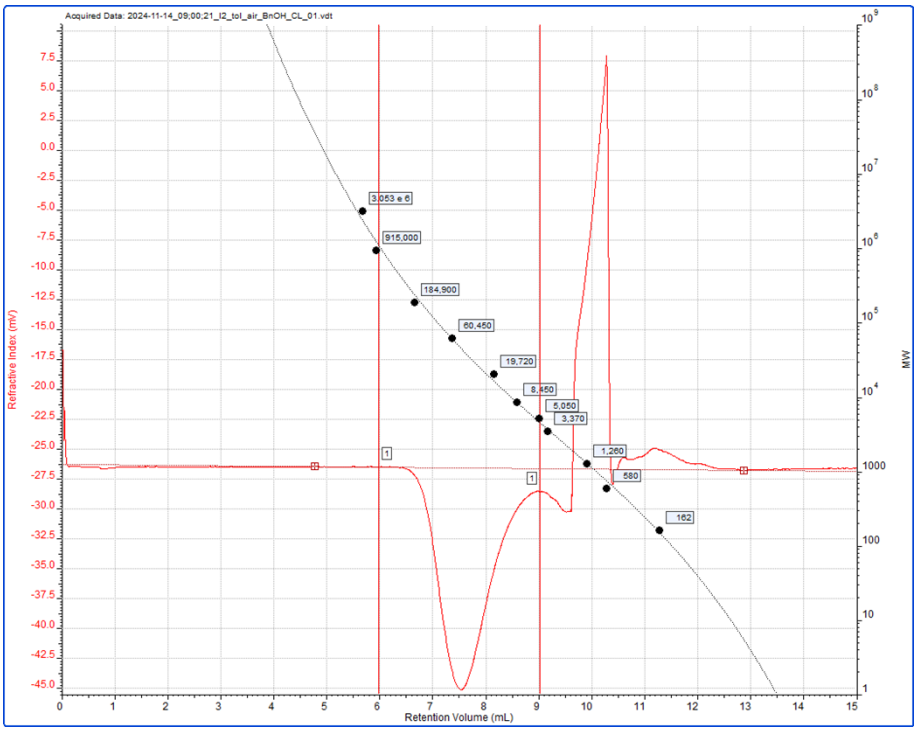
Acquired Data: 2024-11-14_09;00;21_l2_tol_air_BnOH_CL_01.vdt
Refractive Index (mV)
MW
Retention Volume (mL)
3.053 e 6
915,000
184,900
60,450
19,720
8,450
5,050
3,370
1,260
580
162

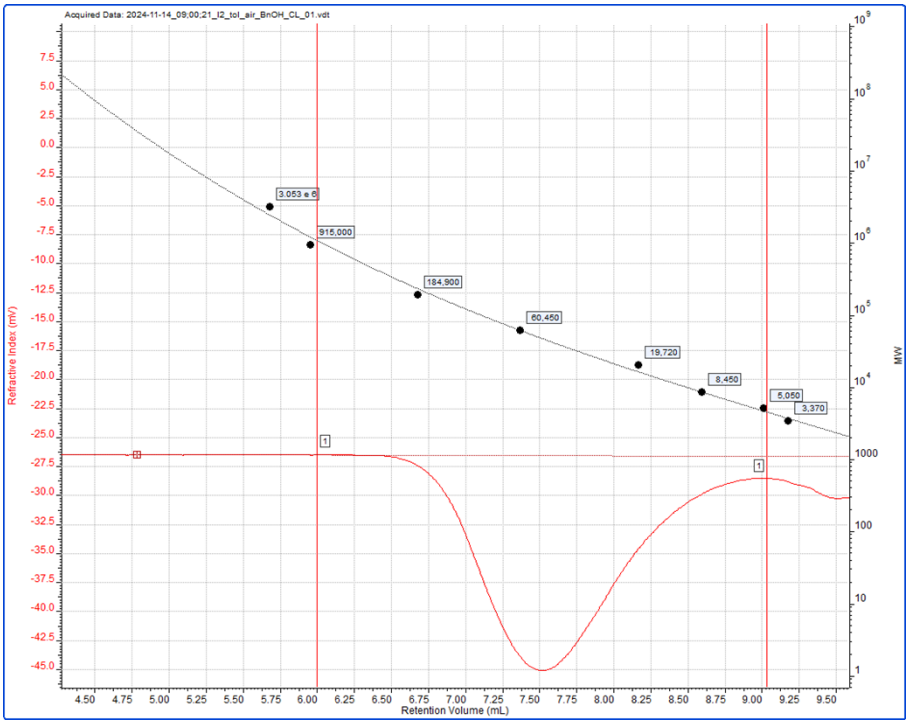
Acquired Data: 2024-11-14_09;00;21_l2_tol_air_BnOH_CL_01.vdt
Refractive Index (mV)
MW
Retention Volume (mL)
3.053 e 6
915,000
184,900
60,450
19,720
8,450
5,050
3,370

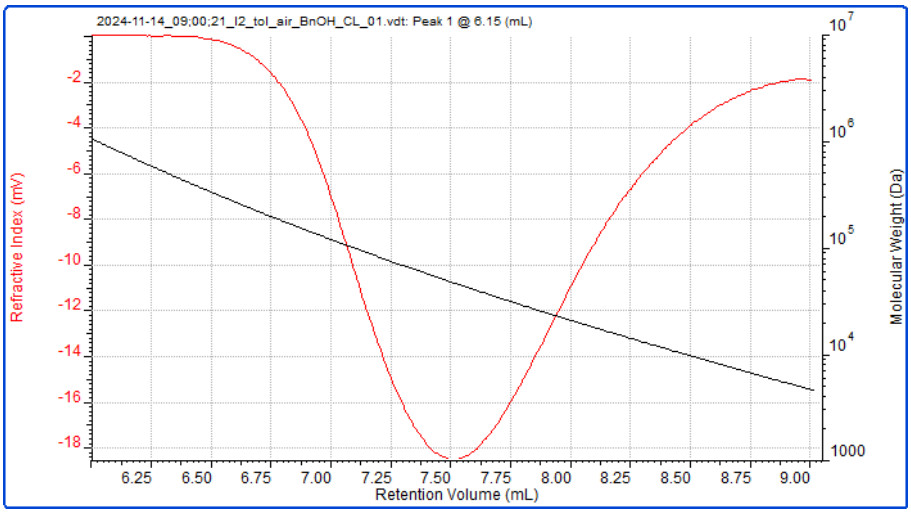


**Figure S30**. GPC trace for PCL from entry 21, Table 1.

Peak 1

Ret Vol (mL) 6.152

*M*n (Da) 26,138

*M*w (Da) 47,851

*M*z (Da) 69,380

*M*p (Da) 725,955

*M*w/*M*n 1.831

I2V N2 melt CL

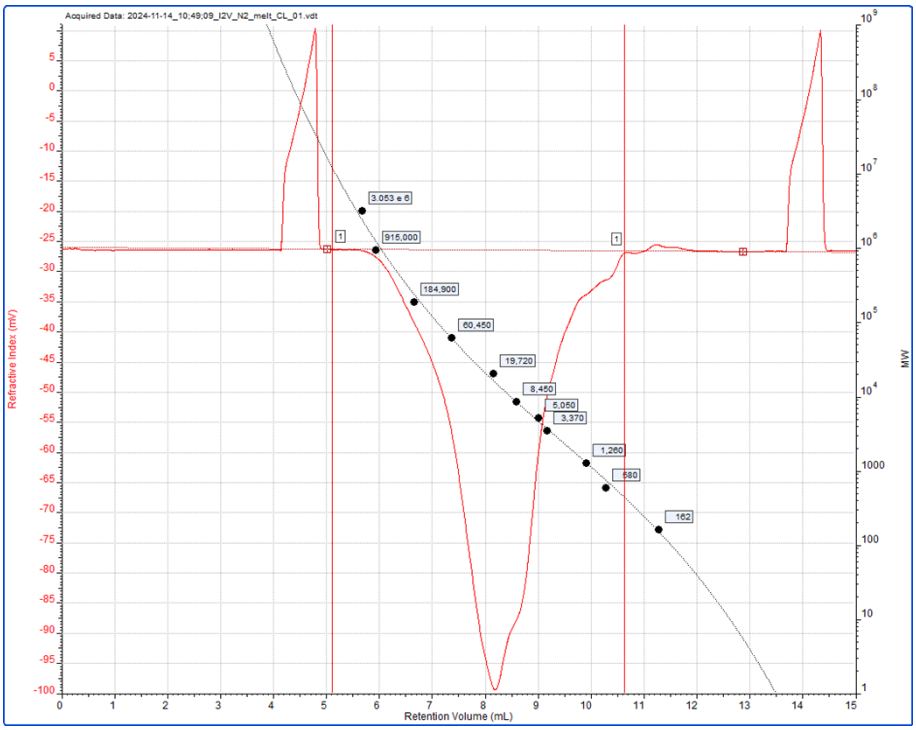
Acquired Data: 2024-11-14_10:49:09_I2V_N2_melt_CL_01.vdt
Refractive Index (mV)
MW
Retention Volume (mL)
3.053 e 6
915,000
184,900
60,450
19,720
8,450
5,050
3,370
1,260
580
162

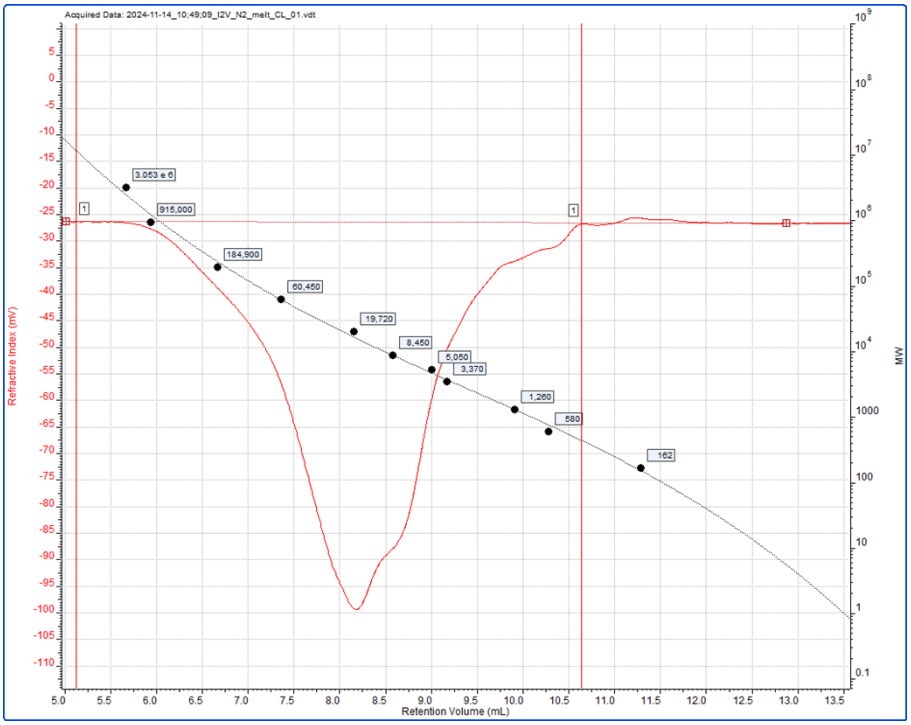
Acquired Data: 2024-11-14_10:49:09_I2V_N2_melt_CL_01.vdt
Refractive Index (mV)
MW
Retention Volume (mL)
3.053 e 6
915,000
184,900
60,450
19,720
8,450
5,050
3,370
1,260
580
162

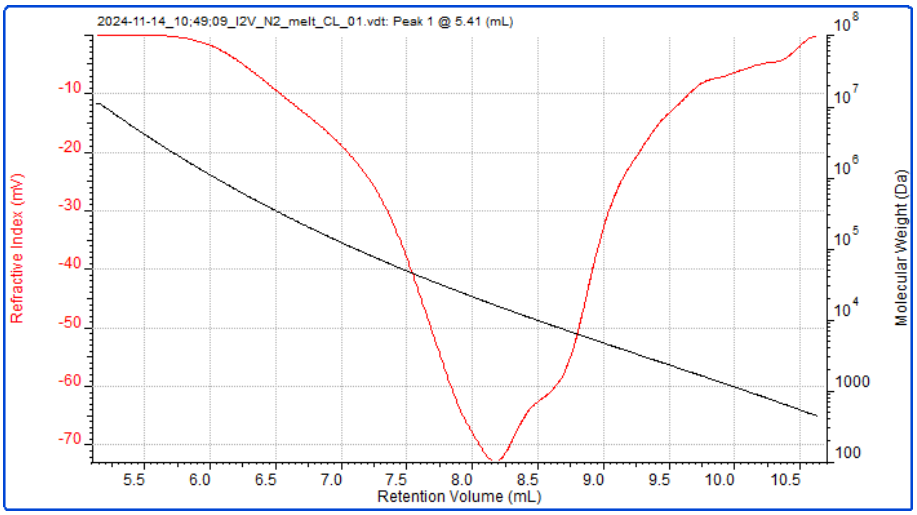


**Figure S31**. GPC trace for PCL from entry 22, Table 1.

Peak 1

Ret Vol (mL) 5.409

*M*n (Da) 7,811

*M*w (Da) 44,636

*M*z (Da) 324,862

*M*p (Da) 4.927 e 6

*M*w/*M*n 5.714

I2-CL-melt-N2-BnOH

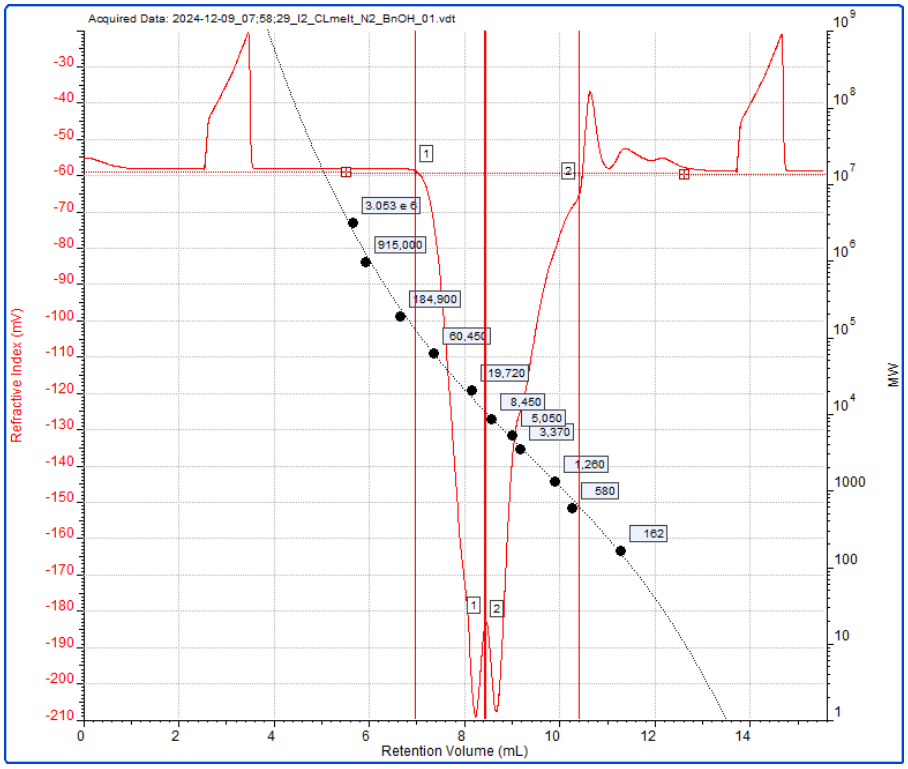
Acquired Data: 2024-12-09_07;58;29_I2_CLmelt_N2_BnOH_01.vdt
Refractive Index (mV)
MW
Retention Volume (mL)
3.053 e 6
915,000
184,900
60,450
19,720
8,450
5,050
3,370
1,260
580
162

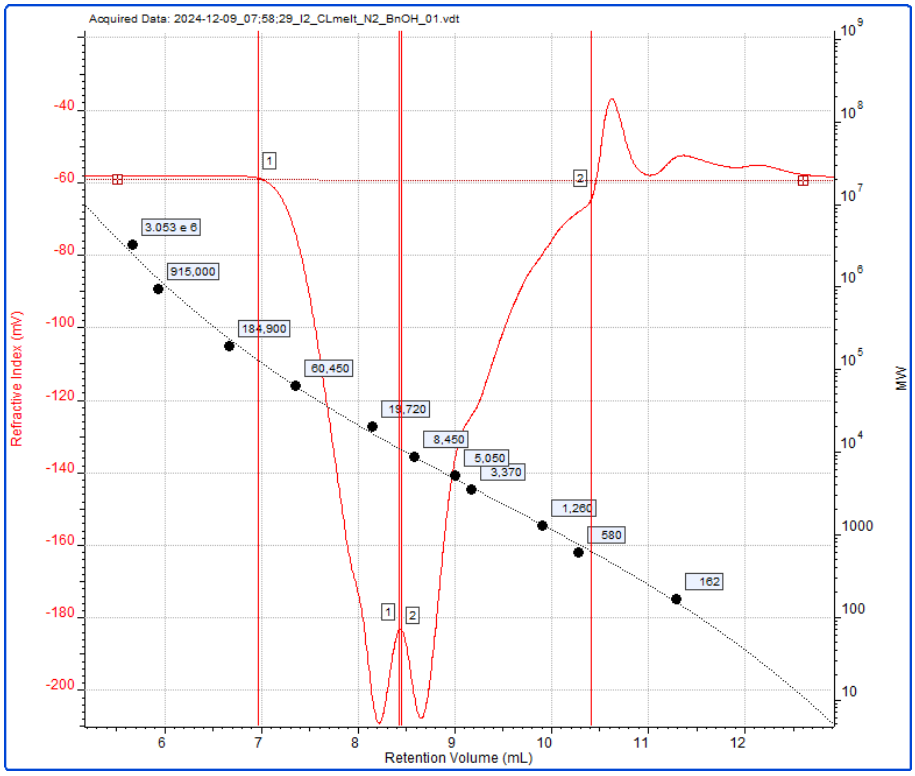
Acquired Data: 2024-12-09_07;58;29_I2_CLmelt_N2_BnOH_01.vdt
Refractive Index (mV)
MW
Retention Volume (mL)
3.053 e 6
915,000
184,900
60,450
19,720
8,450
5,050
3,370
1,260
580
162

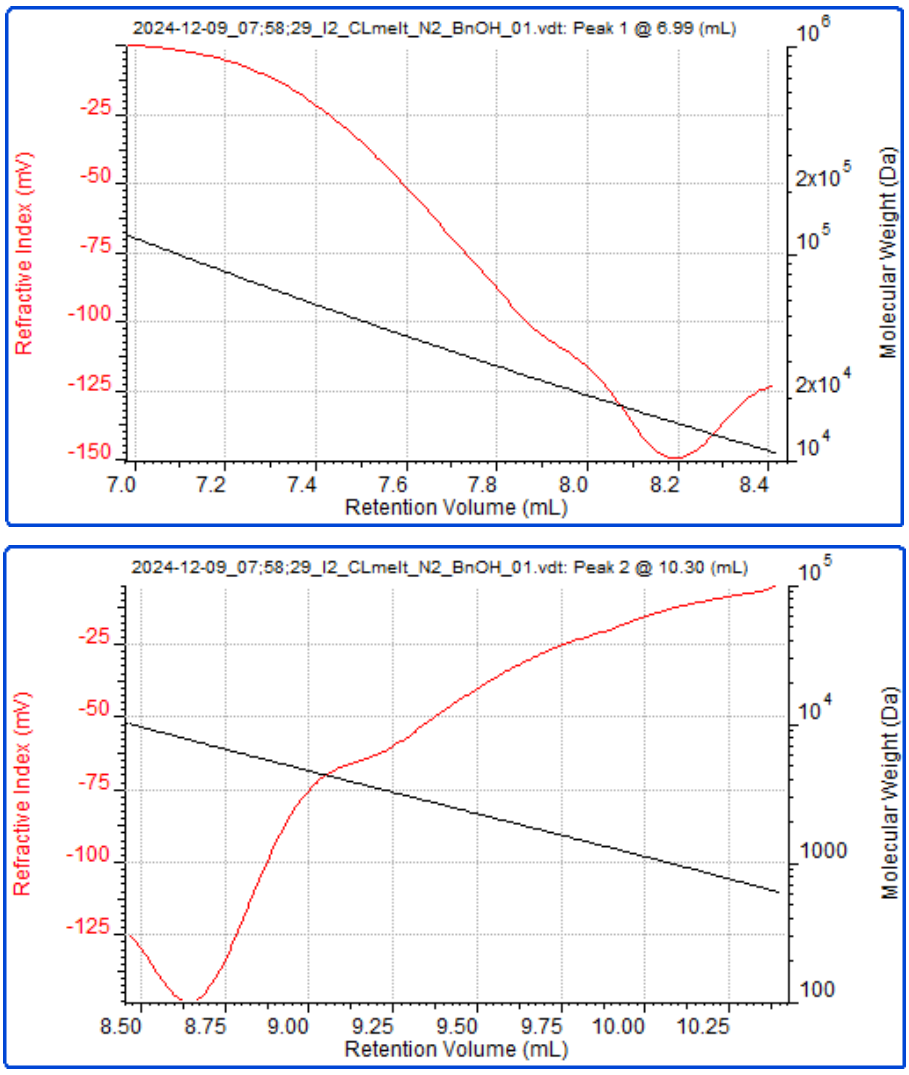


**Figure S32**. GPC trace for PCL from entry 24, Table 1.

| Peak | 1 | 2 |
|---|---|---|
| Ret Vol (mL) | 6.987 | 10.302 |
| *M*n (Da) | 18,898 | 3,921 |
| *M*w (Da) | 23,129 | 5,720 |
| *M*z (Da) | 29,878 | 6,939 |
| *M*p (Da) | 121,366 | 712 |
| *M*w/*M*n | 1.224 | 1.459 |

## *δ-Valerolactone*

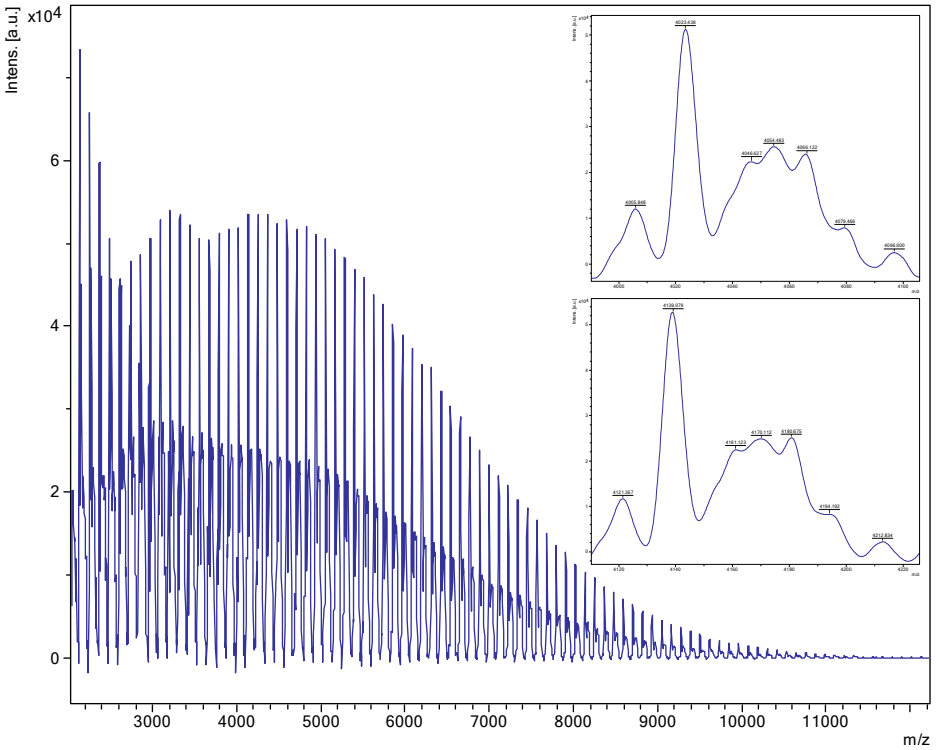


**Figure S33.** MALDI-ToF spectrum of PVL using **2** in toluene at 130 °C under air in the presence of BnOH (entry 3, table 2). Present are chain polymers of the type H-PVL-OH, [M = 17 (OH) + 1(H) + n × 100.12 (VL)] (e.g. for n = 40: calculated peak 4022.8; observed peak 4023.4; and H-PVL-OBn, $Na^+$ n = 40 calc 4135.9, observed 4139.1.

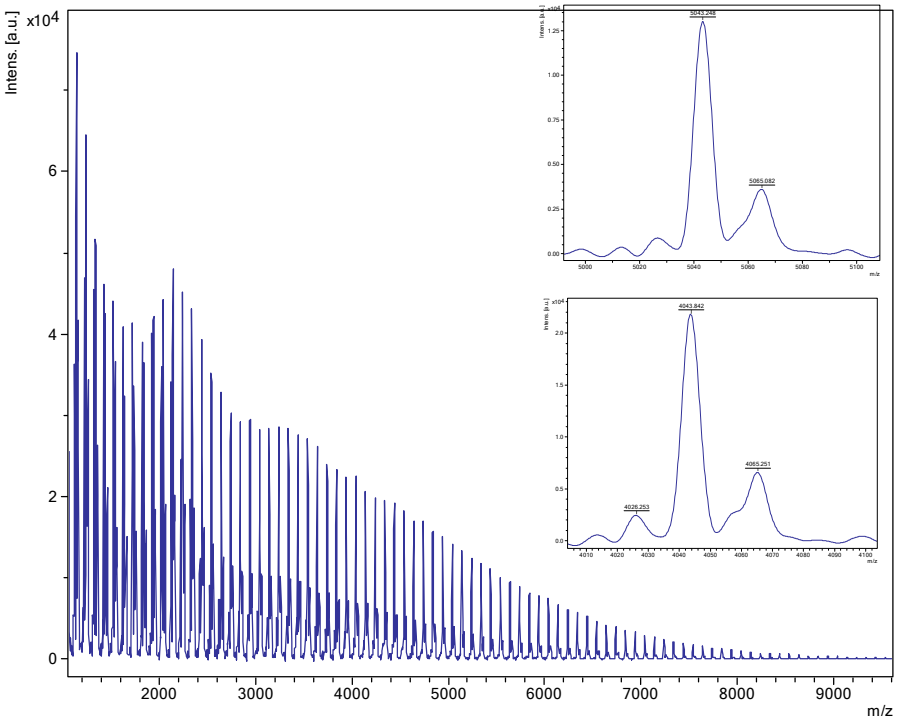


**Figure S34.** MALDI-ToF spectrum of PVL using **10** in toluene at 130 °C under air in the presence of BnOH (entry 20, table 2). Present are chain polymers of the type H-PVL-OH, $Na^+$ (e.g. for n = 40: calculated peak 4045.8; observed peak 4043.6; for n = 50: calculated peak 5047.0; observed peak 5043.2).

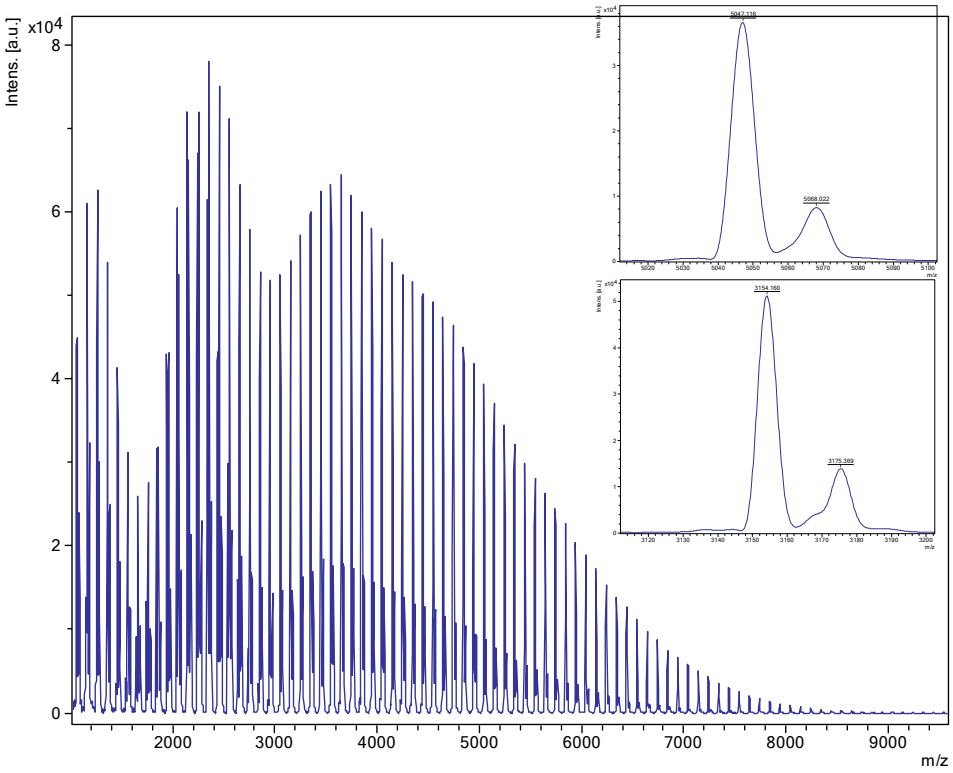


**Figure S35**. MALDI-ToF spectrum of PVL using **10** in toluene under $N_2$ in the presence of BnOH (entry 25, table 2). Present are chain polymers of the type H-PVL-OH, $Na^+$ (e.g. for n = 50, calc 5047.0 obsv. 5047.1; and chain polymers of the type H-PVL-OBn, $K^+$ n = 30: calc 3150.8, obsv. 3154.1.

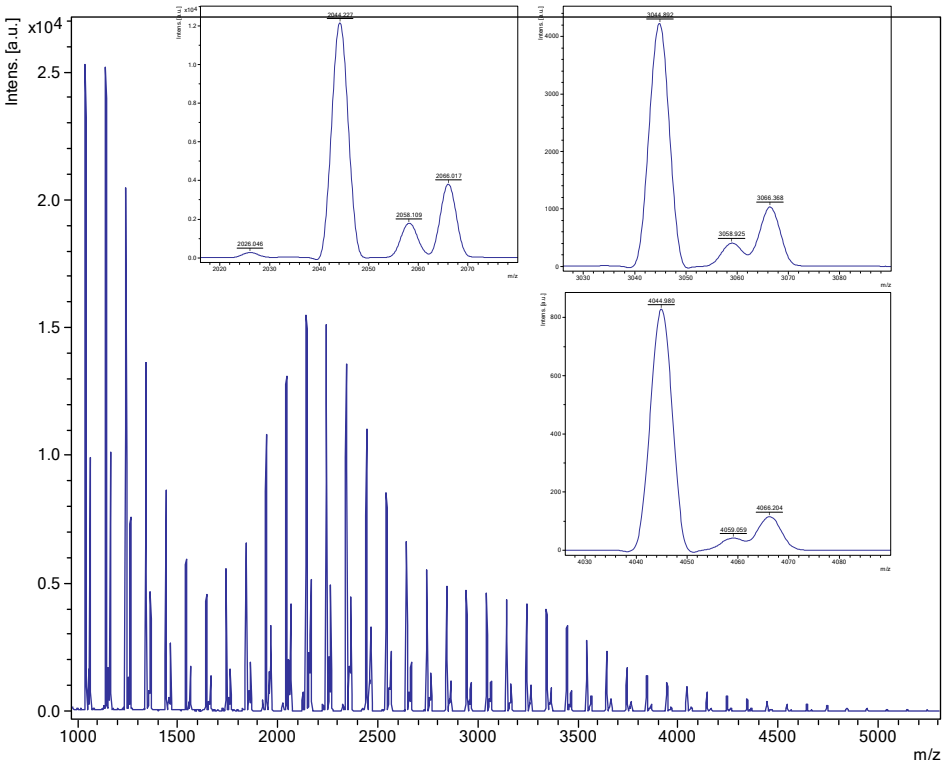


**Figure S36.** MALDI-ToF spectrum of PVL using **10** as a melt under $N_2$ in the presence of BnOH (entry 25, table 2). Present are chain polymers of the type H-PVL-OH, $Na^+$ (e.g. for n = 20:

calculated peak 2043.4; observed peak 2044.2; for n = 30: calculated peak 3044.6; observed peak 3044.8; for n = 40: calculated peak 4045.8; observed peak 4045.0).

**Kinetic runs for δ-VL**

No 2 VO(O*i*Pr)

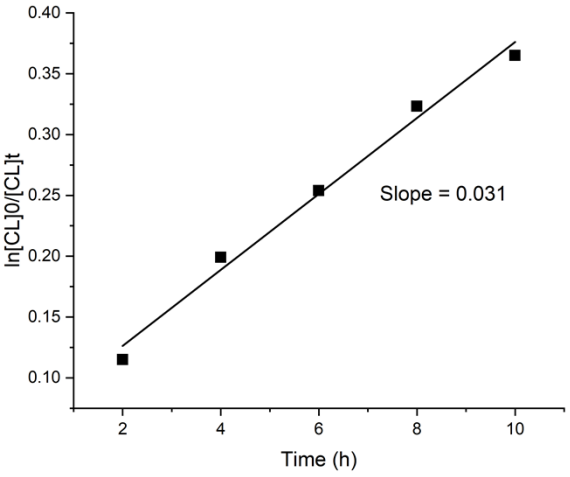


**Figure S37**. Kinetic run for compound **2** with δ-VL.

**OEt No. 3**

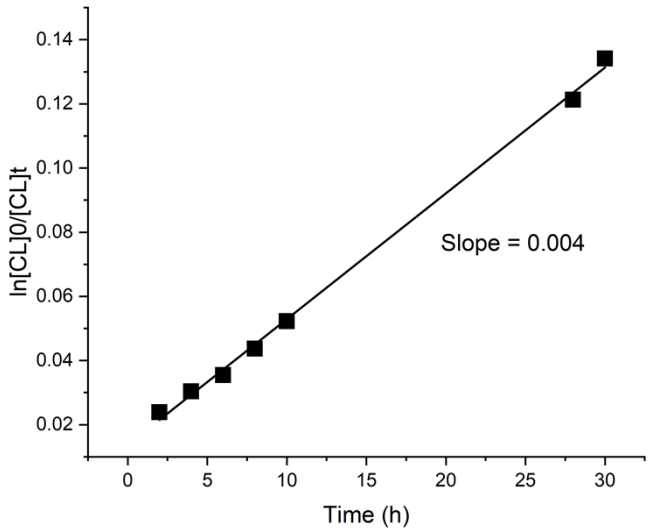


**Figure S38**. Kinetic run for compound **3** with δ-VL.

Njc5

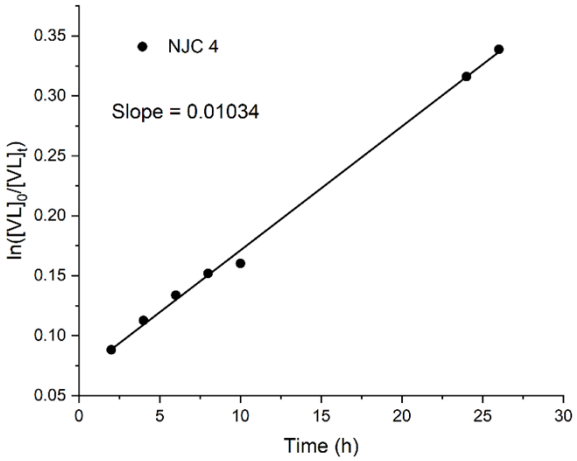


**Figure S39**. Kinetic run for compound **5** with δ-VL.

**Me2V**

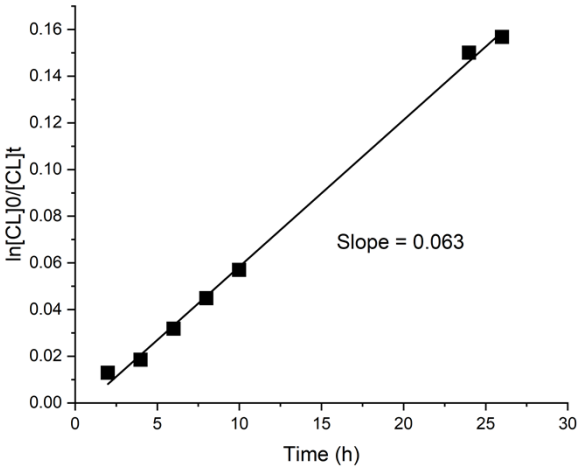


**Figure S40**. Kinetic run for compound **7** with δ-VL.

**3,5-Cl2: 8**

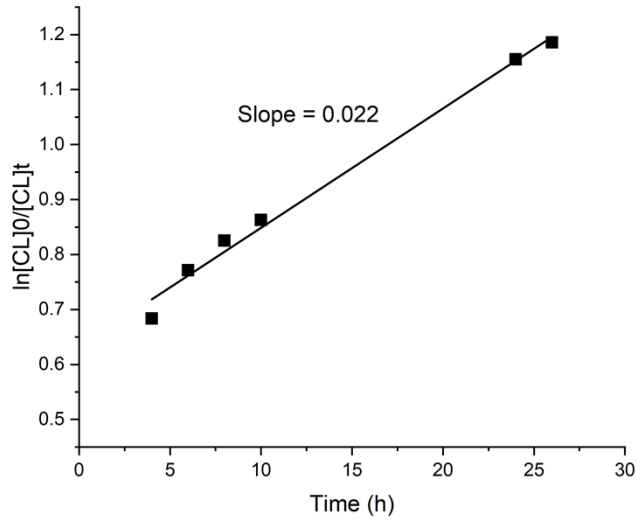


**Figure S41**. Kinetic run for compound **8** with δ-VL.

**3,5-I2- = 10**

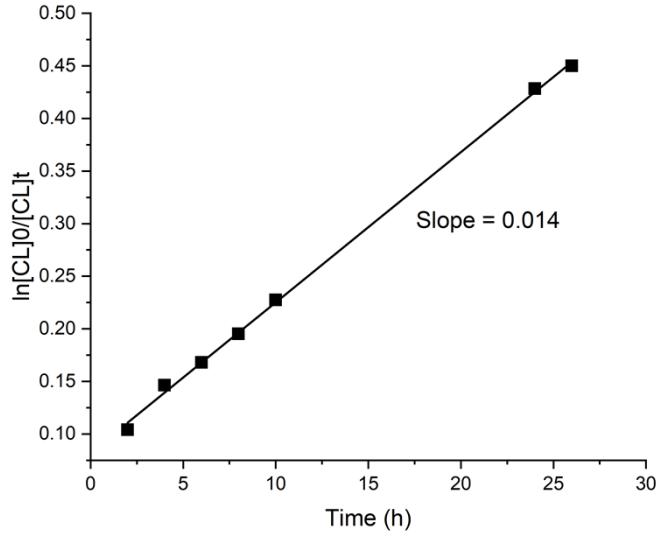


**Figure S42**. Kinetic run for compound **10** with δ-VL.

# GPC traces for PVL

Njc2 air melt vl

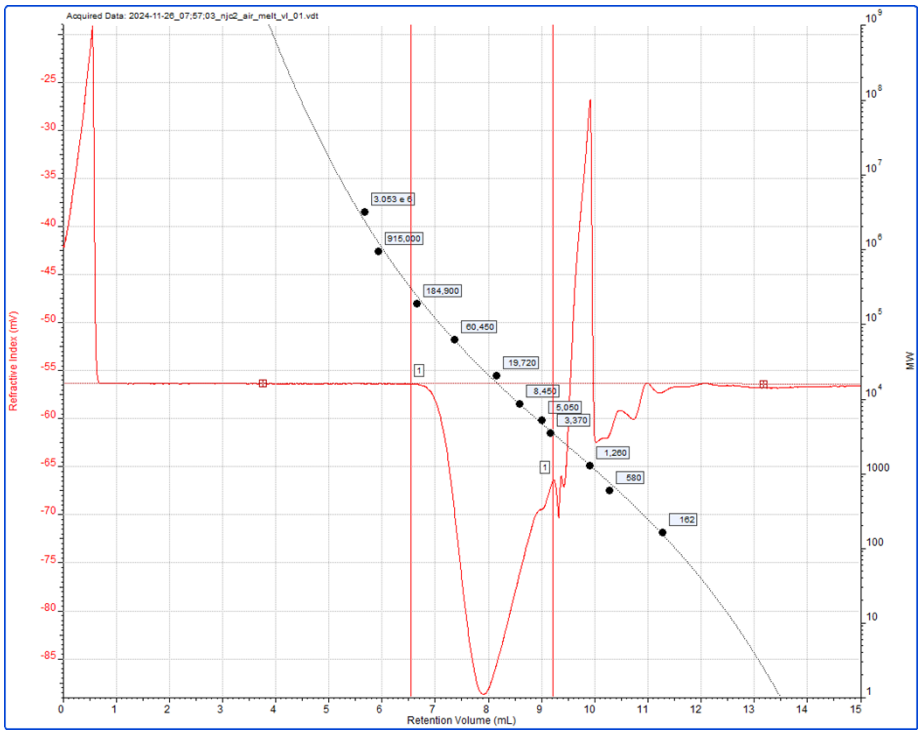


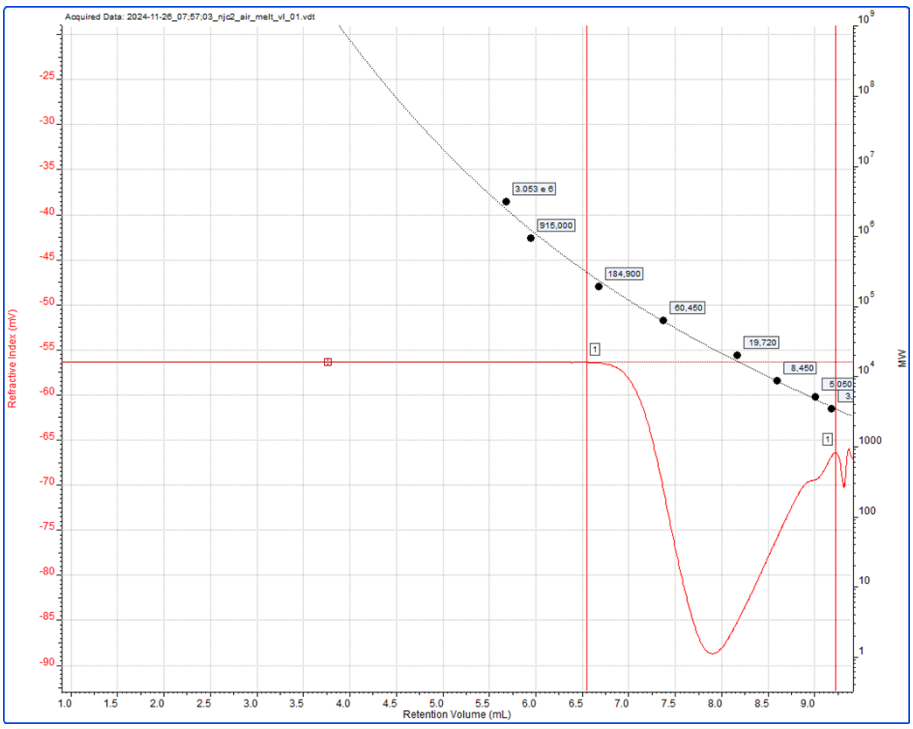

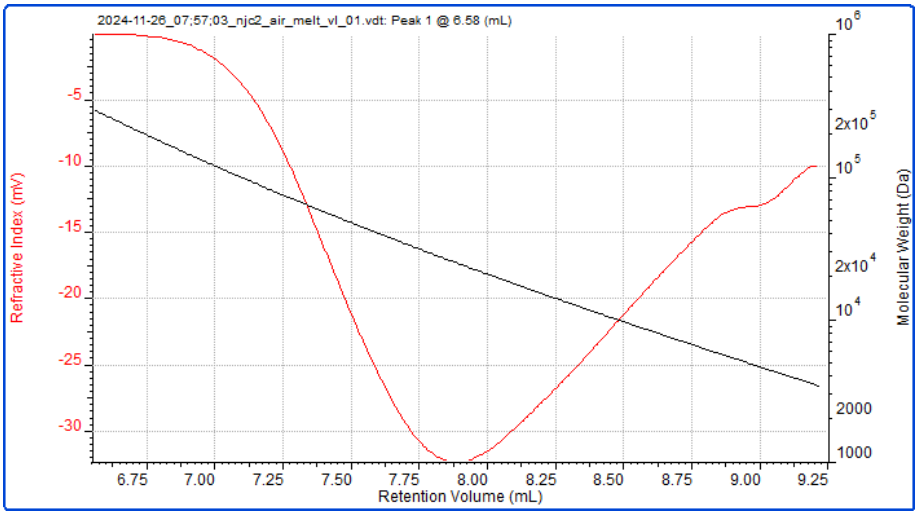


**Figure S43**. GPC trace for PVL from entry 4, Table 2.

Peak 1
Ret Vol (mL) 6.584
*M*n (Da) 13,012
*M*w (Da) 24,498
*M*z (Da) 42,357
*M*p (Da) 270,599
*M*w/*M*n 1.883

Njc4 tol n2 VL

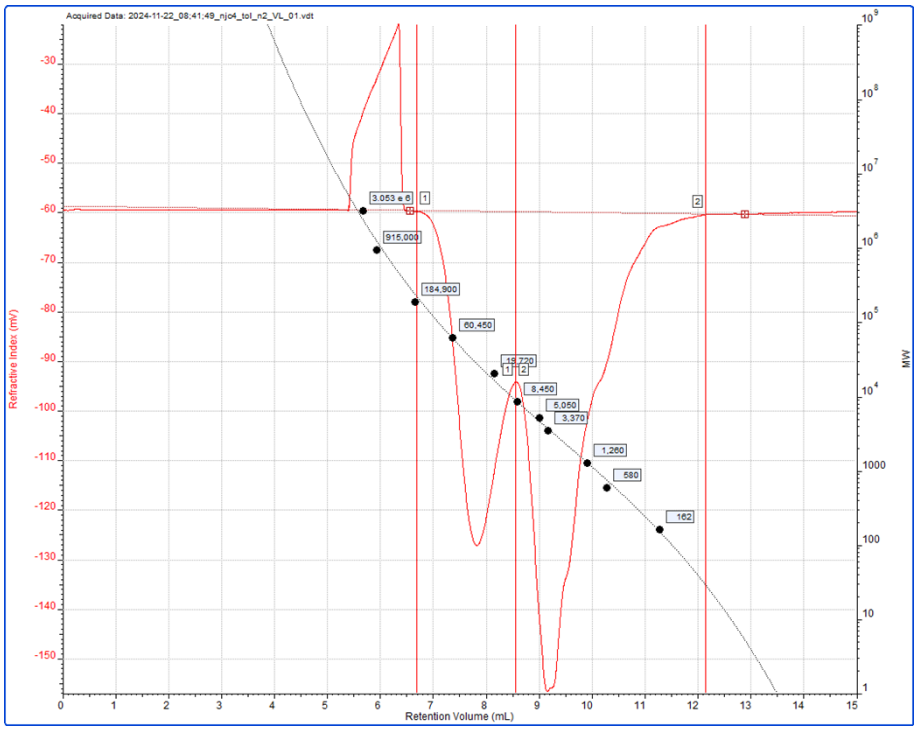

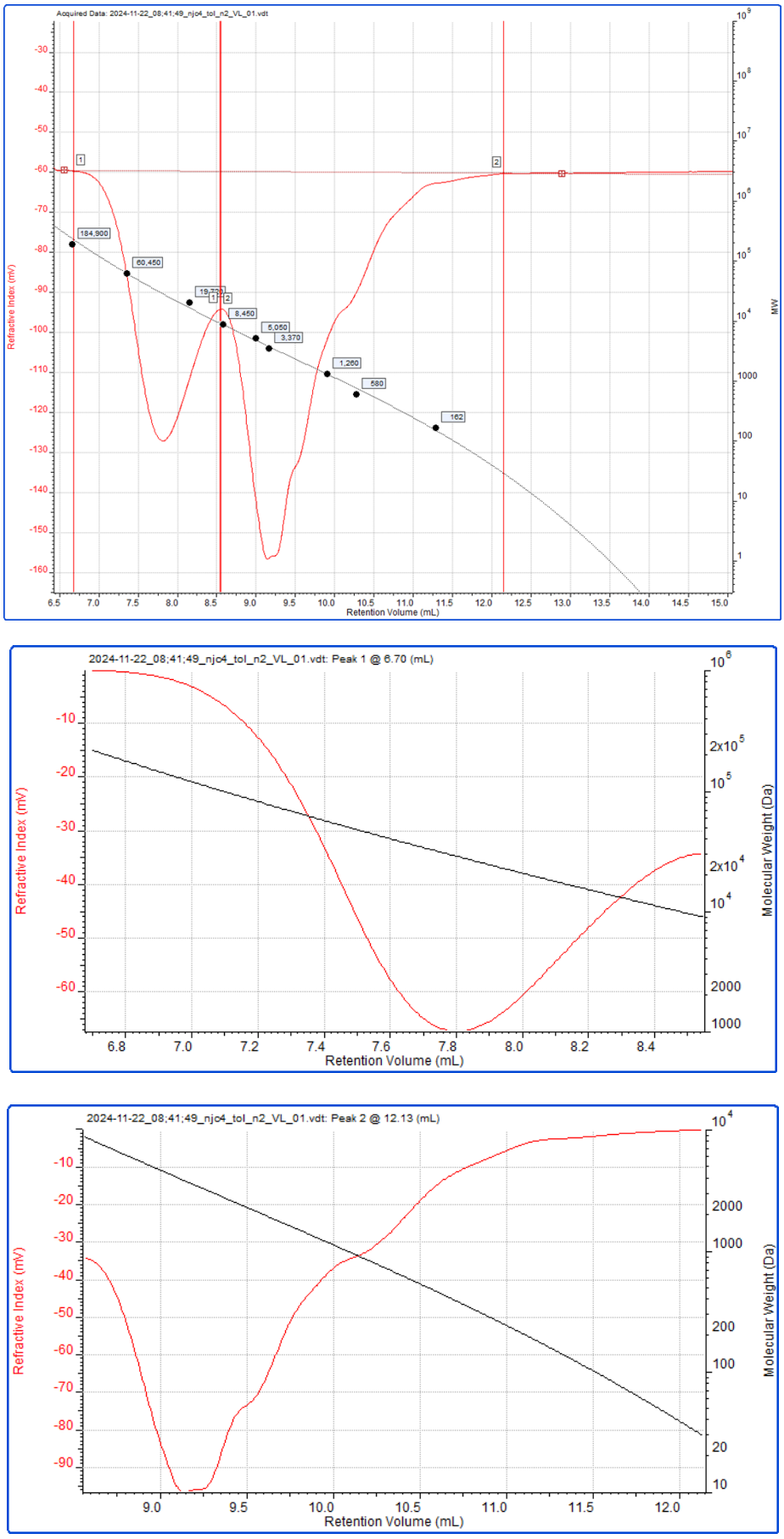


**Figure S44**. GPC trace for PVL from entry 5, Table 2.

| Peak | 1 | 2 |
|---|---|---|
| Ret Vol (mL) | 6.698 | 12.129 |
| *M*n (Da) | 21,915 | 8,528 |
| *M*w (Da) | 30,499 | 8,528 |
| *M*z (Da) | 43,351 | 8,529 |
| *M*p (Da) | 216,480 | 30 |
| *M*w/*M*n | 1.392 | 1.000 |

Njc4 air vl tol bnoh

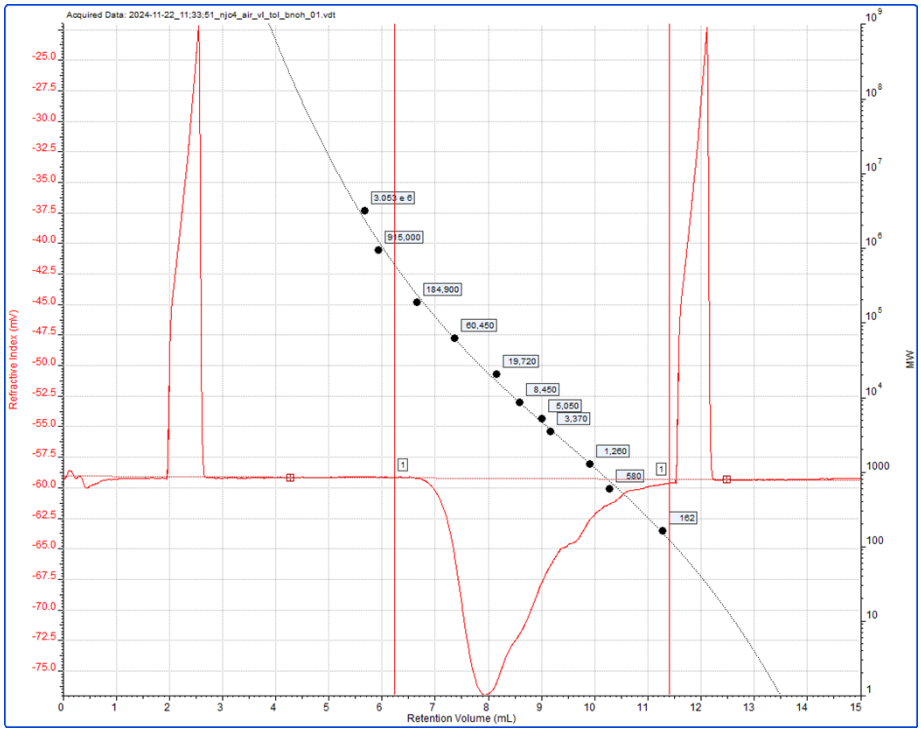

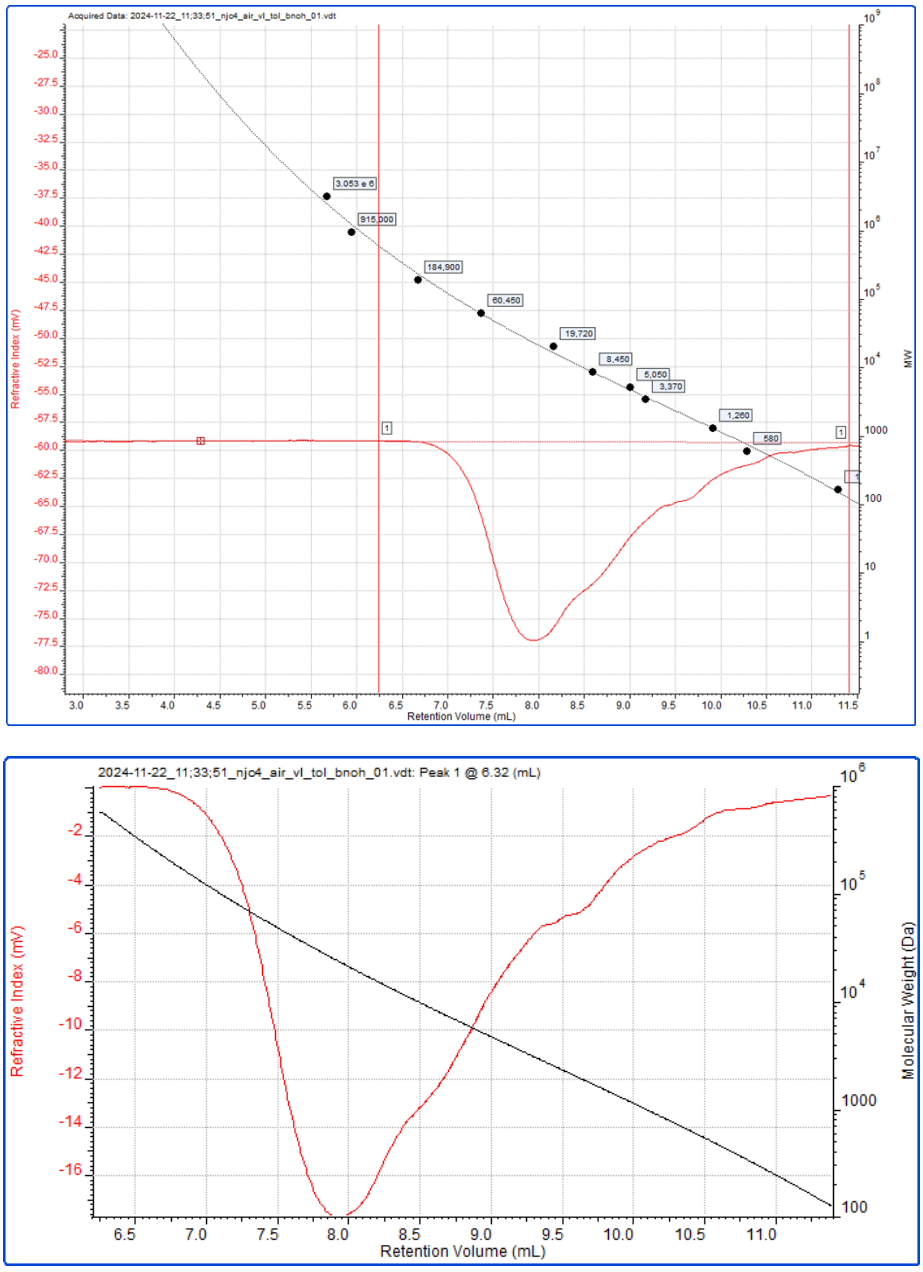


**Figure S45**. GPC trace for PVL from entry 8, Table 2.

Peak 1
Ret Vol (mL) 6.319
*M*n (Da) 4,126
*M*w (Da) 19,056
*M*z (Da) 35,268
*M*p (Da) 484,404
*M*w/*M*n 4.618

tol n2 vl cl2CV

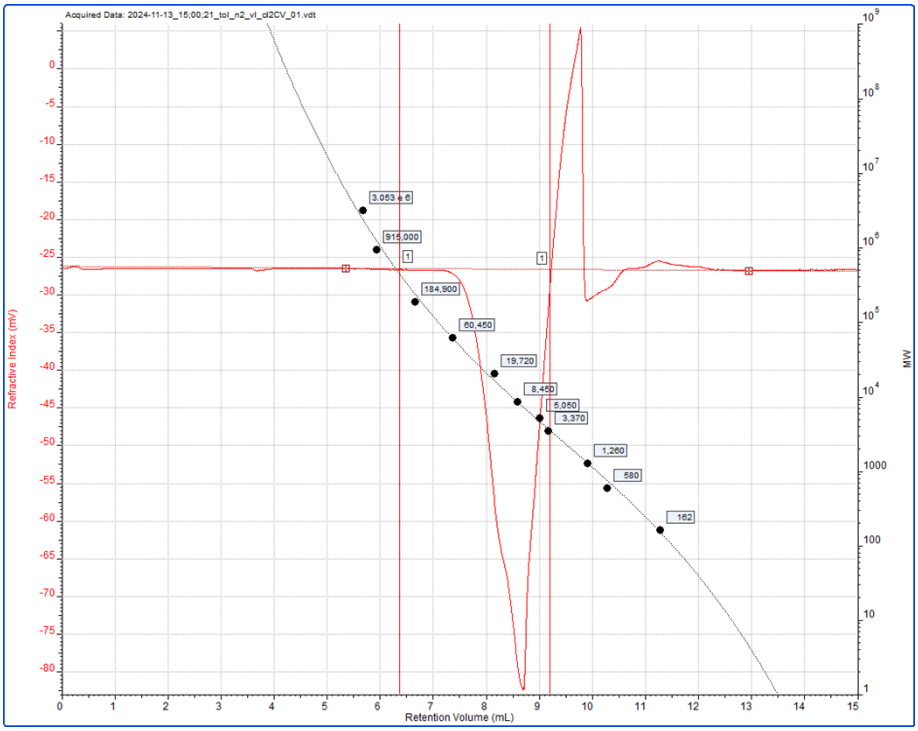


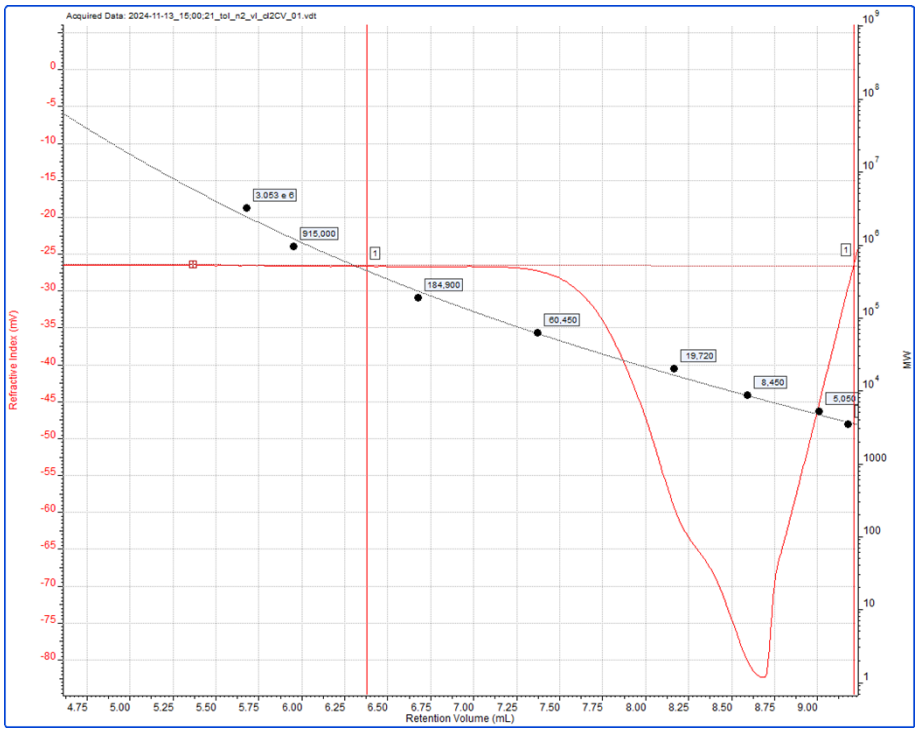

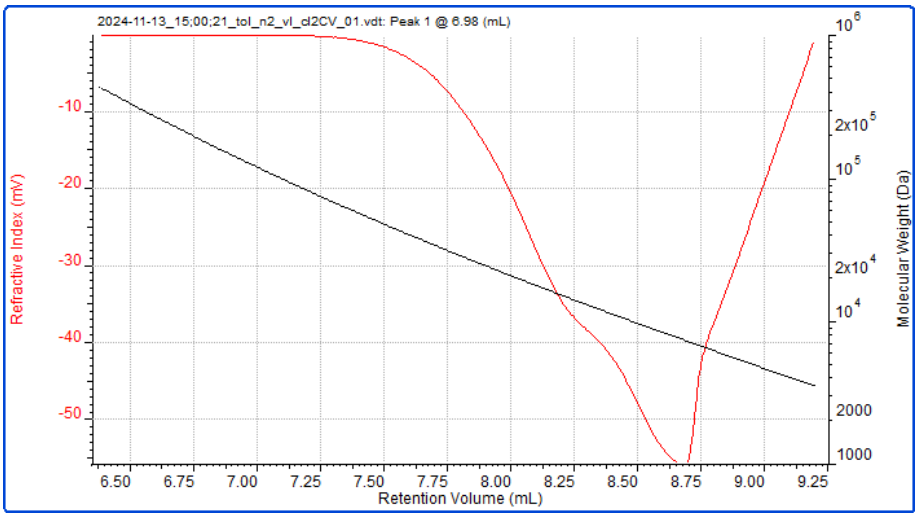


**Figure S46**. GPC trace for PVL from entry 11, Table 2.

Peak 1

Ret Vol (mL) 6.979

*M*n (Da) 9,045

*M*w (Da) 12,403

*M*z (Da) 21,904

*M*p (Da) 121,828

*M*w/*M*n 1.371

Cl2 tol air VL

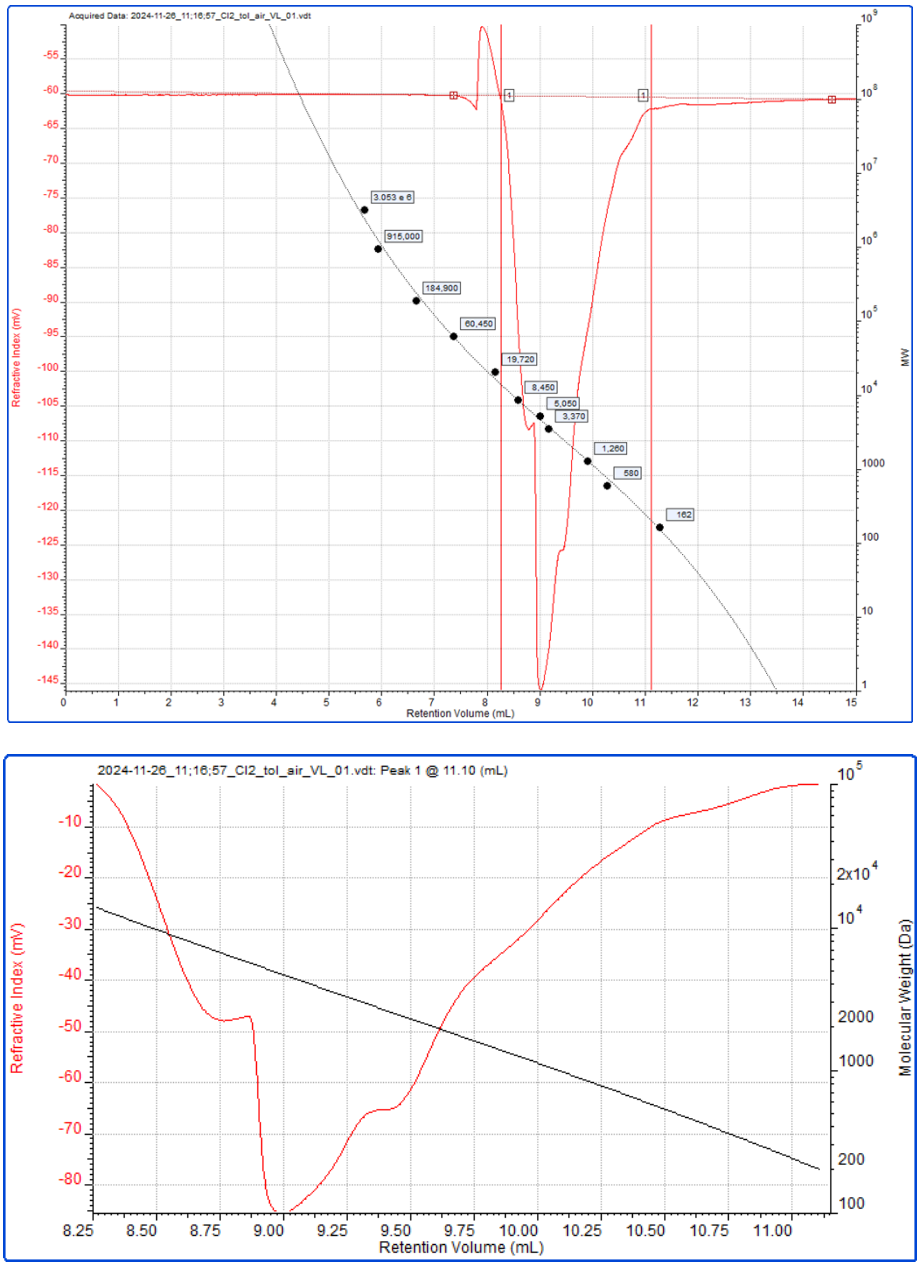


**Figure S47**. GPC trace for PVL from entry 12, Table 2.

Peak 1
Ret Vol (mL) 11.098
*M*n (Da) 3,507
*M*w (Da) 6,795
*M*z (Da) 8,919
*M*p (Da) 201
*M*w/*M*n 1.937

Cl2V-VL-Air-Tol-BnOH

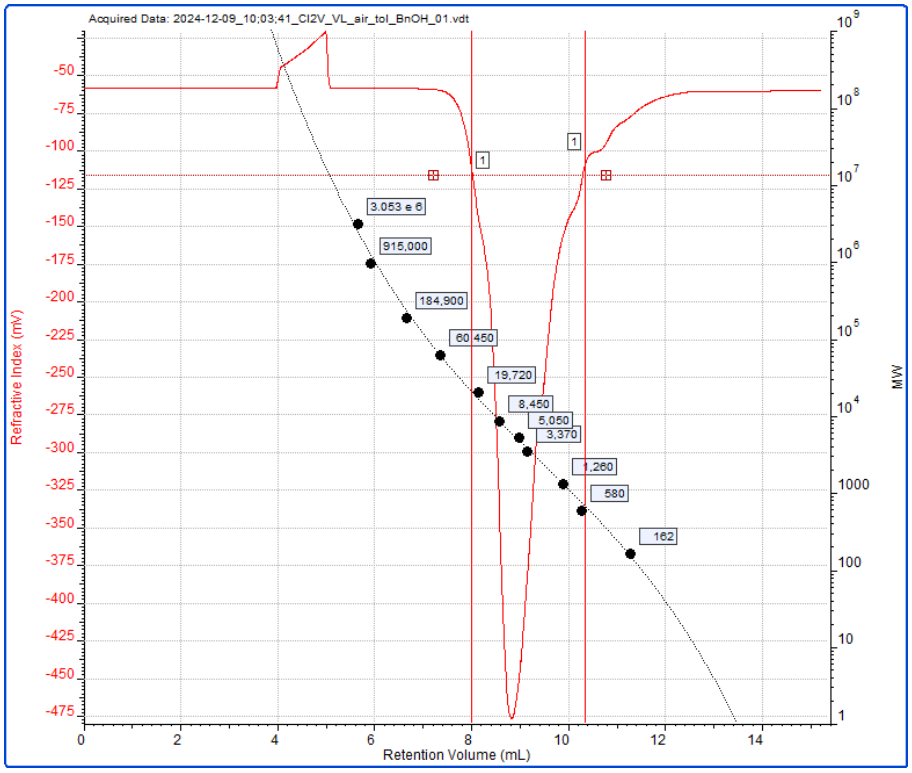
Acquired Data: 2024-12-09_10;03;41_CI2V_VL_air_tol_BnOH_01.vdt
Refractive Index (mV)
MW
Retention Volume (mL)
3.053 e 6
915,000
184,900
60,450
19,720
8,450
5,050
3,370
1,260
580
162

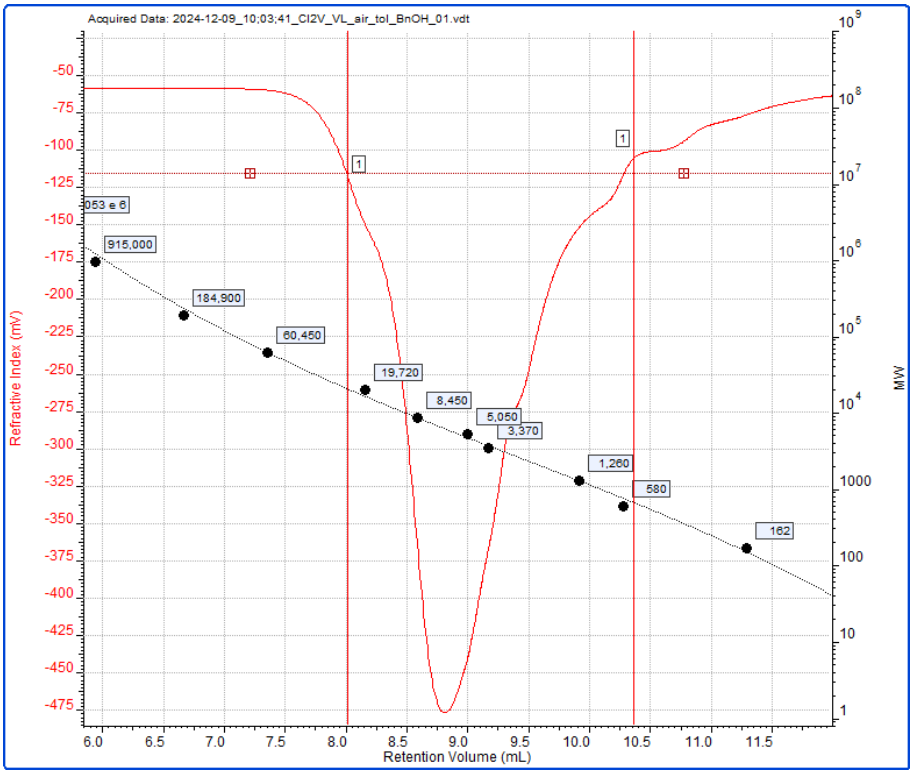
Acquired Data: 2024-12-09_10;03;41_CI2V_VL_air_tol_BnOH_01.vdt
Refractive Index (mV)
MW
Retention Volume (mL)
915,000
184,900
60,450
19,720
8,450
5,050
3,370
1,260
580
162

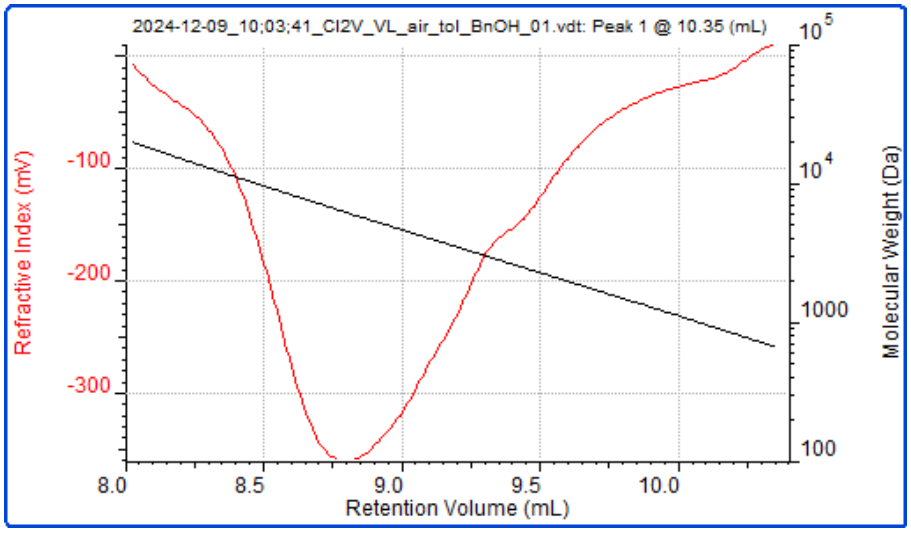


**Figure S48**. GPC trace for PVL from entry 14, Table 2.

Peak 1
Ret Vol (mL) 10.347
*M*n (Da) 4,083
*M*w (Da) 5,639
*M*z (Da) 7,292
*M*p (Da) 667
*M*w/*M*n 1.381

melt N2 Cl2V VL

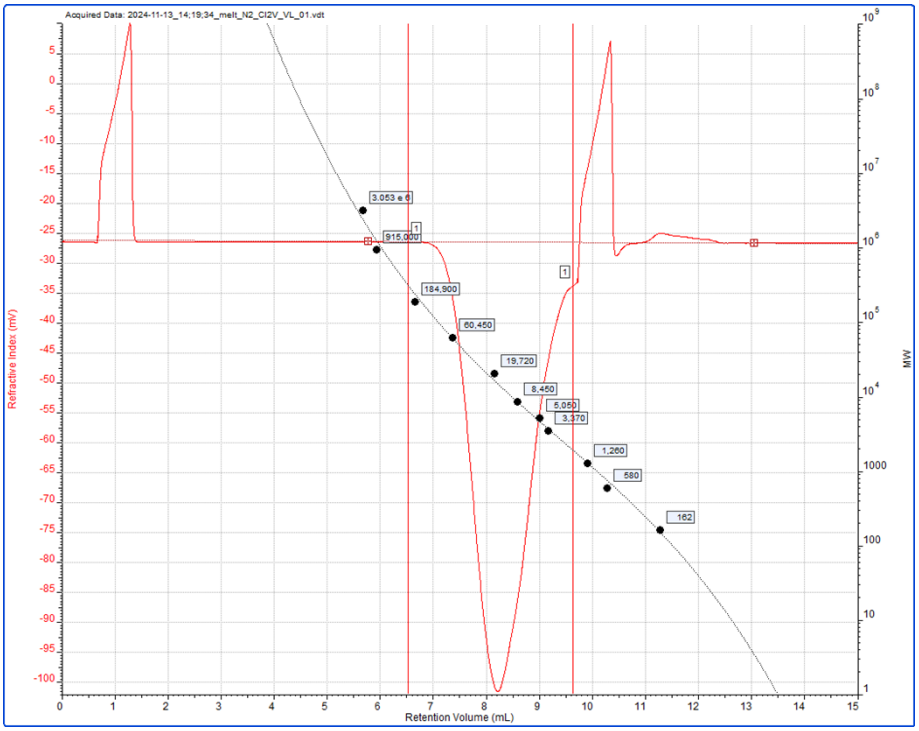

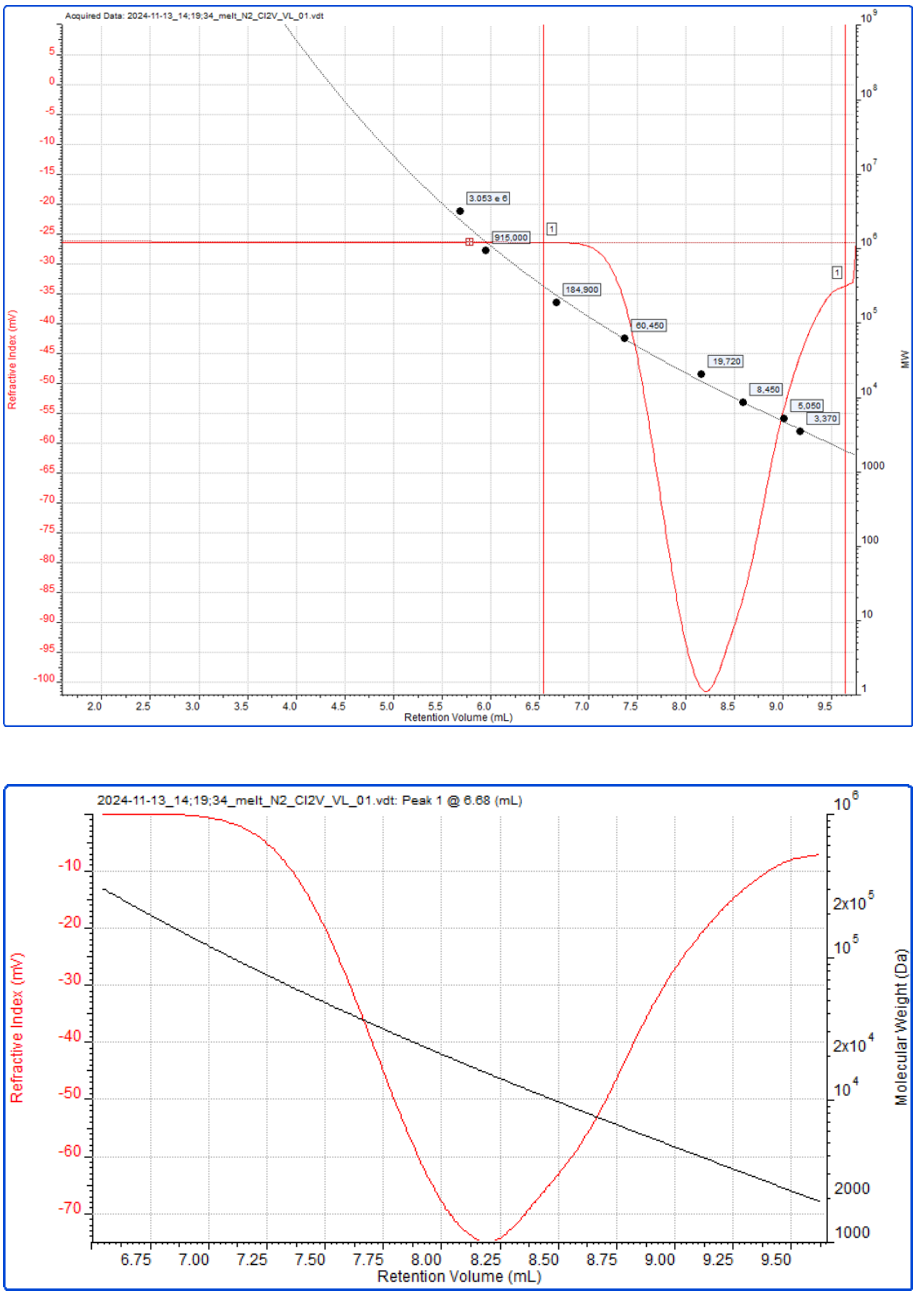


**Figure S49**. GPC trace for PVL from entry 15, Table 2.

Peak 1

Ret Vol (mL) 6.683

*M*n (Da) 9,735

*M*w (Da) 16,976

*M*z (Da) 27,720

*M*p (Da) 219,915

*M*w/*M*n 1.744

Cl2V melt N2 BnOH VL

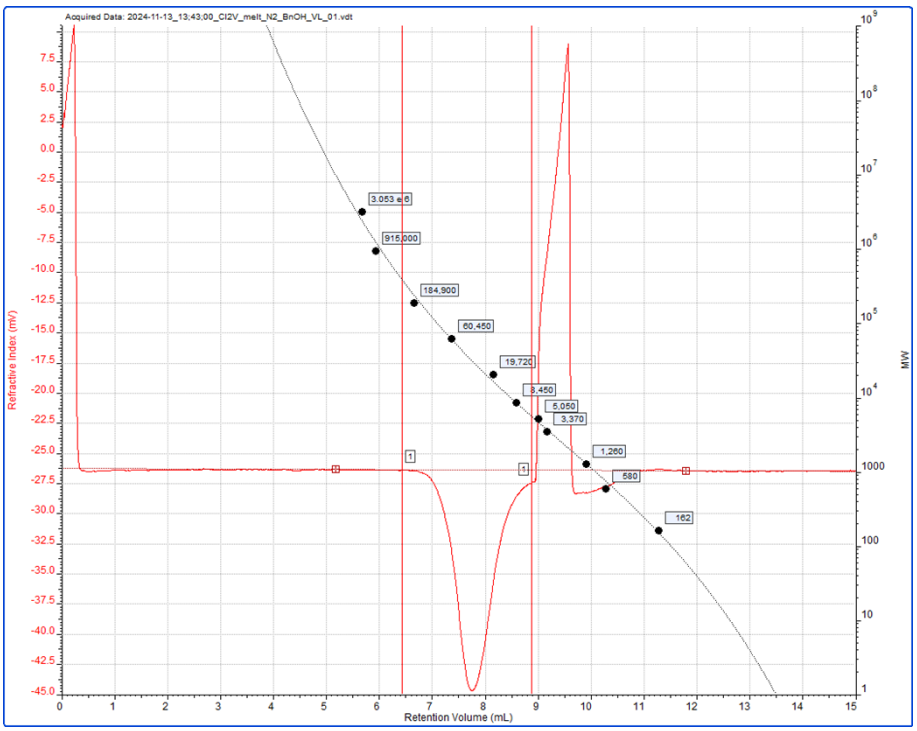


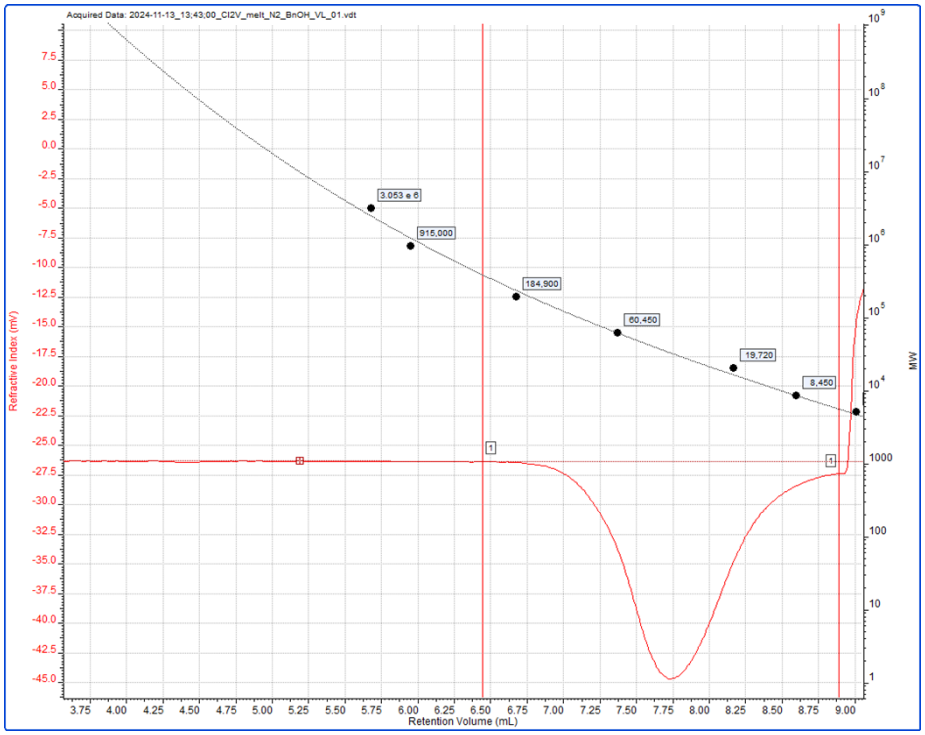

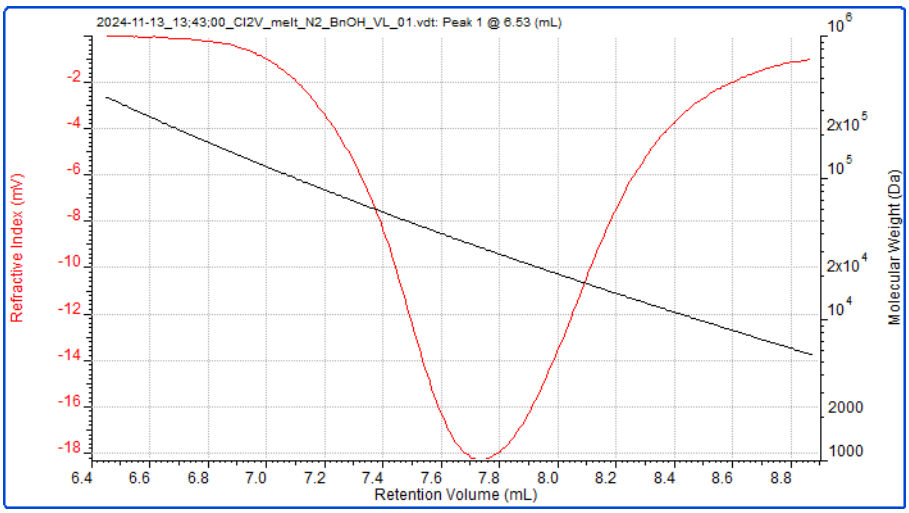


**Figure S50**. GPC trace for PVL from entry 17, Table 2.

Peak 1

Ret Vol (mL) 6.532

*M*n (Da) 23,921

*M*w (Da) 33,741

*M*z (Da) 48,157

*M*p (Da) 302,901

*M*w/*M*n 1.411

I2 VL tol N2

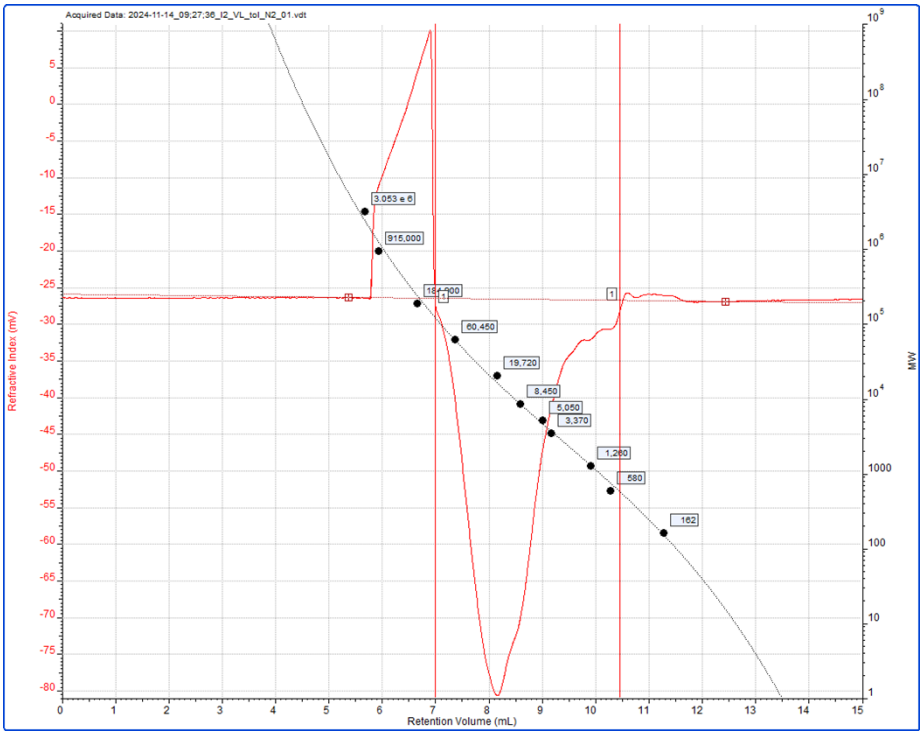
Acquired Data: 2024-11-14_09;27;36_I2_VL_tol_N2_01.vdt
Refractive Index (mV)
MW
Retention Volume (mL)
3,053 e 6
915,000
60,450
19,720
8,450
5,050
3,370
1,260
580
162

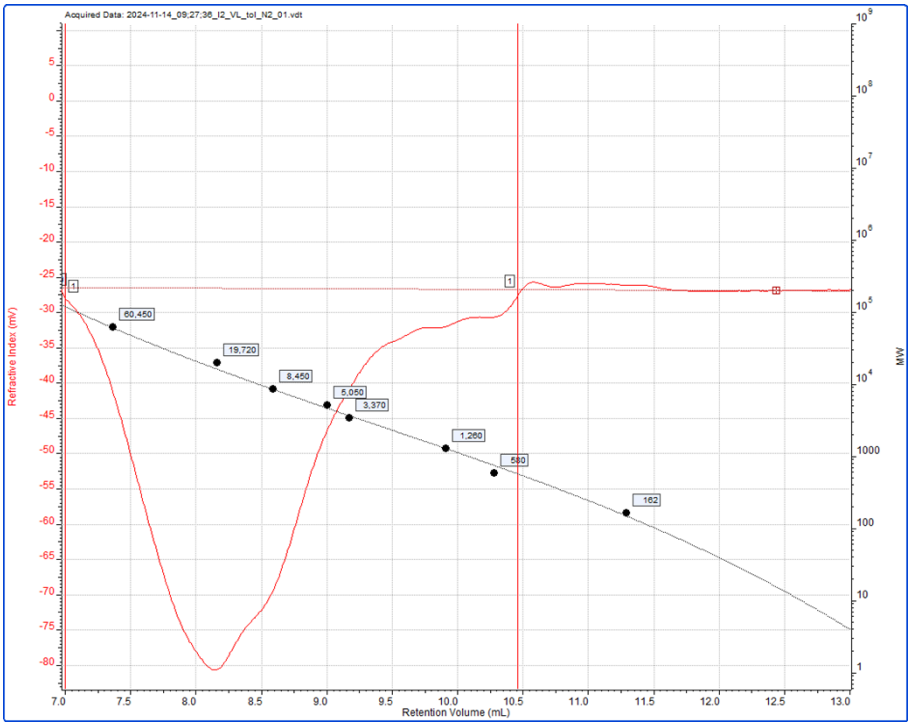
Acquired Data: 2024-11-14_09;27;36_I2_VL_tol_N2_01.vdt
Refractive Index (mV)
MW
Retention Volume (mL)
60,450
19,720
8,450
5,050
3,370
1,260
580
162

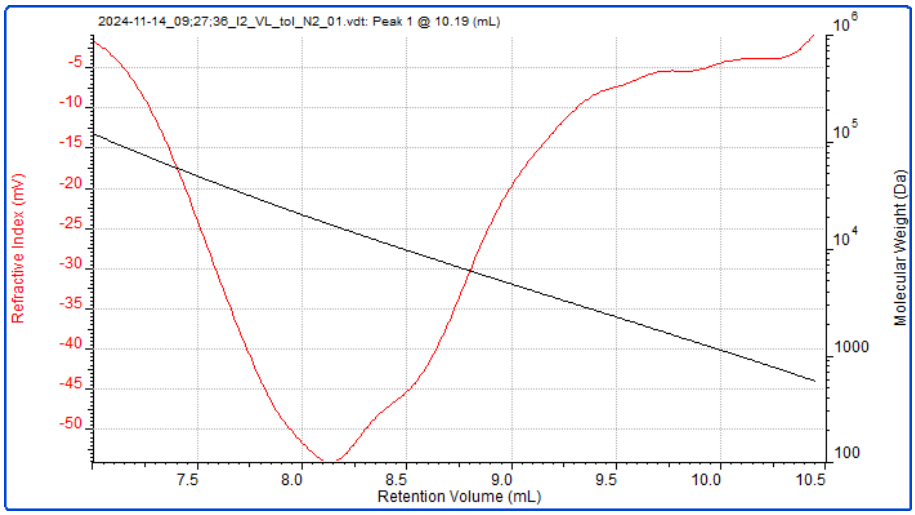


**Figure S51**. GPC trace for PVL from entry 19, Table 2.

Peak 1

Ret Vol (mL) 10.195

*M*n (Da) 27,582

*M*w (Da) 60,957

*M*z (Da) 78,262

*M*p (Da) 835

*M*w/*M*n 2.210

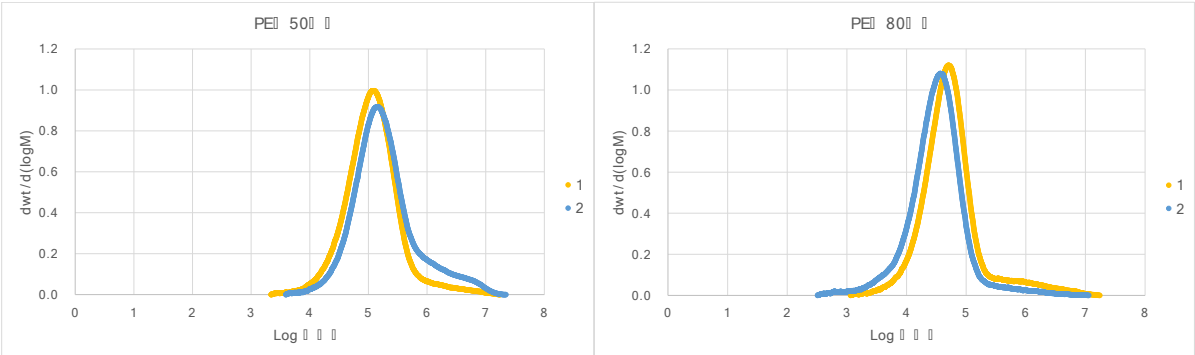


**Figure S52.** GPC curves of polyethylene formed by **1** and **2** using DEAC as co-catalyst. Entry designations refer to Table 5.

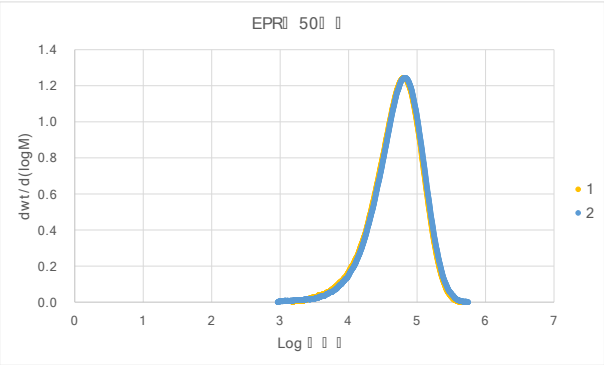


**Figure S53.** GPC curves of ethylene/propylene copolymer formed by **1** and **2** using DEAC as co-catalyst. Entry designations refer to Table 6.

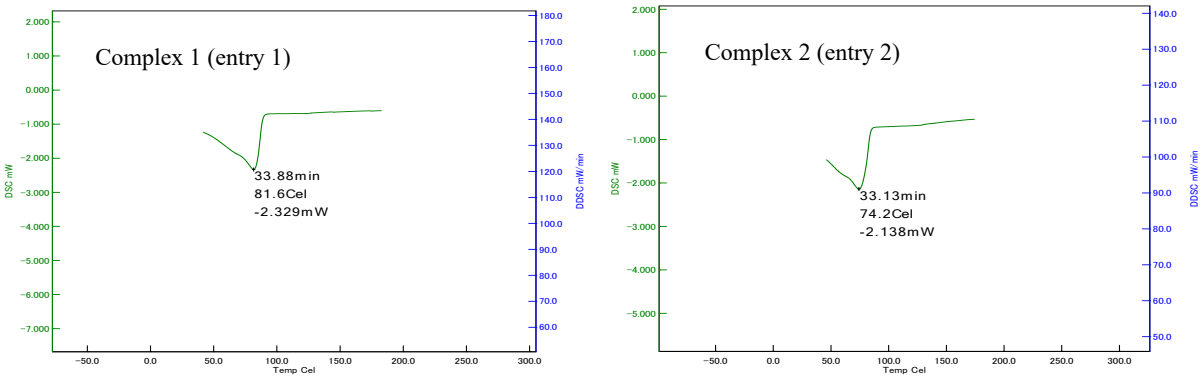


**Figure S54.** DSC thermograms of ethylene/propylene copolymer formed by **1** and **2** using DEAC as co-catalyst. Entry designations refer to Table 6.

Complex 1

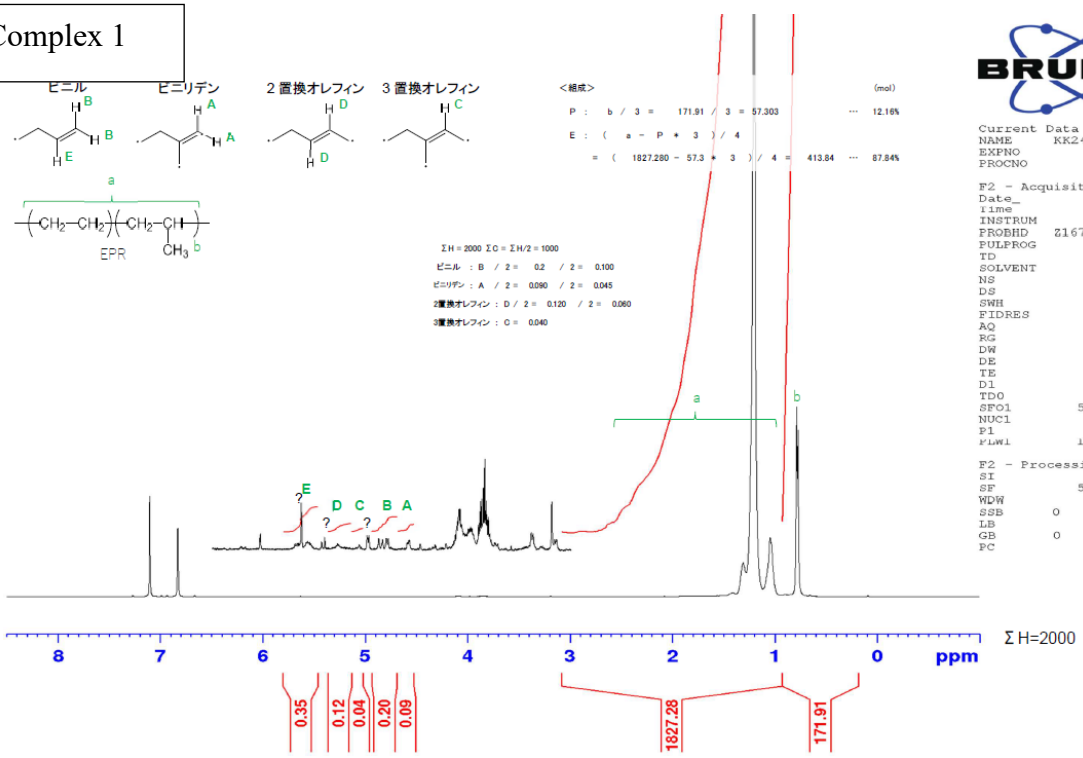



Current Data Parameters
NAME KK24010246_Shibata_E-F
EXPNO 40
PROCNO 1

F2 - Acquisition Parameters
Date_ 20240205
Time 11.12 h
INSTRUM spect
PROBHD Z167097_0001 (
PULPROG zg45
TD 65536
SOLVENT ODCB-d4
NS 64
DS 1
SWH 10000.000 Hz
FIDRES 0.305176 Hz
AQ 3.2767999 sec
RG 29.1379
DW 50.000 usec
DE 10.00 usec
TE 393.0 K
D1 3.72315001 sec
TDO 1
SFO1 500.0120000 MHz
NUC1 1H
P1 10.00 usec
PLW1 15.64700031 W

F2 - Processing parameters
SI 32768
SF 500.0099931 MHz
WDW EM
SSB 0
LB 0.15 Hz
GB 0
PC 1.00


Complex 2

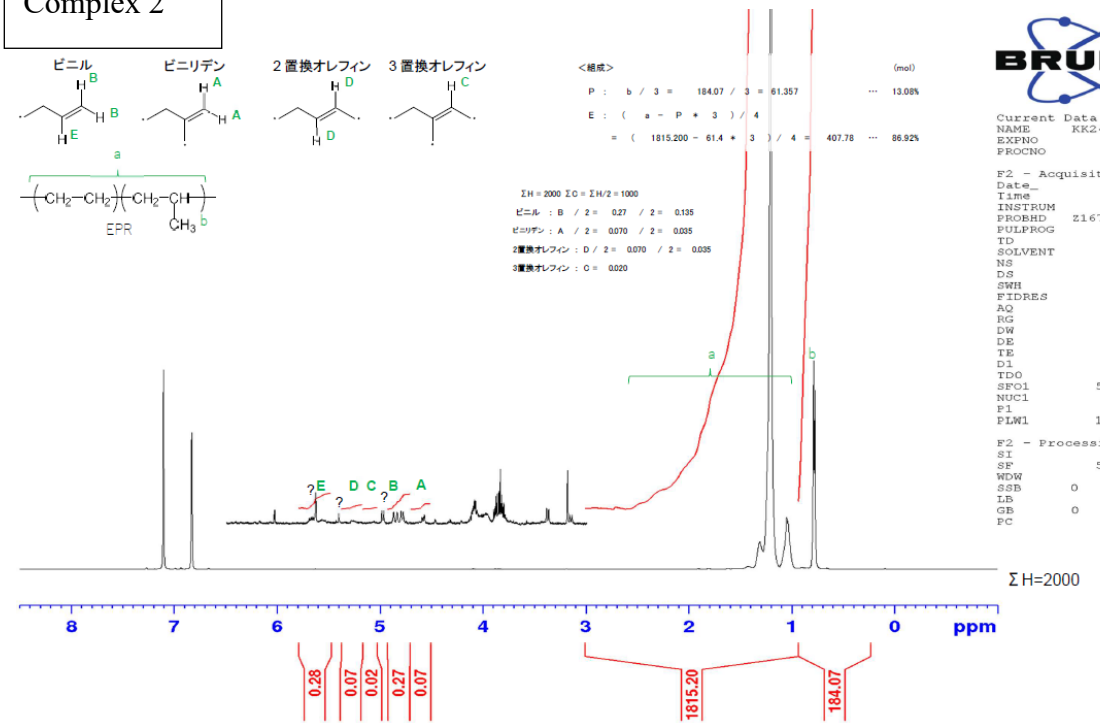



Current Data Parameters
NAME KK24010246_Shibata_E-F
EXPNO 50
PROCNO 1

F2 - Acquisition Parameters
Date_ 20240205
Time 11.33 h
INSTRUM spect
PROBHD Z167097_0001 (
PULPROG zg45
TD 65536
SOLVENT ODCB-d4
NS 64
DS 1
SWH 10000.000 Hz
FIDRES 0.305176 Hz
AQ 3.2767999 sec
RG 33.6207
DW 50.000 usec
DE 10.00 usec
TE 393.0 K
D1 3.72315001 sec
TDO 1
SFO1 500.0120000 MHz
NUC1 1H
P1 10.00 usec
PLW1 15.64700031 W

F2 - Processing parameters
SI 32768
SF 500.0101286 MHz
WDW EM
SSB 0
LB 0.15 Hz
GB 0
PC 1.00

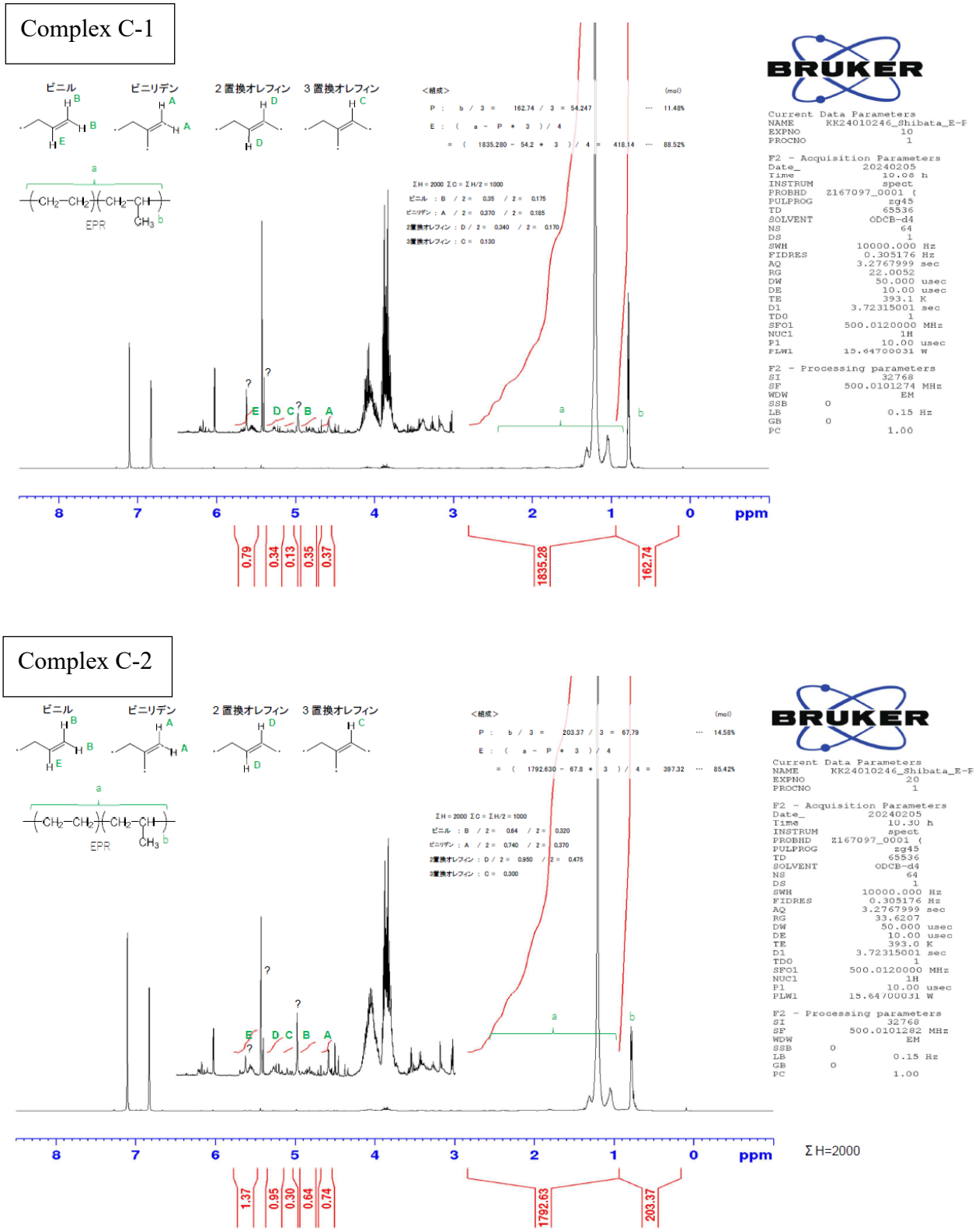


**Figure S55.** $^{1}$H NMR spectra of ethylene/propylene co-polymer was recorded using o-dichlorobenzene at 120 °C, and spectra were referenced versus main chain methylene proton peak (1.2 ppm). Entry designations refer to Table 6.

## References

[S1] M. Hu, X. Song, F. Wang, W. Zhang, W. Ma and F. Han, Ring-opening polymerization of *rac*-lactide catalyzed by magnesium and zinc complexes supported by an NNO ligand. *New J. Chem*. **2022**, *46*, 1175-1181. Doi: org/10.1039/D1NJ05157A